INACIO THOMAZ BUENO

OPTIMIZING DISTURBANCE MAPPING IN SEASONAL BIOMES BASED ON AN ENSEMBLE FRAMEWORK

LAVRAS – MG
2022

INACIO THOMAZ BUENO

OPTIMIZING DISTURBANCE MAPPING IN SEASONAL BIOMES BASED ON AN ENSEMBLE FRAMEWORK

Tese apresentada à Universidade Federal de Lavras, como parte das exigências do Programa de Pós-Graduação em Engenharia Florestal, área de concentração em Manejo Florestal, para a obtenção do título de Doutor.

Prof. Dr. Fausto Weimar Acerbi Júnior
Orientador

LAVRAS – MG
2022

Ficha catalográfica elaborada pelo Sistema de Geração de Ficha Catalográfica da Biblioteca Universitária da UFLA, com dados informados pelo(a) próprio(a) autor(a).

Bueno, Inacio Thomaz.
Optimizing disturbance mapping in seasonal biomes based on an ensemble framework / Inacio Thomaz Bueno. - 2022.
147 p. : il.

Orientador(a): Fausto Weimar Acerbi Júnior.

Tese (doutorado) - Universidade Federal de Lavras, 2022.
Bibliografia.

1. Sensoriamento remoto. 2. LandTrendr. 3. Regionalização. I. Acerbi Júnior, Fausto Weimar. II. Título.

INACIO THOMAZ BUENO

OPTIMIZING DISTURBANCE MAPPING IN SEASONAL BIOMES BASED ON AN ENSEMBLE FRAMEWORK

OTIMIZAÇÃO DO MAPEAMENTO DE MUDANÇAS EM BIOMAS SAZONAIS BASEADO EM UMA METODOLOGIA DE AGRUPAMENTO

Tese apresentada à Universidade Federal de Lavras, como parte das exigências do Programa de Pós-Graduação em Engenharia Florestal, área de concentração em Manejo Florestal, para a obtenção do título de Doutor.

APROVADA em 14/01/2022.

Prof. Dr. Luís Marcelo Tavares de Carvalho	UFLA
Prof. Dr. Sérgio Teixeira da Silva	UFLA
Prof. Dr. Sérgio Henrique Godinho Silva	UFLA
Prof. Dr. Allan Arantes Pereira	IF Sul de Minas Gerais

Prof. Dr. Fausto Weimar Acerbi Júnior

Orientador

LAVRAS – MG
2022

To my beloved family and dear friends

In memory of Demétrius Aguiar Barbosa Prado

AGRADECIMENTOS

À Deus, por ceder o dom da vida.

À minha família: pais, avós, tios, irmãos e primos, que com a simplicidade de um valor, nunca deixaram e vão deixar de influenciar na formação do meu caráter. Ana Claudia pelo companheirismo e motivação.

Às minhas grandes amizades que conquistei por onde passei em especial aos amigos de Lavras e Juruaia pelos grandes momentos compartilhados.

À Universidade Federal de Lavras e a Universidade de Calgary, juntamente com todo seu corpo docente pelo conhecimento transmitido, em especial ao Laboratório de Estudos e Projetos em Manejo Florestal, LEMAF, pelo suporte durante esse tempo.

Ao Programa de Pós Graduação em Engenharia Florestal pela oportunidade concedida para a realização deste trabalho.

À Coordenação de Aperfeiçoamento de Pessoal de Nível Superior (CAPES), pela concessão da bolsa de doutorado, código de financiamento 001.

Ao meu grande amigo e mestre, Professor Fausto, que sempre auxiliou na construção do profissional que sou hoje com toda sua sabedoria, paciência e orientação.

Aos membros da banca examinadora, que gentilmente aceitaram o meu convite e pelas valiosas contribuições.

Aos meus colegas de trabalho do Brasil e Canadá, em especial, Aliny, Duda e Jennifer por toda a ajuda e parceria.

E por fim, à aqueles que indiretamente, mesmo que sendo com um simples bom dia no corredor, me passaram confiança para a realização deste trabalho, o meu muito obrigado.

RESUMO GERAL

O mapeamento e monitoramento de mudanças na vegetação nativa fornece suporte para o desenvolvimento de estratégias de gestão, implementação de iniciativas de políticas e fornecimento de dados para modelagem de processos ecológicos e ambientais. Porém, biomas sazonais são naturalmente heterogêneos em termos de clima, solo, biodiversidade e ameaças representadas por atividades humanas e ocupação do solo. Neste cenário, esta tese tem como objetivo principal otimizar o mapeamento de mudanças na vegetação nativa baseado no método *ensemble*, que visa a combinar vários modelos básicos para produzir um modelo preditivo ideal. Para tanto, esta tese foi organizada em três artigos. No primeiro artigo (1), mapas de mudanças de diferentes índices espectrais foram avaliados em biomas sazonais em relação à concordância espacial entre mapas e entre uma base de dados de referência. Os resultados indicaram que houve uma baixa taxa de concordância espacial entre mapas, a qual não foi influenciada pelos biomas. Também foi encontrada uma relação entre índices e biomas, onde determinados índices performaram melhor em determinados biomas. Já no segundo artigo (2), foi avaliada a efetividade de um método *ensemble* e regionalizações baseadas em diferentes bases de dados no mapeamento de mudanças. O método ensemble combinou mapas de mudança do algoritmo LandTrendr e o algoritmo Random Forest. Os resultados mostraram que o método *ensemble* retornou ganhos em acurácia quando comparado com métodos mais simples. Além disso, o método de regionalização também mostrou ganhos em acurácia quando comparado ao método não regionalizado, sendo variáveis climáticas e sazonais as que mais se destacaram no ganho de acurácia. Por fim, o terceiro artigo (3), utilizou análise orientada ao objeto, e avaliou variáveis preditoras do LandTrendr e de semivariograma, no mapeamento e caracterização das mudanças na cobertura do solo. Três classes de mudanças na cobertura do solo (não mudança, perda de vegetação e pós mudança) foram mapeadas utilizando três bases de dados: LandTrendr, Semivariograma e Híbrida. A base de dados Híbrida retornou as maiores acurácias. Este estudo também indicou que variáveis do semivariograma podem capturar padrões de mudança no uso e cobertura do solo. Assim, a crescente necessidade em se mapear e monitorar mudanças na vegetação em biomas sazonais sugere que novas abordagens aqui propostas, sejam aplicáveis em larga escala e que retornem acurácias satisfatórias.

Palavras-chave: Sensoriamento remoto. BFAST. LandTrendr. Regionalização. Semivariograma.

GENERAL ABSTRACT

Mapping and monitoring disturbance in vegetation provide support for developing management strategies, implementing policy initiatives, and providing inputs for modeling ecological and environmental processes. However, seasonal biomes are naturally heterogeneous in terms of climate, soil, biodiversity, and threats posed by human activities and land occupation. In this thesis, mapping and monitoring disturbances in native vegetation were optimized based on ensemble techniques, which uses multiple or committee classifiers combining their predictions. For this purpose, this thesis was organized in three articles. In the first one (1) disturbance maps of seasonal biomes from different spectral indices were evaluated based on the spatial agreement between maps and their accuracies. The results indicated a low rate of spatial agreement among index-based disturbance maps, which was minimally influenced by vegetation domain. In addition, index-based disturbance maps reflected site-specific sensitivity. In the second article (2), the effectiveness of a heterogeneous ensemble classification and data-driven regionalization for improving vegetation disturbance mapping accuracies over large areas was assessed. The ensemble method combined disturbance maps from the LandTrendr algorithm and Random Forest. The results indicated gains in accuracy by the ensemble method compared to non-ensemble methods of disturbance mapping. In addition, data-driven regionalization addressed complexities arising from variability in vegetation types, local climate, and topography across our study area, identifying climate and seasonal metrics as important variables for reducing uncertainties in vegetation disturbance maps. Finally, the third article (3) used object-based image analysis and evaluated predictor variables from both LandTrendr and semivariogram for mapping and characterizing land cover changes. Three classes of land cover changes: non-change, vegetation loss, and pos-change, were set combined with three datasets: LandTrendr, Semivariogram, and Blended. The Blended datasets returned the best accuracies. This article also indicated that semivariogram variables faithfully captured patterns of vegetation loss and recovery. Thus, the increasing need for mapping and monitoring disturbances in seasonal biomes suggests that the methods and algorithms presented in this thesis, return satisfactory accuracies and may be suitable for large-area applications.

Keywords: Remote sensing. BFAST. LandTrendr. Regionalization. Semivariogram.

LISTA DE FIGURAS
LIST OF FIGURES

SEGUNDA PARTE – ARTIGOS

ARTIGO 1

ARTIGO 2

ARTIGO 3

LISTA DE TABELAS

LIST OF TABLES

SEGUNDA PARTE – ARTIGOS

ARTIGO 1

ARTIGO 2

ARTIGO 3

SUMÁRIO

FIRST PART

1 INTRODUCTION

Anthropogenic disturbances in tropical forest environments (e.g., selective logging and wildfires) are considered one of the major drivers of biodiversity loss (BARLOW *et al.*, 2016) and the second largest source of anthropogenic greenhouse gas emissions (VAN DER WERF *et al.*, 2009). Thus, detecting and monitoring forest disturbance is of vital importance as they are also linked to economic activities, governmental investments and funding, or product supply for local or international markets (TRUMBORE; BRANDO; HARTMANN, 2015).

Seasonal biomes in Brazil, for example, the Brazilian savanna, the semi-arid woodland, and the Atlantic forest are among the most threatened environments in the world due to high rates of conversion, and few conservation efforts focusing on these seasonal areas (ACERBI JÚNIOR *et al.*, 2015). The Atlantic forest was subjected to considerable deforestation in the past, which reduced its occurrence to approximately 14% of its original area (RIBEIRO *et al.*, 2009). Savannas and semi-arid woodlands have been subject to more recent disturbance scenarios with increasing rates of land conversion. From 1990 to 2010, 266,000 km^2 and 90,000 km^2 of vegetation were cleared in savanna and semi-arid woodland areas, respectively (BEUCHLE *et al.*, 2015).

Current research on vegetation disturbance mapping aims to accurate and timely detection of disturbances, and remote sensing data are the only feasible way to detect and monitor disturbances over large areas. However, this is not a trivial task, as disturbance detection is subject to a variety of noise factors including cloud cover, atmospheric scattering, and geometric errors (SCHULTZ *et al.*, 2016). In addition, seasonal biomes are naturally heterogeneous in terms of climate, soil, biodiversity, and threats posed by human activities and land occupation, which may difficult conservation efforts in terms of automatically mapping and monitoring (TRANCOSO; SANO; MENESES, 2015).

The opening of the Landsat archive in 2008 allowed the development of new disturbance mapping approaches (WULDER *et al.*, 2019). Free global mid-resolution (30 m) remote sensing imagery and a long-term record of observations have enabled more accurate land change analysis, the characterization of disturbance drivers, and the monitoring of post-disturbance conditions (WULDER *et al.*, 2012). Methods and algorithms to detect and monitor vegetation disturbances have been developed to exploit the Landsat data archive and to examine long-term vegetation trends. For example, the Breaks For Additive Season and Trend (BFAST)

recently emerged as a reliable automated algorithm for detecting vegetation disturbances across the tropics (DEVRIES *et al.*, 2015; DUTRIEUX *et al.*, 2015; SCHULTZ *et al.*, 2016b, 2018). It computes long-term trends and abrupt disturbances in a dense time series of a spectral index and then it produces sub-annual information on disturbances and trends (VERBESSELT *et al.*, 2010a). Another popular Landsat-based algorithm is the Landsat-based detection of Trends in Disturbance and Recovery, or LandTrendr (KENNEDY; YANG; COHEN, 2010). LandTrendr uses a pixel-based segmentation method to investigate land trajectories by modeling time series and computing straight-line segments, returning outputs as the magnitude, duration, and timing of a land disturbance. Although first developed to detect disturbances in forest environments (KENNEDY *et al.*, 2012), LandTrendr has become popular for other vegetation analyses, such as disturbances in cropland patterns (ZHU *et al.*, 2019a), natural disturbances in mangrove areas (DE JONG *et al.*, 2021), and post-fire vegetation recovery (BRIGHT *et al.*, 2019).

Despite these promising results, some questions still remain. Most authors recognize that an optimal disturbance mapping technique does not yet exist since a single method might be not sensitive to the spatio-temporal heterogeneity of varied and continuous landscapes (HUSSAIN *et al.*, 2013). An alternative to choosing a single method or algorithm for mapping disturbances is utilizing multiple classifier systems or a multi-algorithm ensemble. The ensemble technique for classification systems is based on multiple or committee classifiers combining their predictions. The objective is to exclude individual weaknesses and to benefit from particular advantages of each individual algorithm, reducing the generalization error (OZA; TUMER, 2008). In remote sensing studies, ensemble classification has produced better results than individual systems (BRUZZONE; COSSU; VERNAZZA, 2004; COHEN *et al.*, 2020; RODRIGUEZ-GALIANO *et al.*, 2012; SHIMIZU *et al.*, 2019).

In this context, the main objective of this thesis was to optimize disturbance mapping in seasonal biomes using ensemble techniques. For this purpose, this thesis was organized in three articles. In the first one (1), the suitability of several spectral indices for mapping disturbances in different tropical vegetation domains using the BFAST Monitor algorithm was assessed and compared. The specific objectives of this first article were: to evaluate the spatial agreement between disturbance maps produced using seven spectral indices derived from Landsat Thematic Mapper/Operational Land Imager and input into BFAST Monitor, and the influence of vegetation domain on this agreement; and to evaluate the accuracies of these index-derived disturbance maps and their relationship with vegetation domain.

In the second article (2), the effectiveness of a heterogeneous ensemble classification and data-driven regionalization for improving vegetation disturbance mapping accuracies over

large areas was evaluated. This paper first evaluated the performance of an ensemble method on mapping disturbances in a heterogenous vegetated area, investigating the benefit of using multiple classifiers by exploring their particular advantages. Second, a land regionalization scheme based on environmental and anthropogenic information was tested, where it was hypothesized that the grouping of land units and their respective variability will significantly improve the performance of disturbance mapping algorithms over traditional methods because these algorithms will be customized to each individual unit and their respective disturbance observations, returning gains in accuracy.

In the third article (3), the accuracy of LandTrendr algorithm and the semivariogram features derived from NDVI images to map and characterize land-use and land-cover changes was evaluated. In this article, disturbance mapping accuracies from LandTrendr, semivariogram, and their combination as predictor variables were evaluated first; then gains and losses in accuracies were analyzed based on the relationship between classification accuracies and the number of classes plus land-use and land-cover change types. In addition, this article also analyzed patterns of change in accordance with the temporal behavior of the semivariogram parameters to infer vegetation loss and recovery.

2 LITERATURE REVIEW

2.1 Tropical Seasonal Biomes in Southeast Brazil

Tropical seasonal biomes play a key role in a global context. A particular characteristic that influences the stability of the Earth's climate system consists of the fact that these forests store 200–300 Pg C (10^{15} grams of carbon), about a third as much as stored in the atmosphere (PAN *et al.*, 2011). This cycle is very dynamic, represented by tropical trees performing about 60% of the world's photosynthesis, capturing around 72 Pg C from the atmosphere every year, and releasing back a similar amount through respiration of both trees themselves and other living organisms (MITCHARD, 2018). Tropical seasonal biomes have long been recognized as one of the largest pools of biodiversity comprising more than half of the known species worldwide with a large number of rare and hyper-rare species (TOVO *et al.*, 2017). In the tropics, forests have an important influence on the climate system as a major regulator of global climate by exchanging more water and carbon with the atmosphere than any other biome (LAWRENCE; VANDECAR, 2015). This multiplicity of forest functions and services directly rely on 1.5 billion people (LEWIS; EDWARDS; GALBRAITH, 2015).

In southeast Brazil, tropical seasonal biomes are divided into three major vegetation domains or biomes: Atlantic Forest, Savanna, also known as Cerrado, and Seasonal Dry Tropical Forest, or Caatinga (Figure 1). The first one occurs along the coast, with a 'dry diagonal' of seasonally dry forest, woodland, and savanna vegetation formations (MIRANDA *et al.*, 2018).

Figure 1 – Tropical seasonal biomes in southeast Brazil.

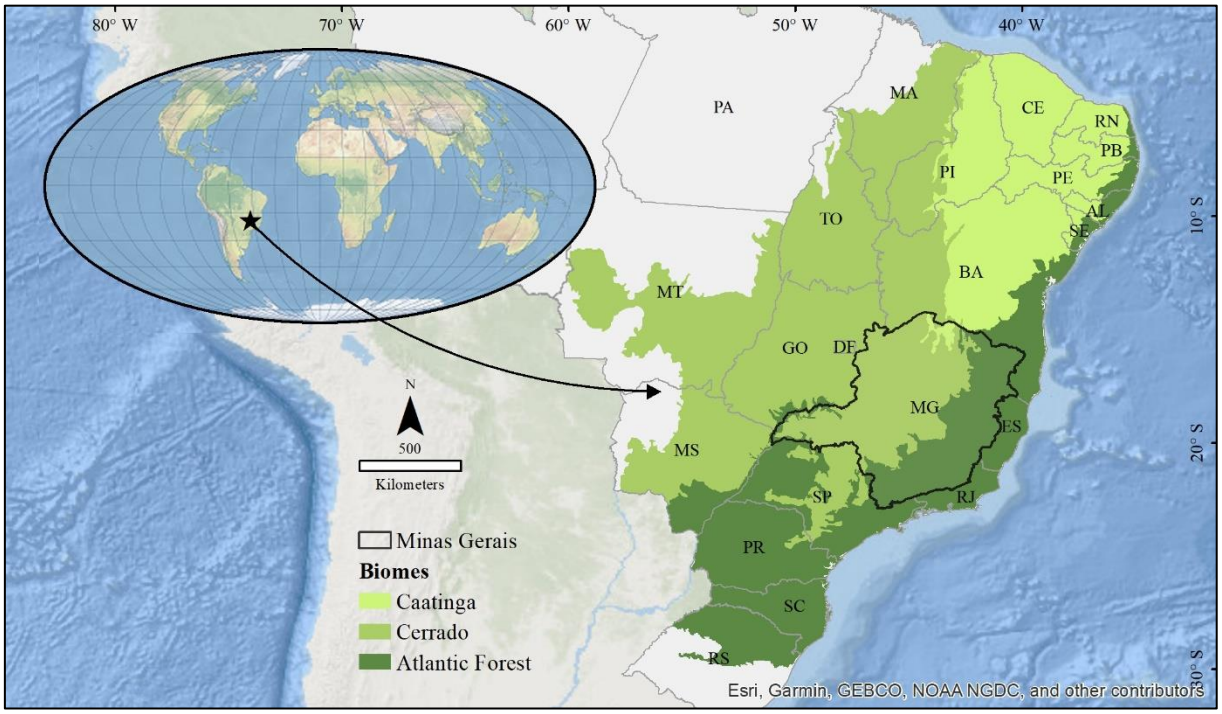

Source: Author (2022).

The Atlantic forest is composed of different types of vegetation, mostly including rainforests, semi-deciduous forests, as well as high-altitude grasslands. This vegetation domain has outstanding levels of species endemism, making the Atlantic forest a biodiversity hotspot (MYERS *et al.*, 2000).

The Cerrado biome has a unique vertically structured mosaic of plant formations among the savannas in the world (FERREIRA *et al.*, 2003). It ranges from forest formations with a dense canopy cover to grasslands with sparse and short twisted trees, also being considered a biodiversity hotspot (MYERS *et al.*, 2000). Approximately 90% of the rains are concentrated from October to April with annual precipitation ranging from 1200 to 1800 mm.

The dry season is quite distinct with monthly precipitation reaching zero millimeters, inducing a wide range of adaptive phenological strategies in vegetation formations in order to overcome water scarcity. Semi-arid woodland, also known as the Caatinga biome, is an ecosystem occupied by a mixture of deciduous forests and herbaceous understory. It receives less than 750 millimeters per year of extremely irregular rainfall, where more than 75% of the total annual rainfall can occur within three months. In addition, annual variations in semi-arid woodland are large where droughts can last for a couple of years.

2.2 Vegetation Disturbances

According to Lewis, Edwards and, Galbraith (2015), three major trends, caused by human activity, dominated tropical biomes over the years: the conversion to non-forest, mostly for expansion of farmlands and mining; degradation of remaining forest, i.e. by selective logging or fire; and regeneration of the secondary forest. Human-induced deforestation, defined as forest clearance and conversion to another land use, is probably the most direct ecosystem issue causing the permanent loss of forest cover (PRĂVĂLIE, 2018). Deforestation is driven by socioeconomic factors that range from local use to international markets and that occur legally and illegally, making their focalization and mitigation complex (LEWIS; EDWARDS; GALBRAITH, 2015).

Vegetation disturbance quantification has received special attention in recent years by scientific studies. At the global scale, Keenan *et al.* (2015), based on the 2015 FAO Global Forest Resources Assessment (FAO, 2015), founded a decrease of tropical forests by ~1.9 M km² in the past twenty-five years, from 19.6 M km² in 1990 to 17.7 M km² in 2015. Achard *et al.* (2014), using sample blocks of Landsat images and considering forested pixels with >30% canopy in a 3 ha of minimum mapping unit, calculated a decrease of 1.3 M km² in twenty years, from 16.4 M km² in 1990 to 15.1 M km² in 2010. And Hansen *et al.* (2013), based on Landsat images, found a decrease of tropical forests by ~1.1 M km², considering canopy closure greater than 25% for all vegetation taller than 5m in height.

Tropical deforestation has various environmental implications at global scales (PRĂVĂLIE, 2018). With regards to carbon emission, Pan *et al.* (2011) estimated a total emission (gross deforestation emission minus forest regrowth) of 1.3 (±0.7) Pg C per year (1990–2007), being the second-largest anthropic source of atmospheric CO_2 after fossil fuel burning. Climate variation is also directly impacted from local to global scales, where a total tropical deforestation scenario could result in global warming equivalent to that caused by the burning of fossil fuels since 1850 (LAWRENCE; VANDECAR, 2015). In addition, forest removal is the main cause of land degradation by the water erosion process in drylands (PRĂVĂLIE, 2016). The impact on biodiversity is another relevant issue since animal and plant communities in forests fragmented by agriculture continue to decline after human impacts have occurred (EDWARDS *et al.*, 2014).

Although Brazil exhibited the largest decline in annual forest loss among tropical countries (40 K km².year^{-1} in 2003 to 2004 to 20 K km²/year in 2010 to 2011) accounted by Hansen *et al.* (2013), it also retains the deforestation scenario in South America in Amazon and

Seasonal biomes (KEENAN *et al.*, 2015). In the Amazon, the decline in annual forest loss is observed in new large forest clearings (> 0.5 km²) drop of 46% over 2001 to 2014, while the number of new small clearings (< 0.01 km²) increased by 34% between the same period (KALAMANDEEN *et al.*, 2018). Conversely, Savanna and Seasonal Dry Tropical biomes have been under increasing anthropic pressure for many years, indicated by ~266 K km² and ~90 K km² of gross forest loss in the past twenty years, respectively (BEUCHLE *et al.*, 2015). The authors also demonstrated a decrease of the annual rate of loss in Savanna from 0.79% yr^{-1} to 0.44% yr^{-1}, while Dry Forests increased from 0.19% yr^{-1} to 0.44% yr^{-1}.

2.3 Remote Sensing and Disturbance Detection

The remote sensing science extracts information of a target on Earth's surface through a set of data provided by a sensor placed at an airplane or satellite (SCHOWENGERDT, 2007). Solar energy is the main source of energy in passive remote sensing and sensors are responsible to convert radiance received from a target into digital images or remote sensing images (SCHOWENGERDT, 2007). Thus, remote sensing is very important and efficient for land cover mapping and monitoring purposes because it is generally faster and less costly than the information collected at the ground level. It also provides an aerial perspective that allows a better understanding of the spatial relationships and invisible data to human sense such as spectral information in the infrared region (CONGALTON; GREEN, 2009). Thus, remote sensing science has become a universal practice in government agencies, environmental organizations, industrial sector, and research institutions (KENNEDY; YANG; COHEN, 2010).

Among a collection of applications in remote sensing science, detecting disturbances on the Earth's surface is the process of identifying differences between images at different times. Remote sensing-based disturbance detection has developed many different methods over the past decades of satellite remote sensing, which have been reviewed by several authors (BANSKOTA *et al.*, 2014; COPPIN *et al.*, 2004; HUSSAIN *et al.*, 2013; LU *et al.*, 2004; TEWKESBURY *et al.*, 2015; ZHU, 2017). Some of these review studies provided a comprehensive division of a disturbance detection project in different levels and aspects, such as the disturbance target, sensor characteristics, image frequency, pre-processing, unit of analysis, disturbance detection technique, and accuracy assessment (ZHU, 2017). Thus, disturbance detection is a highly variable and ever-expanding area of research with multiple fields of interest, i.e. deforestation, damage assessment, disasters monitoring, urban expansion, planning, and land management (HUSSAIN *et al.*, 2013).

In forest environments, deforestation and degradation are the main disturbance targets, and the sensor is directly related to the scale of analysis. At the global scale, forest disturbance detection studies started with low spatial resolution sensors as Achard *et al.* (2002) using 1 km resolution Advanced Very High Resolution Radiometer – AVHRR images, and Mayaux *et al.* (2005) using 1 km resolution SPOT-4. Coarse resolution Moderate Resolution Imaging Spectroradiometer – MODIS image with 500m pixel size was used to detect forest disturbances (HANSEN; STEHMAN; POTAPOV, 2010). In recent years, an overwhelming increase in computing provided a foundation for Landsat forest disturbance over the globe by wall to wall mapping (GONG *et al.*, 2013; HANSEN *et al.*, 2013) or grouped into blocks (ACHARD *et al.*, 2014). At regional scales, the use of Landsat imagery increases due to free and open access, relatively high spatial resolution, and effectiveness in time series analysis (ZHU, 2017). In addition, very high spatial resolution imagery, such as Rapideye imagery (5m pixel size), became computational feasible to map forest disturbances (GÄRTNER; FÖRSTER; KLEINSCHMIT, 2016; MARX; TETTEH, 2017).

Unit of analysis and disturbance detection technique are quite related. Although the unit of analysis is basically divided into pixel-based disturbance detection and object-based disturbance detection, Tewkesbury *et al.* (2015) subdivided it into the pixel, kernel, image-object overlay, image-object comparison, multi-temporal image-object, vector polygon, and hybrid. The pixel is the most fundamental element of an image and it is still widely used in most disturbance detection, mainly in large areas where object-based analysis can be very time consuming (ACHARD *et al.*, 2014; GONG *et al.*, 2013; HANSEN *et al.*, 2013; HANSEN; LOVELAND, 2012).

Many disturbance detection methods are demonstrated in the literature, which were divided by Zhu (2017) into six major categories: thresholding, differencing, segmentation, trajectory classification, statistical boundary, and regression. Although the author reviewed these methodologies in Landsat time series and in multiple land cover and land use classes, they can be adapted for forest disturbance detection with similar Earth Observation instruments.

I. Thresholding: assigns a predefined threshold for identifying disturbances in land cover, detected when there are significant deviations from the value as applied by Pickell *et al.* (2014) detecting anthropic forest disturbance combining autonomous disturbance detection procedure and a spectral threshold classification.
II. Differencing: compares images acquired at different times, which was considered very effective in large areas, as demonstrated by Potapov *et al.* (2015) while quantifying

forest cover disturbance across Eastern Europe since the 1980s using supervised bagged classification in difference images.

III. Trajectory classification: first extracts information from Landsat time series, and later uses this information to further classify every unit of analysis in time. Developed by Kennedy, Yang and, Cohen (2010), the LandTrendr method classifies pixel trajectories in forests by segmenting them into discrete periods of growth, disturbance, or recovery.

IV. Statistical boundary: assigns an area as disturbance, when it follows a statistical boundary, i.e. Brooks *et al.* (2014) developed the Exponentially Weighted Moving Average Change Detection, an algorithm based on statistical quality control charts for detecting forest disturbance.

V. Regression: assumes a linear or non-linear relationship between the time observations and the response variables using regression to estimate the output. They are relatively simple to use, but heavily reliant on accurate calibration when using different sensors (ZHU, 2017).

Accuracy assessment of forest disturbance maps indicates the quality in a quantitative and meaningful fashion. Olofsson *et al.* (2014) recommended good practices for assessing accuracy in land change regarding sampling design, response design, and analysis.

2.4 The Challenge of Detecting Disturbances in Seasonal Biomes

To track disturbances over time, mapping methods rely on the selection of imagery in time, which needs the selection of appropriate imagery from the archive from which to derive disturbance information. An important challenge in the selection of imagery for such disturbance detection methods is the loss of data due to a number of contaminations. Clouds and cloud shadow significantly influence remote sensing imagery. The brightening effect of clouds and the darkening effect of cloud shadows significantly influence the reflectance of spectral bands. Screening of such contaminations is especially crucial for disturbance detection methods because undetected cloud and cloud shadow will likely result in the identification of disturbance where none occurred (ZHU; WOODCOCK, 2014).

Another important challenge is the great variety of large-scale vegetation phenologies, which renders mapping and characterization difficult, including issues related to highly diverse seasonality, forest types, or forest densities and height (WHITE *et al.*, 2010). A key challenge in remote sensing disturbance detection is to accurately identify disturbances in vegetation while not accounting for those associated with phenological differences, which is an intrinsic characteristic of seasonal biomes (TRANCOSO; SANO; MENESES, 2015). When images

from different seasons are acquired, disturbances caused by phenology in vegetation are inevitable and can be easily confused with forest disturbance (LU *et al.*, 2016).

2.5 Recent Advances for Vegetation Disturbance Detection

Over the past several years, there have been significant advances in disturbance mapping algorithms that use Landsat data, taking advantage of the high-quality data archive that became freely available in 2008. Users of forest disturbance maps now have a palette of new products becoming available to choose from and they need to understand which are best suited to their needs (ZHU, 2017).

2.5.1 Methods and Algorithms

Not too recent but still important, object-based image analysis combines segmentation and remote sensing information along with analyst experience with image objects in order to model geographic entities (BLASCHKE, 2010; CHEN *et al.*, 2012). Segmentation is the most common approach for building objects in images (VIEIRA *et al.*, 2012), which has the objective of creating groups of pixels spectrally similar and spatially adjacent from an image with the purpose of minimizing the within-object variability compared to the between-object variability (DESCLÉE; BOGAERT; DEFOURNY, 2006). According to (CHEN *et al.*, 2012), the advantages of object-based based approach on pixel-based disturbance detection methods are the segmentation procedure, which characterizes landscape elements by groups of homogeneous pixels; reduction salt and pepper effect attributed by small spurious disturbances; and the extraction of sophisticated information of the image objects as geometry and texture. Among the object-based disturbance detection methodologies described in scientific literature, Chen *et al.* (2012) classified them into four groups.

I. Image-object change detection: it is similar to pixel-based when two or more segmented images are directly compared by the extraction of spectral and/or spatial information.
II. Class-object change detection: a comparison “from-to” of image-objects defined by landscape classes, so additional classification information is required.
III. Multi-temporal object change detection: objects are generated by two or more images with temporal information, where a set of images create one segmentation.
IV. Hybrid change detection: involves the use of both object and pixel methodologies.

As well as traditional spectral statistics, shape and texture descriptors extracted from objects, other textural or structural features derived from geostatistical functions can be

obtained (BALAGUER *et al.*, 2010). In recent years, the semivariogram has gained a place among object-based disturbance detection procedures. Object-based classifications have been made using semivariogram features to mitigate the presence of phenological effects from time series to detect disturbances over forest ecosystems (ACERBI JÚNIOR *et al.*, 2015; SILVEIRA *et al.*, 2019, 2018a, 2018b). In Hermosilla *et al.* (2012), semivariogram features were used with other spectral, textural, and shape features extracted from high-resolution imagery for object classification in a disturbance detection problem in peri-urban areas with heterogeneous landscapes. Balaguer *et al.* (2010) demonstrated better performance of the combination of features derived from the semivariogram and spectral information with respect to the texture features derived from the gray-level co-occurrence matrix and spectral information. Powers *et al.* (2015) used semivariogram features for object-based classification to map industrial disturbances in forest areas. Gil-Yepes *et al.* (2016) explored a set of temporal features derived from geostatistical functions for object-based land-use/land-cover change detection using high-resolution images. Silveira *et al.* (2017b) studied the semivariogram features to detect land cover changes resulting from a Brazilian dam failure using an object-based approach.

Focusing now on the algorithms used in this thesis, the Breaks For Additive Season and Trend (BFAST) recently emerged as a reliable automated algorithm for detecting vegetation disturbances across the tropics (DEVRIES *et al.*, 2015; DUTRIEUX *et al.*, 2015; SCHULTZ *et al.*, 2016b, 2018). BFAST was originally developed for detecting vegetation disturbances from a 16-day Moderate Resolution Imaging Spectroradiometer time series. It computes long-term trends and abrupt disturbances in a dense time series of a spectral index then produces sub-annual information on disturbances and trends (VERBESSELT *et al.*, 2010a). Later, BFAST Monitor emerged as a near-real-time means of identifying disturbances from a stable history period (VERBESSELT; ZEILEIS; HEROLD, 2012). Recent research has demonstrated the utility of BFAST algorithms and Landsat time series using different spectral indices over a variety of vegetation domains. For example, using Landsat time series and the normalized difference vegetation index, BFAST tracked small-scale disturbances in an Afromontane forest (DEVRIES *et al.*, 2015), and identified annual land cover disturbances and their effect on vegetation greenness in a coastal region (LI *et al.*, 2019). The algorithm was also useful for detecting burned areas in savanna regions, outperforming coarse-resolution burned area products (LIU *et al.*, 2018). Moisture-related spectral indices, such as the normalized difference moisture index, were also assessed for detecting and attributing causes of disturbances in the Colombian Andes (MURILLO-SANDOVAL *et al.*, 2018), and to identify forest degradation in mixed savanna and dry forest areas (SCHULTZ *et al.*, 2018). Positive trends in vegetation were

evaluated by quantifying vegetation regrowth using the soil-adjusted total vegetation index of abandoned well pads in semi-arid lands (WALLER *et al.*, 2018).

The Landsat-based detection of Trends in Disturbance and Recovery, or LandTrendr (KENNEDY; YANG; COHEN, 2010), uses a pixel-based segmentation method to investigate land trajectories by modeling time series and computing straight-line segments. Trajectory-based segments are further used for identifying forest disturbance events and capturing the associated information such as the year of event, duration, and magnitude of disturbance. Although first developed to detect disturbances in forest environments (KENNEDY *et al.*, 2012), LandTrendr has become popular for other vegetation analyses, such as disturbances in cropland patterns (ZHU *et al.*, 2019a), natural disturbances in mangrove areas (DE JONG *et al.*, 2021), and post-fire vegetation recovery (BRIGHT *et al.*, 2019). In forest disturbance studies, Cohen *et al.* (2018) used LandTrendr to map forest disturbances across the conterminous United States. Yang *et al.* (2018) assessed the capability of the LandTrendr algorithm and Landsat imagery in surface mining area to detect the vegetation disturbance and characterize the historical dynamics. In Bueno, Silveira, and Acerbi Júnior (2019), the accuracy of LandTrendr disturbance maps in different tropical seasonal biomes (savanna and Atlantic Forest) was analyzed. De Marzo *et al.* (2021) detected disturbances related to forest degradation across the entire Argentine Dry Chaco using LandTrendr and dense Landsat time series. Souza *et al.* (2020a) evaluated the dynamics of savanna clearings and land degradation using LandTrendr and different satellite products.

Another fast-growing trend in disturbance detection methodologies is the use of machine learning, especially deep learning algorithms, in the fields of geosciences (ZHU *et al.*, 2017). Deep learning refers to machine learning algorithms that construct hierarchical architectures of increasing sophistication, with features that would normally be problematic for traditional machine learning to extract (REICHSTEIN *et al.*, 2019). Applications to problems in land cover change are presented by Khan *et al.* (2017) detecting forest cover disturbances over a period of 29 years by filling incomplete data using deep neural networks, thus performing disturbance analysis at a finer temporal resolution and automatically improving the learning of disturbance features. Zhao and Du (2016) used a multiscale convolutional neural network to learn spatial-related deep features for hyperspectral remote imagery classification, generating a significant increase in classification accuracies. Zhang *et al.* (2016) used deep-architecture-based feature learning to detect disturbances in multi-resolution image-pairs although demonstrating the effectiveness and superiority of the method.

2.5.2 Accurate Datasets

There have been positive developments in the Landsat program over the past years (WULDER *et al.*, 2019). The most important advance to get accurate datasets was the free and open access to the Landsat archive, which has greatly benefited operational applications, scientific studies, and discoveries informed by analyses of large numbers of Landsat images (ZHU *et al.*, 2019b). For example, global mapping of annual forest disturbance has been achieved using all available Landsat observations from 2000 to 2012, reporting a net forest loss of 1.5 million km^2 (HANSEN *et al.*, 2013). Another important advance was the effort to deliver high-quality Landsat data, such as the establishment of an on-demand atmospherically collected surface reflectance product capability for all Landsat Thematic Mapper, Enhanced Thematic Mapper plus, and Operational Land Imager imagery (ROY *et al.*, 2014). In recognition of the need for improved usability and consistency among Landsat sensors, all data were reprocessed as Collection 1 with reprocessing finished May 2017 (DWYER *et al.*, 2018).

In 2014, the Global Forest Watch launched a web service that provides data for monitoring global forest disturbance over time. Worldwide maps of tree cover loss support the monitoring of more than 50 million hectares of forest (HANSEN *et al.*, 2013). The dataset is now widely used by researchers, conservationists, and local communities with more than 2 million users by 2018 (CURTIS *et al.*, 2018). For example, Jutras-Perreault, Gobakken, and Ørka (2021) evaluated Global Forest Watch and LandTrendr maps to infer forest cover disturbance in a boreal environment, while Zhang *et al.* (2020) evaluated the accuracy and suitability of the GFW dataset for analyzing China's forest cover. Other examples of worldwide maps are represented by Pekel *et al.* (2016) mapping global surface water, and Ying *et al.* (2017) mapping bare soils. Recently, another important dataset, MapBiomas, has become available that provides annual national-level land cover and land use maps for Brazil. MapBiomas, available from 1985 to 2020, classifies annual land cover and land uses using machine learning algorithms in multiple classes, such as forest formations, non-forest natural formations, farming, non-vegetated areas, and water (SOUZA *et al.*, 2020b).

2.5.3 Big Data Analysis

High-performance and cloud computing systems are becoming popular over the last years as well as large archives of remote sensing data have become freely available on global scales (MA *et al.*, 2015). Nowadays, the establishment of the Google Earth Engine platform provided many advances in disturbance detection studies, such as quick access of public geospatial data catalog, straightforward management of time series stacks, and agile

computation through parallel processing. These advances enable the creation of large-scale disturbance maps, and also a user-friendly format to run disturbance detection algorithms (GORELICK *et al.*, 2017), such as the implementation of the widely used disturbance detection algorithms (HAMUNYELA *et al.*, 2020; KENNEDY *et al.*, 2018), availability of forest disturbance maps (HANSEN *et al.*, 2013), and agile mapping in large areas (MIDEKISA *et al.*, 2017).

3 FINAL CONSIDERATIONS

Methods and algorithms to detect and monitor vegetation disturbances have been developed to exploit the Landsat data archive and to examine long-term vegetation trends; however, an optimal disturbance mapping technique does not yet exist since a single method might be not sensitive to the spatio-temporal heterogeneity of varied and continuous landscapes. In addition, more research is required to investigate the capabilities of different spectral indices and algorithms combined with new methodologies in mapping disturbances of seasonal biomes.

4 REFERENCES

ACERBI JÚNIOR, F. W. et al. Change Detection in Brazilian Savannas Using Semivariograms Derived from NDVI Images. **Ciência e Agrotecnologia**, v. 39, n. 2, p. 103–109, abr. 2015. DOI: 10.1590/S1413-70542015000200001.

ACHARD, F. et al. Determination of deforestation rates of the world's humid tropical forests. **Science**, v. 297, n. 5583, p. 999–1002, 9 ago. 2002. DOI: 10.1126/science.1070656.

ACHARD, F. et al. Determination of tropical deforestation rates and related carbon losses from 1990 to 2010. **Global Change Biology**, v. 20, n. 8, p. 2540–2554, 1 ago. 2014. DOI: 10.1111/gcb.12605.

BALAGUER, A. et al. Definition of a comprehensive set of texture semivariogram features and their evaluation for object-oriented image classification. **Computers & Geosciences**, v. 36, n. 2, p. 231–240, fev. 2010. DOI: 10.1016/j.cageo.2009.05.003.

BANSKOTA, A. et al. Forest Monitoring Using Landsat Time Series Data: A Review. **Canadian Journal of Remote Sensing**, v. 40, n. 5, p. 362–384, 3 set. 2014. DOI: 10.1080/07038992.2014.987376.

BARLOW, J. et al. Anthropogenic disturbance in tropical forests can double biodiversity loss from deforestation. **Nature**, v. 535, n. 7610, p. 144–147, 6 jul. 2016. DOI: 10.1038/nature18326.

BEUCHLE, R. et al. Land cover changes in the Brazilian Cerrado and Caatinga biomes from 1990 to 2010 based on a systematic remote sensing sampling approach. **Applied Geography**, v. 58, p. 116–127, mar. 2015. DOI: 10.1016/j.apgeog.2015.01.017.

BLASCHKE, T. Object based image analysis for remote sensing. **ISPRS Journal of Photogrammetry and Remote Sensing**, v. 65, n. 1, p. 2–16, jan. 2010. DOI: 10.1016/j.isprsjprs.2009.06.004.

BRIGHT, B. C. et al. Examining post-fire vegetation recovery with Landsat time series analysis in three western North American forest types. **Fire Ecology**, v. 15, n. 1, 1 dez. 2019. DOI: 10.1186/s42408-018-0021-9.

BROOKS, E. B. et al. On-the-Fly Massively Multitemporal Change Detection Using Statistical

Quality Control Charts and Landsat Data. **IEEE Transactions on Geoscience and Remote Sensing**, v. 52, n. 6, p. 3316–3332, jun. 2014. DOI: 10.1109/TGRS.2013.2272545.

BRUZZONE, L.; COSSU, R.; VERNAZZA, G. Detection of land-cover transitions by combining multidate classifiers. **Pattern Recognition Letters**, v. 25, n. 13, p. 1491–1500, 1 out. 2004. DOI: 10.1016/j.patrec.2004.06.002.

BUENO, I. T. et al. Object-Based Change Detection in the Cerrado Biome Using Landsat Time Series. **Remote Sensing**, v. 11, n. 5, p. 570, 8 mar. 2019. DOI: 10.3390/rs11050570.

BUENO, I. T.; SILVEIRA, E. M. O.; ACERBI JÚNIOR, F. W. Assessing forest change detection in tropical seasonal biomes through LandTrendr algorithm. *In* ANAIS DO XIX SIMPÓSIO BRASILEIRO DE SENSORIAMENTO REMOTO, 2019, Santos. **Anais eletrônicos...** São José dos Campos, INPE, 2019. Disponível em: https://proceedings.science/sbsr-2019/papers/assessing-forest-change-detection-in-tropical-seasonal-biomes-through-landtrendr-algorithm. Acesso em: 20 out. 2020.

CHEN, G. et al. Object-based change detection. **International Journal of Remote Sensing**, v. 33, n. 14, p. 4434–4457, 20 jul. 2012. DOI: 10.1080/01431161.2011.648285.

COHEN, W. B. et al. A LandTrendr multispectral ensemble for forest disturbance detection. **Remote Sensing of Environment**, v. 205, p. 131–140, 1 fev. 2018. DOI: 10.1016/J.RSE.2017.11.015.

COHEN, W. B. et al. Diversity of Algorithm and Spectral Band Inputs Improves Landsat Monitoring of Forest Disturbance. **Remote Sensing**, v. 12, n. 10, p. 1673, 23 maio 2020. DOI: 10.3390/rs12101673.

CONGALTON, R. G.; GREEN, K. **Assessing the accuracy of remotely sensed data: principles and practices**. 2. ed. Boca Raton: CRC Press, 2009.

COPPIN, P. et al. Digital change detection methods in ecosystem monitoring: a review. **International Journal of Remote Sensing**, v. 25, n. 9, p. 1565–1596, maio 2004. DOI: 10.1080/0143116031000101675.

CURTIS, P. G. et al. Classifying drivers of global forest loss. **Science**, v. 361, n. 6407, p. 1108–1111, 14 set. 2018. DOI: 10.1126/science.aau3445.

DE JONG, S. M. et al. Mapping mangrove dynamics and colonization patterns at the Suriname coast using historic satellite data and the LandTrendr algorithm. **International Journal of Applied Earth Observation and Geoinformation**, v. 97, p. 102293, 1 maio 2021. DOI: 10.1016/j.jag.2020.102293.

DE MARZO, T. et al. Characterizing forest disturbances across the Argentine Dry Chaco based on Landsat time series. **International Journal of Applied Earth Observation and Geoinformation**, v. 98, p. 102310, 1 jun. 2021. DOI: 10.1016/j.jag.2021.102310.

DESCLÉE, B.; BOGAERT, P.; DEFOURNY, P. Forest change detection by statistical object-based method. **Remote Sensing of Environment**, v. 102, n. 1–2, p. 1–11, maio 2006. DOI: 10.1016/j.rse.2006.01.013.

DEVRIES, B. et al. Robust monitoring of small-scale forest disturbances in a tropical montane forest using Landsat time series. **Remote Sensing of Environment**, v. 161, p. 107–121, maio 2015. DOI: 10.1016/j.rse.2015.02.012.

DUTRIEUX, L. P. et al. Monitoring forest cover loss using multiple data streams, a case study of a tropical dry forest in Bolivia. **ISPRS Journal of Photogrammetry and Remote Sensing**, v. 107, p. 112–125, set. 2015. DOI: 10.1016/j.isprsjprs.2015.03.015.

DWYER, J. L. et al. Analysis Ready Data: Enabling Analysis of the Landsat Archive. **Remote Sensing 2018, Vol. 10, Page 1363**, v. 10, n. 9, p. 1363, 28 ago. 2018. DOI: 10.3390/RS10091363.

EDWARDS, D. P. et al. Maintaining ecosystem function and services in logged tropical forests. **Trends in Ecology & Evolution**, v. 29, n. 9, p. 511–520, 1 set. 2014. DOI: 10.1016/J.TREE.2014.07.003.

FAO. **Global Forest Resources Assessment 2015. FAO Forestry Paper No. 1**. Rome: UN Food and Agriculture Organization, 2015.

FERREIRA, L. et al. Seasonal landscape and spectral vegetation index dynamics in the Brazilian Cerrado: An analysis within the Large-Scale Biosphere–Atmosphere Experiment in Amazônia (LBA). **Remote Sensing of Environment**, v. 87, n. 4, p. 534–550, 15 nov. 2003. DOI: 10.1016/j.rse.2002.09.003.

GÄRTNER, P.; FÖRSTER, M.; KLEINSCHMIT, B. The benefit of synthetically generated RapidEye and Landsat 8 data fusion time series for riparian forest disturbance monitoring. **Remote Sensing of Environment**, v. 177, p. 237–247, 1 maio 2016. DOI: 10.1016/J.RSE.2016.01.028.

GIL-YEPES, J. L. et al. Description and validation of a new set of object-based temporal geostatistical features for land-use/land-cover change detection. **ISPRS Journal of Photogrammetry and Remote Sensing**, v. 121, p. 77–91, nov. 2016. DOI: 10.1016/j.isprsjprs.2016.08.010.

GONG, P. et al. Finer resolution observation and monitoring of global land cover: first mapping results with Landsat TM and ETM+ data. **International Journal of Remote Sensing**, v. 34, n. 7, p. 2607–2654, 10 abr. 2013. DOI: 10.1080/01431161.2012.748992.

GORELICK, N. et al. Google Earth Engine: Planetary-scale geospatial analysis for everyone. **Remote Sensing of Environment**, v. 202, p. 18–27, dez. 2017. DOI: 10.1016/j.rse.2017.06.031.

HAMUNYELA, E. et al. Implementation of BFASTmonitor Algorithm on Google Earth Engine to support large-area and sub-annual change monitoring using earth observation data. **Remote Sensing**, v. 12, n. 18, p. 2953, 11 set. 2020. DOI: 10.3390/RS12182953.

HANSEN, M. C. et al. High-Resolution Global Maps of 21st-Century Forest Cover Change. **Science**, v. 342, n. 6160, p. 850–853, 15 nov. 2013. DOI: 10.1126/science.1244693.

HANSEN, M. C.; LOVELAND, T. R. A review of large area monitoring of land cover change using Landsat data. **Remote Sensing of Environment**, v. 122, p. 66–74, jul. 2012. DOI: 10.1016/j.rse.2011.08.024.

HANSEN, M. C.; STEHMAN, S. V.; POTAPOV, P. V. Quantification of global gross forest cover loss. **Proceedings of the National Academy of Sciences of the United States of America**, v. 107, n. 19, 11 maio 2010. DOI: 10.1073/pnas.0912668107.

HERMOSILLA, T. et al. Change Detection in Peri-urban Areas Based on Contextual Classification. **Photogrammetrie - Fernerkundung - Geoinformation**, v. 2012, n. 4, p. 359–370, 1 ago. 2012. DOI: 10.1127/1432-8364/2012/0123.

HUSSAIN, M. et al. Change detection from remotely sensed images: From pixel-based to object-based approaches. **ISPRS Journal of Photogrammetry and Remote Sensing**, v. 80, p. 91–106, jun. 2013. DOI: 10.1016/j.isprsjprs.2013.03.006.

JUTRAS-PERREAULT, M.-C.; GOBAKKEN, T.; ØRKA, H. O. Comparison of two algorithms for estimating stand-level changes and change indicators in a boreal forest in Norway. **International Journal of Applied Earth Observation and Geoinformation**, v. 98, p. 102316, 1 jun. 2021. DOI: 10.1016/J.JAG.2021.102316.

KALAMANDEEN, M. et al. Pervasive Rise of Small-scale Deforestation in Amazonia. **Scientific Reports**, v. 8, n. 1, p. 1600, 25 dez. 2018. DOI: 10.1038/s41598-018-19358-2.

KEENAN, R. J. et al. Dynamics of global forest area: Results from the FAO Global Forest Resources Assessment 2015. **Forest Ecology and Management**, v. 352, p. 9–20, 7 set. 2015. DOI: 10.1016/J.FORECO.2015.06.014.

KENNEDY, R. et al. Implementation of the LandTrendr Algorithm on Google Earth Engine. **Remote Sensing**, v. 10, n. 5, p. 691, 1 maio 2018. DOI: 10.3390/rs10050691.

KENNEDY, R. E. et al. Spatial and temporal patterns of forest disturbance and regrowth within the area of the Northwest Forest Plan. **Remote Sensing of Environment**, v. 122, p. 117–133, 1 jul. 2012. DOI: 10.1016/j.rse.2011.09.024.

KENNEDY, R. E.; YANG, Z.; COHEN, W. B. Detecting trends in forest disturbance and recovery using yearly Landsat time series: 1. LandTrendr — Temporal segmentation algorithms. **Remote Sensing of Environment**, v. 114, n. 12, p. 2897–2910, 15 dez. 2010. DOI: 10.1016/j.rse.2010.07.008.

KHAN, S. H. et al. Forest Change Detection in Incomplete Satellite Images With Deep Neural Networks. **IEEE Transactions on Geoscience and Remote Sensing**, v. 55, n. 9, p. 5407–5423, set. 2017. DOI: 10.1109/TGRS.2017.2707528.

LAWRENCE, D.; VANDECAR, K. Effects of tropical deforestation on climate and agriculture. **Nature Climate Change**, v. 5, n. 1, p. 27–36, 18 jan. 2015. DOI: 10.1038/nclimate2430.

LEWIS, S. L.; EDWARDS, D. P.; GALBRAITH, D. Increasing human dominance of tropical

forests. **Science**, v. 349, n. 6250, p. 827–832, 21 ago. 2015. DOI: 10.1126/science.aaa9932.

LI, D. et al. Quantifying annual land-cover change and vegetation greenness variation in a coastal ecosystem using dense time-series Landsat data. **GIScience and Remote Sensing**, v. 56, n. 5, p. 769–793, 4 jul. 2019. DOI: 10.1080/15481603.2019.1565104.

LIU, J. et al. Burned area detection based on Landsat time series in savannas of southern Burkina Faso. **International Journal of Applied Earth Observation and Geoinformation**, v. 64, p. 210–220, 1 fev. 2018. DOI: 10.1016/j.jag.2017.09.011.

LU, D. et al. Change detection techniques. **International Journal of Remote Sensing**, v. 25, n. 12, p. 2365–2401, 20 jun. 2004. DOI: 10.1080/0143116031000139863.

LU, M. et al. Land cover change detection by integrating object-based data blending model of Landsat and MODIS. **Remote Sensing of Environment**, v. 184, p. 374–386, out. 2016. DOI: 10.1016/j.rse.2016.07.028.

MA, Y. et al. Remote sensing big data computing: Challenges and opportunities. **Future Generation Computer Systems**, v. 51, p. 47–60, 1 out. 2015. DOI: 10.1016/j.future.2014.10.029.

MARX, A.; TETTEH, G. O. A Forest Vitality and Change Monitoring Tool Based on RapidEye Imagery. **IEEE Geoscience and Remote Sensing Letters**, v. 14, n. 6, p. 801–805, jun. 2017. DOI: 10.1109/LGRS.2017.2675164.

MAYAUX, P. et al. Tropical forest cover change in the 1990s and options for future monitoring. **Philosophical Transactions of the Royal Society B: Biological Sciences**, v. 360, n. 1454, p. 373–384, 28 fev. 2005. DOI: 10.1098/rstb.2004.1590.

MIDEKISA, A. et al. Mapping land cover change over continental Africa using Landsat and Google Earth Engine cloud computing. **PLOS ONE**, v. 12, n. 9, p. e0184926, 27 set. 2017. DOI: 10.1371/journal.pone.0184926.

MIRANDA, P. L. S. et al. Using tree species inventories to map biomes and assess their climatic overlaps in lowland tropical South America. **Global Ecology and Biogeography**, v. 27, n. 8, p. 899–912, ago. 2018. DOI: 10.1111/geb.12749.

MITCHARD, E. T. A. The tropical forest carbon cycle and climate change. **Nature**, v. 559, n.

7715, p. 527–534, 25 jul. 2018. DOI: 10.1038/s41586-018-0300-2.

MURILLO-SANDOVAL, P. et al. Detecting and Attributing Drivers of Forest Disturbance in the Colombian Andes Using Landsat Time-Series. **Forests**, v. 9, n. 5, p. 269, 15 maio 2018. DOI: 10.3390/f9050269.

MYERS, N. et al. Biodiversity hotspots for conservation priorities. **Nature**, v. 403, n. 6772, p. 853–858, 24 fev. 2000. DOI: 10.1038/35002501.

OLOFSSON, P. et al. Good practices for estimating area and assessing accuracy of land change. **Remote Sensing of Environment**, v. 148, n. October, p. 42–57, maio 2014. DOI: 10.1016/j.rse.2014.02.015.

OZA, N. C.; TUMER, K. Classifier ensembles: Select real-world applications. **Information Fusion**, v. 9, n. 1, p. 4–20, jan. 2008. DOI: 10.1016/j.inffus.2007.07.002.

PAN, Y. et al. A large and persistent carbon sink in the world's forests. **Science (New York, N.Y.)**, v. 333, n. 6045, p. 988–93, 19 ago. 2011. DOI: 10.1126/science.1201609.

PEKEL, J. F. et al. High-resolution mapping of global surface water and its long-term changes. **Nature**, v. 540, n. 7633, p. 418–422, 15 dez. 2016. DOI: 10.1038/nature20584.

PICKELL, P. D. et al. Monitoring anthropogenic disturbance trends in an industrialized boreal forest with Landsat time series. **Remote Sensing Letters**, v. 5, n. 9, p. 783–792, 2 set. 2014. DOI: 10.1080/2150704X.2014.967881.

POTAPOV, P. V. et al. Eastern Europe's forest cover dynamics from 1985 to 2012 quantified from the full Landsat archive. **Remote Sensing of Environment**, v. 159, p. 28–43, 15 mar. 2015. DOI: 10.1016/J.RSE.2014.11.027.

POWERS, R. P. et al. Remote sensing and object-based techniques for mapping fine-scale industrial disturbances. **International Journal of Applied Earth Observation and Geoinformation**, v. 34, n. 1, p. 51–57, 1 fev. 2015. DOI: 10.1016/J.JAG.2014.06.015.

PRĂVĂLIE, R. Drylands extent and environmental issues. A global approach. **Earth-Science Reviews**, v. 161, p. 259–278, out. 2016. DOI: 10.1016/j.earscirev.2016.08.003.

PRĂVĂLIE, R. Major perturbations in the Earth's forest ecosystems. Possible implications for

global warming. **Earth-Science Reviews**, v. 185, p. 544–571, out. 2018. DOI: 10.1016/j.earscirev.2018.06.010.

REICHSTEIN, M. et al. Deep learning and process understanding for data-driven Earth system science. **Nature**, v. 566, p. 195–204, 2019. DOI: 10.1016/j.earscirev.2018.06.010.

RIBEIRO, M. C. et al. The Brazilian Atlantic Forest: How much is left, and how is the remaining forest distributed? Implications for conservation. **Biological Conservation**, v. 142, n. 6, p. 1141–1153, jun. 2009. DOI: 10.1016/j.biocon.2009.02.021.

RODRIGUEZ-GALIANO, V. F. et al. An assessment of the effectiveness of a random forest classifier for land-cover classification. **ISPRS Journal of Photogrammetry and Remote Sensing**, v. 67, n. 1, p. 93–104, 1 jan. 2012. DOI: 10.1016/j.isprsjprs.2011.11.002.

ROY, D. P. et al. Landsat-8: Science and product vision for terrestrial global change research. **Remote Sensing of Environment**, v. 145, p. 154–172, 5 abr. 2014. DOI: 10.1016/j.rse.2014.02.001.

SCHOWENGERDT, R. A. **Remote sensing: models and methods for image processing**. 3. ed. Cambridge: Academic Press, 2007.

SCHULTZ, M. et al. Error Sources in Deforestation Detection Using BFAST Monitor on Landsat Time Series Across Three Tropical Sites. **IEEE Journal of Selected Topics in Applied Earth Observations and Remote Sensing**, v. 9, n. 8, p. 3667–3679, 1 ago. 2016a. DOI: 10.1109/JSTARS.2015.2477473.

SCHULTZ, M. et al. Performance of vegetation indices from Landsat time series in deforestation monitoring. **International Journal of Applied Earth Observation and Geoinformation**, v. 52, p. 318–327, out. 2016b. DOI: 10.1016/j.jag.2016.06.020.

SCHULTZ, M. et al. Forest Cover and Vegetation Degradation Detection in the Kavango Zambezi Transfrontier Conservation Area Using BFAST Monitor. **Remote Sensing**, v. 10, n. 11, p. 1850, 21 nov. 2018. DOI: 10.3390/rs10111850.

SHIMIZU, K. et al. A comprehensive evaluation of disturbance agent classification approaches: Strengths of ensemble classification, multiple indices, spatio-temporal variables, and direct prediction. **ISPRS Journal of Photogrammetry and Remote Sensing**, v. 158, p. 99–112, dez.

2019. DOI: 10.1016/j.isprsjprs.2019.10.004.

SILVEIRA, E. M. O. et al. Object-based change detection using semivariogram indices derived from NDVI images: The environmental disaster in Mariana, Brazil. **Ciência e Agrotecnologia**, v. 41, n. 5, p. 554–564, set. 2017. DOI: 10.1590/1413-70542017415009817.

SILVEIRA, E. M. O. et al. Object-based land-cover change detection applied to Brazilian seasonal savannahs using geostatistical features. **International Journal of Remote Sensing**, v. 39, n. 8, p. 2597–2619, 18 abr. 2018a. DOI: 10.1080/01431161.2018.1430397.

SILVEIRA, E. M. O. et al. Reducing the effects of vegetation phenology on change detection in tropical seasonal biomes. **GIScience and Remote Sensing**, v. 56, n. 5, p. 699–717, 4 jul. 2019. DOI: 10.1080/15481603.2018.1550245.

SILVEIRA, E. M. O. et al. Using spatial features to reduce the impact of seasonality for detecting tropical forest changes from landsat time series. **Remote Sensing**, v. 10, n. 6, p. 808, 23 maio 2018b. DOI: 10.3390/rs10060808.

SOUZA, A. A. et al. Dynamics of savanna clearing and land degradation in the newest agricultural frontier in Brazil. **GIScience and Remote Sensing**, v. 57, n. 7, p. 965–984, 2 out. 2020a. DOI: 10.1080/15481603.2020.1835080.

SOUZA, C. M. et al. Reconstructing Three Decades of Land Use and Land Cover Changes in Brazilian Biomes with Landsat Archive and Earth Engine. **Remote Sensing 2020, Vol. 12, Page 2735**, v. 12, n. 17, p. 2735, 25 ago. 2020b. DOI: 10.3390/RS12172735.

TEWKESBURY, A. P. et al. A critical synthesis of remotely sensed optical image change detection techniques. **Remote Sensing of Environment**, v. 160, p. 1–14, abr. 2015. DOI: 10.1016/j.rse.2015.01.006.

TOVO, A. et al. Upscaling species richness and abundances in tropical forests. **Science Advances**, v. 3, n. 10, p. e1701438, 1 out. 2017. DOI: 10.1126/sciadv.1701438.

TRANCOSO, R.; SANO, E. E.; MENESES, P. R. The spectral changes of deforestation in the Brazilian tropical savanna. **Environmental Monitoring and Assessment**, v. 187, n. 1, p. 4145, 4 jan. 2015. DOI: 10.1007/s10661-014-4145-3.

TRUMBORE, S.; BRANDO, P.; HARTMANN, H. Forest health and global change. **Science**,

v. 349, n. 6250, p. 814–818, 21 ago. 2015. DOI: 10.1126/science.aac6759.

VAN DER WERF, G. R. et al. CO2 emissions from forest loss. **Nature Geoscience**, v. 2, n. 11, p. 737–738, nov. 2009. DOI: 10.1038/ngeo671.

VERBESSELT, J. et al. Detecting trend and seasonal changes in satellite image time series. **Remote Sensing of Environment**, v. 114, n. 1, p. 106–115, jan. 2010. DOI: 10.1016/j.rse.2009.08.014.

VERBESSELT, J.; ZEILEIS, A.; HEROLD, M. Near real-time disturbance detection using satellite image time series. **Remote Sensing of Environment**, v. 123, p. 98–108, ago. 2012. DOI: 10.1016/j.rse.2012.02.022.

VIEIRA, M. A. et al. Object Based Image Analysis and Data Mining applied to a remotely sensed Landsat time-series to map sugarcane over large areas. **Remote Sensing of Environment**, v. 123, p. 553–562, ago. 2012. DOI: 10.1016/j.rse.2012.04.011.

WALLER, E. K. et al. Landsat time series analysis of fractional plant cover changes on abandoned energy development sites. **International Journal of Applied Earth Observation and Geoinformation**, v. 73, p. 407–419, 1 dez. 2018. DOI: 10.1016/j.jag.2018.07.008.

WHITE, J. C. et al. Characterizing temperate forest structural and spectral diversity with Hyperion EO-1 data. **Remote Sensing of Environment**, v. 114, n. 7, p. 1576–1589, 15 jul. 2010. DOI: 10.1016/J.RSE.2010.02.012.

WULDER, M. A. et al. Opening the archive: How free data has enabled the science and monitoring promise of Landsat. **Remote Sensing of Environment**, v. 122, p. 2–10, jul. 2012. DOI: 10.1016/j.rse.2012.01.010.

WULDER, M. A. et al. Current status of Landsat program, science, and applications. **Remote Sensing of Environment**, v. 225, p. 127–147, 1 maio 2019. DOI: 10.1016/j.rse.2019.02.015.

YANG, Y. et al. Detecting the dynamics of vegetation disturbance and recovery in surface mining area via Landsat imagery and LandTrendr algorithm. **Journal of Cleaner Production**, v. 178, p. 353–362, 20 mar. 2018. DOI: 10.1016/j.jclepro.2018.01.050.

YING, Q. et al. Global bare ground gain from 2000 to 2012 using Landsat imagery. **Remote Sensing of Environment**, v. 194, p. 161–176, 1 jun. 2017. DOI: 10.1016/J.RSE.2017.03.022.

ZHANG, D. et al. Accuracy assessment of the global forest watch tree cover 2000 in China. **International Journal of Applied Earth Observation and Geoinformation**, v. 87, p. 102033, 1 maio 2020. DOI: 10.1016/J.RSE.2017.03.022.

ZHANG, P. et al. Change detection based on deep feature representation and mapping transformation for multi-spatial-resolution remote sensing images. **ISPRS Journal of Photogrammetry and Remote Sensing**, v. 116, p. 24–41, 1 jun. 2016. DOI: 10.1007/S12145-019-00380-5.

ZHAO, W.; DU, S. Learning multiscale and deep representations for classifying remotely sensed imagery. **ISPRS Journal of Photogrammetry and Remote Sensing**, v. 113, p. 155–165, 1 mar. 2016. DOI: 10.1016/J.ISPRSJPRS.2016.01.004.

ZHU, L. et al. Long-Term Monitoring of Cropland Change near Dongting Lake, China, Using the LandTrendr Algorithm with Landsat Imagery. **Remote Sensing**, v. 11, n. 10, p. 1234, 24 maio 2019a. DOI: 10.3390/rs11101234.

ZHU, X. X. et al. Deep Learning in Remote Sensing: A Comprehensive Review and List of Resources. **IEEE Geoscience and Remote Sensing Magazine**, v. 5, n. 4, p. 8–36, dez. 2017. DOI: 10.1109/MGRS.2017.2762307.

ZHU, Z. Change detection using landsat time series: A review of frequencies, preprocessing, algorithms, and applications. **ISPRS Journal of Photogrammetry and Remote Sensing**, v. 130, p. 370–384, ago. 2017. DOI: 10.1016/j.isprsjprs.2017.06.013.

ZHU, Z. et al. Benefits of the free and open Landsat data policy. **Remote Sensing of Environment**, v. 224, p. 382–385, 1 abr. 2019b. DOI: 10.1016/j.rse.2019.02.016.

ZHU, Z.; WOODCOCK, C. E. Automated cloud, cloud shadow, and snow detection in multitemporal Landsat data: An algorithm designed specifically for monitoring land cover change. **Remote Sensing of Environment**, v. 152, p. 217–234, set. 2014. DOI: 10.1016/j.rse.2014.06.012.

SECOND PART – ARTICLES

ARTICLE 1 – SPATIAL AGREEMENT AMONG VEGETATION DISTURBANCE MAPS IN TROPICAL DOMAINS USING LANDSAT TIME SERIES

Inacio Thomaz Bueno [1], Greg McDermid [2], Eduarda Martiniano de Oliveira Silveira [3,*], Jennifer Hird [2], Breno Izidoro Domingos [1], Fausto Weimar Acerbi Júnior [1].

[1] *Department of Forest Science, Federal University of Lavras, Lavras 37200-000, Brazil;*
[2] *Department of Geography, University of Calgary, Calgary T2N 1N4, Canada;*
[3] *SILVIS Lab, Department of Forest and Wildlife Ecology, University of Wisconsin-Madison, Madison WI 53706, USA.*

***** Corresponding author email: esilveira@wisc.edu

Publication status: Published in **Remote Sensing**

DOI: 10.3390/rs12182948

Abstract: Detecting disturbances in native vegetation is a crucial component of many environmental management strategies, and remote sensing-based methods are the most efficient way to collect multi-temporal disturbance data over large areas. Given that there is a large range of datasets for monitoring, analyzing, and detecting disturbances, many methods have been well-studied and successfully implemented. However, factors such as the vegetation type, input data, and change detection method can significantly alter the outcomes of a disturbance-detection study. We evaluated the spatial agreement of disturbance maps provided by the Breaks For Additive Season and Trend (BFAST) algorithm, evaluating seven spectral indices in three distinct vegetation domains in Brazil: Atlantic forest, savanna, and semi-arid woodland, by assessing levels of agreement between the outputs. We computed individual map accuracies based on a reference dataset, then ranked their performance, while also observing their relationships with specific vegetation domains. Our results indicated a low rate of spatial agreement among index-based disturbance maps, which itself was minimally influenced by vegetation domain. Wetness indices produced greater detection accuracies in comparison to greenness-related indices free of saturation. The normalized difference moisture index performed best in the Atlantic forest domains, yet performed poorest in semi-arid woodland, reflecting its specific sensitivity to vegetation and its water content. The normalized difference vegetation index led to high disturbance detection accuracies in the savanna and semi-arid woodland domains. This study offered novel insight into vegetation disturbance maps, their relationship to different ecosystem types, and corresponding accuracies. Distinct input data can produce non-spatially correlated disturbance maps and reflect site-specific sensitivity. Future research should explore algorithm limitations presented in this study, as well as the expansion to other techniques and vegetation domains across the globe.

Keywords: change detection; BFAST; spectral indices; remote sensing; deforestation

1 INTRODUCTION

Anthropogenic disturbances in tropical environments (i.e., selective logging and wildfires) are considered one of the major drivers of biodiversity loss (BARLOW et al., 2016) and the second largest source of anthropogenic greenhouse gas emissions (VAN DER WERF et al., 2009). In the 1990–2010 period, global net losses of tropical forests averaged 6 million hectares per year (approximately 0.38% annually) (ACHARD et al., 2014). Such disturbance rates have received worldwide attention as tropical vegetation domains play such a key role in

global systems. Overall, they store 200–300 Pg. C (10^{15} grams of carbon) (PAN et al., 2011), account for about 60% of the world's terrestrial photosynthesis (MITCHARD, 2018), provide habitats for more than half of the known species worldwide (TOVO et al., 2017), and are a major regulator of global climate (LAWRENCE; VANDECAR, 2015).

Mapping disturbances in tropical domains plays a pivotal role in many environmental management strategies, and remote sensing data are the only feasible way to detect and monitor these disturbances over large areas. However, this is not a trivial task, as disturbance detection is subject to a variety of noise factors including natural forest phenology, cloud cover, atmospheric scattering, and geometric errors (SCHULTZ et al., 2016a). As a result, we require an understanding of the sensitivity and generalizability of disturbance detection methods across a variety of different vegetation types (GROGAN et al., 2016).

The opening of the Landsat archive in 2008 boosted the application of vegetation disturbance detection from satellites. Free global mid-resolution (30 m) remote sensing imagery has enabled more accurate area estimation analysis, characterization of disturbance types, and monitoring post-disturbance conditions (WULDER et al., 2019). In addition, these new capabilities have been leveraged through the development of new time-series techniques for detecting and tracking disturbances (ZHU, 2017). For example, the Breaks For Additive Season and Trend (BFAST) recently emerged as a reliable automated algorithm for detecting vegetation disturbances across the tropics (DEVRIES et al., 2015; DUTRIEUX et al., 2015; SCHULTZ et al., 2016b, 2018). BFAST was originally developed for detecting vegetation disturbances from a 16 day Moderate Resolution Imaging Spectroradiometer (MODIS) time series. It computes long-term trends and abrupt disturbances in a dense time series of a spectral index, then produces sub-annual information on disturbances and trends (VERBESSELT et al., 2010a). Later, BFAST Monitor emerged as a near-real time means of identifying disturbances from a stable history period (VERBESSELT; ZEILEIS; HEROLD, 2012).

Recent research has demonstrated the utility of BFAST algorithms and Landsat time series using different spectral indices over a variety of vegetation domains. For example, using Landsat time series and the normalized difference vegetation index (NDVI), BFAST tracked small-scale disturbances in an Afromontane forest (DEVRIES et al., 2015), and identified annual land cover disturbances and their effect on vegetation greenness in a coastal region (LI et al., 2019). The algorithm was also useful for detecting burned areas in savanna regions, outperforming coarse-resolution burned area products (LIU et al., 2018). Moisture-related spectral indices, such as the normalized difference moisture index (NDMI), were also assessed for detecting and attributing causes of disturbances in the Colombian Andes (MURILLO-

SANDOVAL et al., 2018), and to identify forest degradation in mixed savanna and dry forest areas (SCHULTZ et al., 2018). Positive trends in vegetation were evaluated by quantifying vegetation regrowth using the soil-adjusted total vegetation index (SATVI) of abandoned well pads in semi-arid lands (WALLER et al., 2018).

Different spectral indices can return disparate accuracies when mapping disturbances in tropical forests using BFAST. In tropical dry forests, moisture-related indices achieved better spatial accuracies when compared to greenness-related indices (SMITH et al., 2019). Similar results were found in evergreen forests over the globe, although the canopy-related normalized difference fraction index (NDFI) outperformed moisture-related indices in this instance (SCHULTZ et al., 2016b). Another important element in disturbance detection studies is locational or regional variability, which can influence forest disturbance patterns. Disturbance detection methods over large areas usually opt for generalized vegetation types. A common strategy is to apply a predefined threshold for identifying forested areas and then detecting disturbed pixels when there are significant deviations from the threshold (ACHARD et al., 2014; HANSEN et al., 2013). However, disturbance dynamics can differ across forest types, leading to misclassifications in large-scale analysis (CURTIS et al., 2018). Using BFAST, Schultz et al. (2016) observed different levels of edge effects in different sites while detecting forest disturbances. This led the authors to suggest that local forest disturbance patterns must be understood and algorithms must be tuned to account for regional conditions. Furthermore, Grogan et al. (2016), while observing their error distribution over forest types, found a site-specific sensitivity to error imbalances when using a generalized forest model, i.e., they noted disturbance underestimation in evergreen forests and overestimation in dry forests.

Research into Landsat spectral indices is comprehensive and the BFAST algorithms have received attention in tropical forests. However, no study has examined the algorithm's performance across distinct vegetation domains while also investigating similarities between vegetation disturbance maps derived from different spectral indices. In addition, most recent disturbance detection studies frequently relate to forested areas, while non-forested areas, such as scrublands in savannas or open grasslands in semi-arid lands, are still not yet fully understood.

In this paper, we compare the suitability of several spectral indices for mapping disturbances in different tropical vegetation domains using the BFAST Monitor algorithm. This study addressed the following questions: (1) How do vegetation disturbance maps derived from Landsat-based spectral indices spatially agree? (2) How accurate are these vegetation disturbance maps when compared to a reference dataset? (3) How does the vegetation domain

influence these agreements? Thus, our objectives were: (1) To evaluate the spatial agreement between disturbance maps produced using seven spectral indices derived from Landsat Thematic Mapper/Operational Land Imager (TM/OLI) and input into BFAST Monitor, and the influence of vegetation domain on this agreement; and (2) to evaluate the accuracies of these index-derived disturbance maps and their relationship with vegetation domain. To accomplish these objectives, we used a dense Landsat time series from 2003 to 2017 and calculated seven distinct spectral indices to detect disturbed pixels through the BFAST Monitor algorithm. We evaluated the disturbance maps' accuracies and spatial similarity in three distinct vegetation domains in southeast Brazil: Atlantic forest, savanna, and semi-arid woodland.

2 MATERIAL AND METHODS

2.1 Study Sites

The study area comprises three Worldwide Reference System grid (WRS-2) scenes dispersed across the Minas Gerais state of southeastern Brazil (Figure 1). These regions represent three distinct Brazilian vegetation domains: Atlantic forest (Path/Row: 218/75), savanna (Path/Row: 220/72), and semi-arid woodland (Path/Row: 218/70).

The Atlantic forest is composed of different types of vegetation, mostly including rainforests, semi-deciduous forests, as well as high-altitude grasslands. This vegetation domain has outstanding levels of species endemism, making the Atlantic forest a biodiversity hotspot (MYERS et al., 2000). In the past, it was subjected to substantial disturbance activity and was reduced to approximately 14% of its original vegetation (RIBEIRO et al., 2009), becoming one of most vulnerable hotspots to global change (BELLARD et al., 2014). The greatest extent of the Atlantic forest scene is located in the south of the Minas Gerais state, extending over the states of São Paulo and Rio de Janeiro. The region is represented by a mix of plains in the northwest, and the Serra da Mantiqueira mountain complex in the southeast of the scene. This region receives around 2000 mm annual rainfall with lower values into the continent and higher values found at montane areas. Most of the area does not show a climatological water deficit, leading to a low seasonal signal (MIRANDA et al., 2018).

In Brazil, the savanna vegetation domain is represented by the Cerrado biome, which has a unique vertically structured mosaic of plant formations among the savannas in the world (FERREIRA et al., 2003). It ranges from forest formations with dense canopy cover to grasslands with sparse and short twisted trees, also being considered a biodiversity hotspot (MYERS et al., 2000). The savanna scene is located in western MG crossing to Goiás state,

where approximately 90% of the rains are concentrated from October to April with annual precipitation ranging from 1200 to 1800 mm. The dry season is quite distinct with monthly precipitation reaching zero millimeters, inducing a wide range of adaptive phenological strategies in vegetation formations in order to overcome water scarcity. The Brazilian savanna has been under increasing anthropic pressure due to policy-driven land conversion processes, as indicated by ~266,000 km^2 of gross forest loss in the past twenty years (BEUCHLE et al., 2015).

Semi-arid woodland, also known as the Caatinga biome, is an ecosystem occupied by a mixture of deciduous forests and herbaceous understory. The scene occupies a northeastern portion of MG being mostly concentrated in Bahia state, with an extensive area of the Espinhaço mountain range. It receives less than 750 millimeters per year of extremely irregular rainfall, where more than 75% of the total annual rainfall can occur within three months. In addition, annual variations in semi-arid woodland are large where droughts can last for a couple of years. As the Brazilian savanna, these dry forests have been either converted from their native vegetation or modified in a major way, represented by ~90,000 km^2 of forest loss with an increase from 0.19% yr^{-1} to 0.44% yr^{-1} in the past decades (BEUCHLE et al., 2015).

Figure 1 – The study scenes location and monthly precipitation information for Atlantic forest (AF), savanna (SAV), and semi-arid woodland (SAW) vegetation domains. Both Landsat views in wet and dry season are represented by a false color composition (Red = NIR, Green = shortwave infrared (SWIR), Blue = Red).

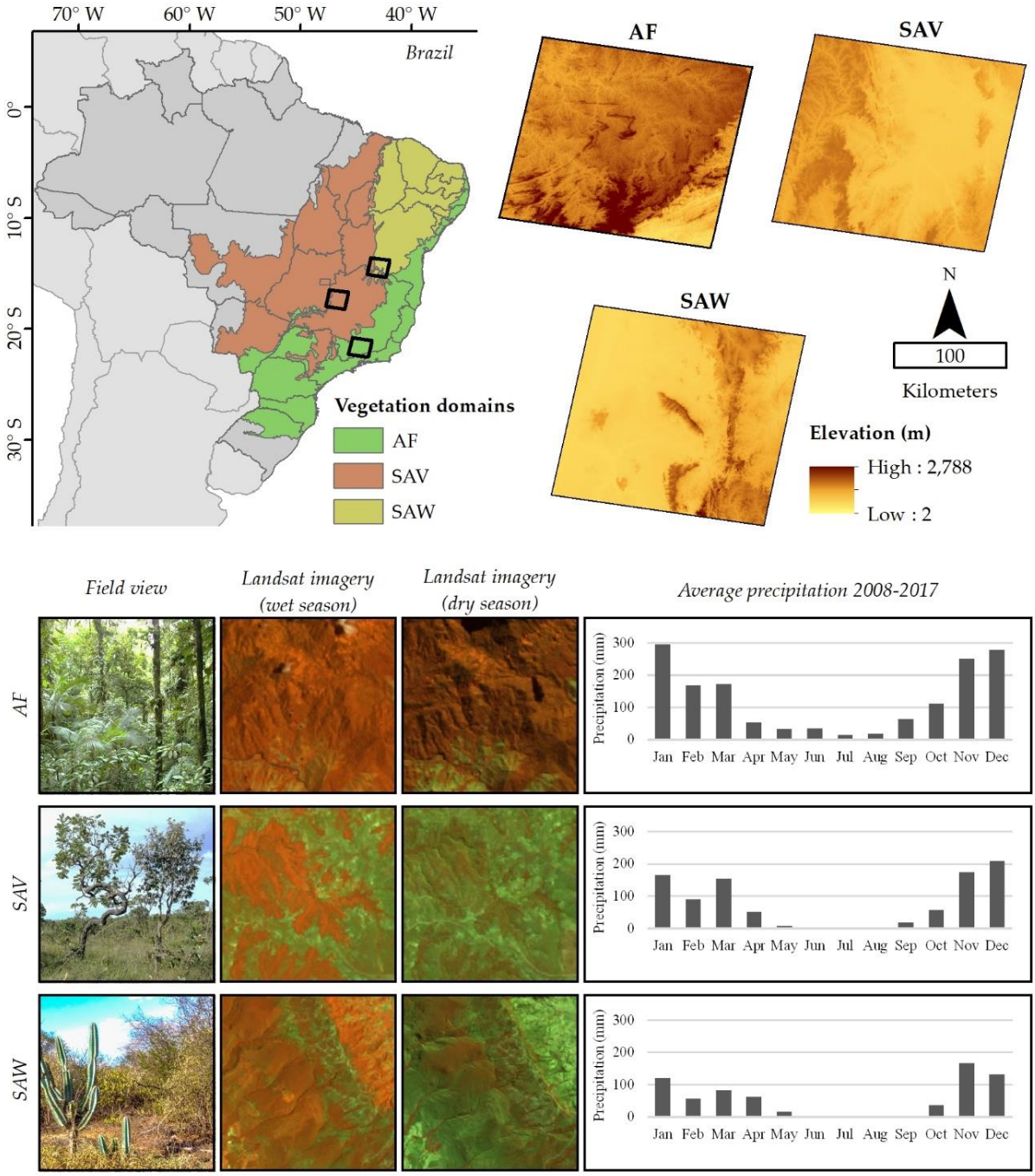

Source: Author (2022).

2.2 Pre-Processing

As our study evaluates disturbances based on a time series modeling algorithm, a non-native vegetation mask is important to limit the procedure to pixels that are established as

vegetation at the beginning of the study period. This avoided unnecessary computation time and further uncertainties. For this reason, we used the land use/land cover map of the Brazil's Rural Environmental Registry (CAR, Cadastro Ambiental Rural in Portuguese) as a vegetation mask. The land use/land cover map used 5 m Rapideye and 30 m Landsat TM imagery to produce a valuable high-resolution large-scale product. This is used as input for land-use, environmental, economic, and territorial policies. CAR's vegetation class comprises forested areas as well as non-forest native vegetation, i.e., lowland and montane grasslands, shrub lands, scrublands, and wetlands. We additionally masked temporary water bodies that were not accounted for by CAR's layer using the Global Surface Water information (PEKEL et al., 2016), which contains Landsat-based annual maps of the location and temporal distribution of surface water from 1984 to 2018. Temporary surface water is commonly located in the savanna and semi-arid woodland domains represented by veredas and wet grasslands, respectively (JUNK et al., 2014). They are composed of temporary ponds or streams where water content may range from water-logged soil to water bodies several meters deep. This natural decrease and increase in water levels based on a dry period of varying duration can be a source of noise in vegetation disturbance analysis.

2.3 Landsat-Derived Spectral Indices

We acquired Landsat TM/OLI-derived spectral index products provided by the U.S. Geological Survey's Earth Resources Observation and Science Center (USGS EROS) (USGS, 2020) from 2003 to 2017 across the three WRS-2 tiles covering the study region. Thematic Mapper (TM) and Operational Land Imager (OLI) products were converted to surface reflectance using the Landsat Ecosystem Disturbance Adaptive Process (LEDAPS) (MASEK et al., 2006) and Land Surface Reflectance Code (LaSRC) (VERMOTE et al., 2016), respectively. We selected all images available with less than 50% of cloud cover using the Function of Mask (Fmask) algorithm (ZHU; WOODCOCK, 2012) to generate cloud-free observations.

A set of seven commonly used indices were downloaded from the USGS EROS website, which saved us from performing data preprocessing steps such as geometric and radiometric calibration, and band math calculations. These indices can be grouped into two broad categories based on their calculations using similar spectral wavelengths, and their resultant response to land surface vegetation. The first group employs a combination of red (Red, TM/OLI (0.630–0.690 µm)) and near-infrared (NIR, TM (0.760–0.900 µm), OLI (0.845–0.885 µm)), and respond to actively photosynthesizing biomass. We label these 'greenness indices.' They

include and are built around the NDVI, the most frequently used index in remote sensing science, that was selected due to its use to quantify vegetation greenness (TUCKER, 1979). It is calculated as a normalized ratio between Red and NIR reflectance values (Equation 1). Higher NDVI values suggest higher amounts of photosynthetic active biomass. As the most popular index, NDVI time series have been used in many forest disturbance detection and monitoring efforts (GAO et al., 2019; WU et al., 2020).

$$NDVI = \frac{NIR - RED}{NIR + RED} \quad (1)$$

We include three more greenness indices in this group, all of which are variations of the NDVI and which are designed to reduce saturation issues identified with this index—the enhanced vegetation index (EVI), the soil-adjusted vegetation index (SAVI), and the modified soil-adjusted vegetation index (MSAVI). The EVI, developed by Huete et al. (1999), was selected due its usefulness in regions with dense vegetation as it does not saturate as quickly as other vegetation indices. It incorporates the blue band (Blue, TM/OLI (0.450–0.520 μm)), which is atmosphere-sensitive and used to correct aerosol influences in the red band, canopy background adjustment L = 1.0, adjustable coefficients of atmospheric resistance C1 = 6 and C2 = 7.5, and the sensor's gain factor G = 2.5 (Equation 2). As an improvement to NDVI regarding saturation issues in highly dense vegetation, EVI also has frequent use in tropical forest disturbance detection (GRINGS; ROITBERG; BARRAZA, 2020).

$$EVI = G \times \left(\frac{NIR - RED}{NIR + C1 \times RED - C2 \times BLUE + L}\right) \quad (2)$$

In contrast to EVI, SAVI corrects NDVI by reducing the influence of soil brightness in areas with sparse vegetation (HUETE, 1988). It has a soil brightness correction factor L = 0.5 (Equation 3), which can be sensitive to deforestation with incomplete forest canopy cover or located at the edge of forest remnants, which is related to forest degradation studies (SCHULTZ et al., 2018).

$$SAVI = (1 + L) \times \left(\frac{NIR - RED}{NIR + RED + L}\right) \quad (3)$$

Our final greenness index, the MSAVI, modifies SAVI by replacing the constant soil adjustment factor L with a self-adjusting function (Equation 4) (QI et al., 1994). In this version of MSAVI, the L factor is self-adjusted to the best vegetation density factor, reducing the soil background effects. The MSAVI is shown to increase the dynamic range of the vegetation signal while further minimizing the soil background influences, resulting in greater vegetation sensitivity as defined by a vegetation signal-to-soil noise ratio, showing usefulness for forest degradation studies (MATRICARDI et al., 2010).

$$MSAVI = \frac{2 \times NIR + 1 - \sqrt{(2 \times NIR + 1)^2 - 8 \times (NIR - RED)}}{2} \quad (4)$$

In addition to these four greenness indices, we include in our analysis three 'wetness indices.' These employ a combination of NIR and shortwave infrared (SWIR) reflectance in their formulae. The latter has shown lower reflectance in vegetation areas compared to other spectral regions due to absorption caused by water and the biochemical content of vegetation. However, they are frequently used in forest fire mapping (COLLINS et al., 2018) and forest recovery (BRIGHT et al., 2019), and due to water-related responses, these indices have also been used in forest disturbances related to anthropic practices (BUENO et al., 2019; SMITH et al., 2019). The wetness indices included in our analyses are: The normalized burn ratio (NBR), a second version of the NBR (NBR2), and the NDMI. The first two were originally designed for estimating post-wildfire burned area, and burn severity, while the latter is commonly used to track vegetation water content, water stress, and plant biomass changes more closely (WILSON; SADER, 2002).

The NBR is calculated as a normalized ratio between NIR and the second Landsat SWIR band (SWIR2, TM (2.080–2.350 µm), OLI (2.100–2.300 µm)) reflectance (Equation 5) (KEY; BENSON, 2006).

$$NBR = \frac{NIR - SWIR2}{NIR + SWIR2} \quad (5)$$

The second version of normalized burn ratio (NBR2) modifies NBR by replacing the NIR band with the first Landsat SWIR band (SWIR1, TM (1.550–1.750 µm), OLI (1.560–1.660 µm)) (Equation 6) in order to highlight water sensitivity in vegetation (DEVRIES et al., 2016).

By using both shortwave infrared channels, this index is very sensitive to leaf moisture and is suitable for deforestation mapping (BUENO et al., 2019).

$$NBR2 = \frac{SWIR1 - SWIR2}{SWIR1 + SWIR2} \quad (6)$$

Finally, the NDMI adjusts the normalized difference formula by replacing the SWIR2 band used in Equation (5) with SWIR1 (Equation 7). The NDMI has shown good accuracies in forest degradation (SCHULTZ et al., 2018), as well disturbances associated with forest type and harvest intensity (JIN; SADER, 2005).

$$NDMI = \frac{NIR - SWIR1}{NIR + SWIR1} \quad (7)$$

2.4 Vegetation Disturbance Maps

In this study, we defined 'disturbance' as negative changes to the native vegetation induced by human activity that completely alters the land cover. The main process for this is the conversion of native vegetation to pastures or bare soil by logging practices. To detect these disturbances in native vegetation, we used the R package 'bfastSpatial' (VERBESSELT; ZEILEIS; HEROLD, 2012). BFAST Spatial applies BFAST Monitor over each stack of Landsat indices, where each pixel is represented by a time series. The method of detection is based on fitting a seasonal model on a period defined as having a stable land cover history and then checking the stability of this model during the disturbance analysis period.

We assigned the stable history period to the years 2003 to 2007 and tuned BFAST Monitor to fit a first-order harmonic model in order to describe the native vegetation trajectories under seasonal changes. A first-order harmonic model helps to model the irregular distribution of Landsat observations that can result in model over-fitting (DEVRIES et al., 2015). Subsequentially, the monitoring period was assigned to the years 2008 to 2017 where the algorithm detects whether a new observation deviates from the stable history model. By computing a moving sum of the residuals based on an ordinary least squares model, a breakpoint is flagged when the moving sum deviates from zero beyond a 95% significance threshold.

We extracted the magnitude-of-change from model breakpoints, where negative magnitude values are associated with vegetation loss (i.e., deforestation, wildfires, forest

degradation) and positive values are with vegetation cover gain (i.e., forest regeneration). However, model breakpoints may be associated with near-zero disturbance magnitudes that are not related to anthropic events; thus, a secondary classification arises as an important step to better distinguish anthropogenic disturbances from stable areas affected by seasonal variations (DEVRIES et al., 2015). For this reason, we defined a threshold of disturbance to obtain a binary map (disturbed, undisturbed).

We then applied a threshold-based method to determine the binary changes by setting a fixed percentile of 10% (5% on each tail) of the data distribution. Particularly, a pixel was assigned as disturbed (value = 1) when its magnitude-of-change value was less than 5% of negative values or greater than 5% of positive values. Otherwise, it was assigned as undisturbed (value = 0). Positive change magnitude values (vegetation cover gain) were also classified as disturbance because a vegetation pixel with low reflectance values, i.e., scrublands, may be abruptly converted to high-reflectance land use, i.e., agriculture lands, which can result in a positive value of change along the time series. The selection of a suitable threshold value to identify change has been reported as a difficult task and is arbitrary as it is directly related to the exclusion and inclusion of change areas (HUSSAIN et al., 2013). However, this procedure guarantees the inclusion of an equal number of pixels of the index gain and loss, making it suitable to compare how change maps are similar through a unique change algorithm.

It is worth recalling that our purpose here was not to produce the most accurate disturbance maps, but rather to compare effects of spectral indices and vegetation domain on different disturbance maps produced with consistent (and reasonable) workflows.

2.5 Spatial Agreement and Accuracy Analysis

Our procedure consisted of a spatial analysis of disturbed pixels adapted from Cohen et al. (2017) and performed on individual study scenes. We then compared disturbance maps with one another (spatial agreement analysis) to a reference dataset (see 2.5.3 Accuracy analysis) as illustrated in Figure 2. The first component—spatial agreement—was divided into two parts: (a) Overall agreement among the seven disturbance maps, and (b) paired agreement between maps.

Figure 2 – Schematic illustrating the data agreement analysis. Vegetation domains are represented by Atlantic forest (AF), savanna (SAV), and semi-arid woodland (SAW).

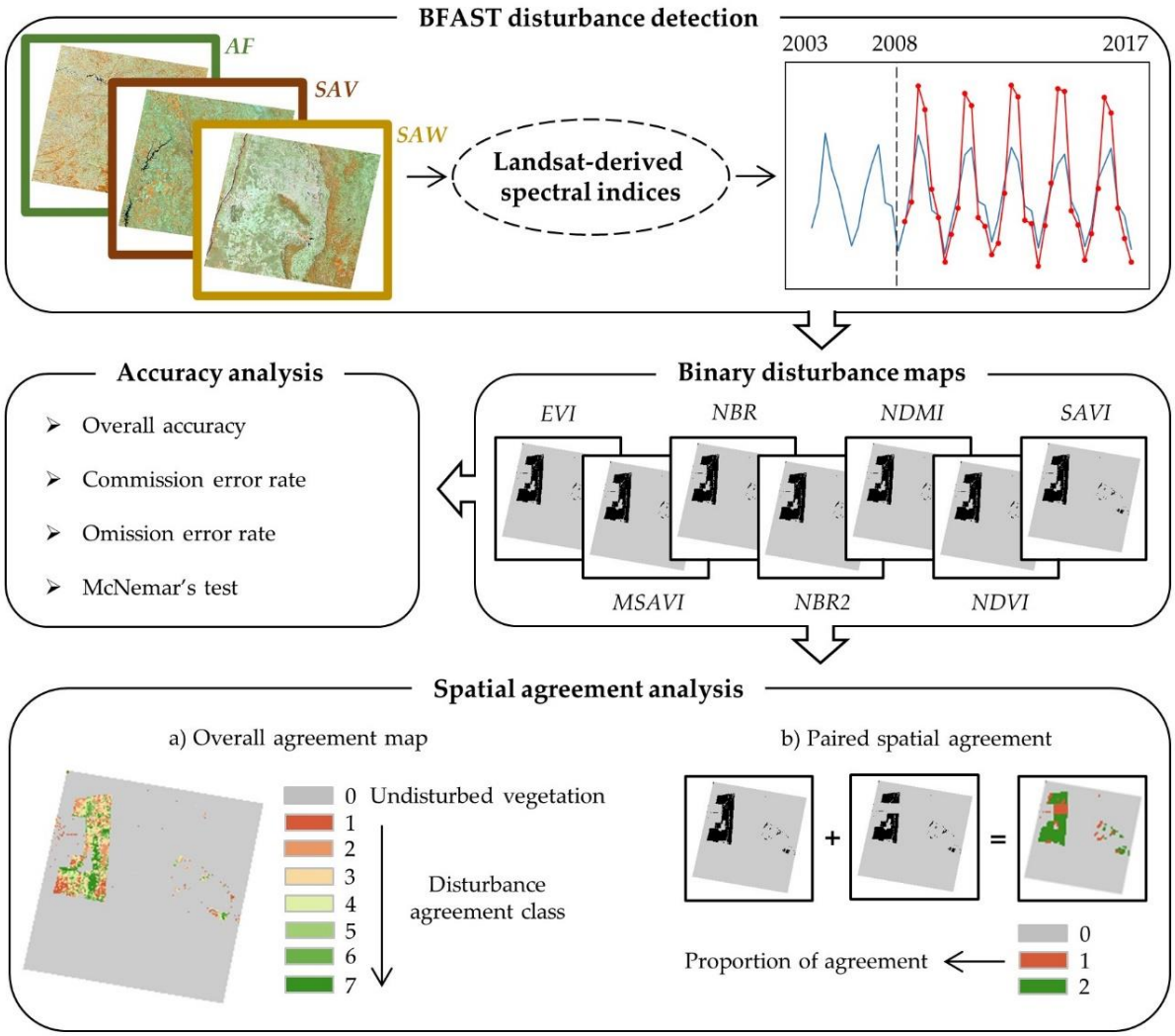

Source: Author (2022).

2.5.1 Overall Spatial Agreement

The overall-agreement analysis consisted of summing the seven binary disturbance maps, producing an overall agreement map by vegetation domain. For each pixel, the number of maps labels that pixel as disturbance, producing an overall agreement map with eight numerical classes. These classes varied from one (meaning that only one particular spectral index detected a disturbance in a particular pixel) to seven (meaning a total agreement among disturbance maps for a disturbed pixel). The total agreement for undisturbed pixels was assigned as undisturbed vegetation. The number of pixels per class was extracted and plotted across the vegetation domains. In addition, we isolated classes 'one' and 'two' from the overall

agreement map (hereafter labeled as ‘class1‘ and ‘class2’), then analyzed these by ranking what indices most contributed for these low agreement counts. $Class_1$ and $class_2$ describe the lowest amounts of spatial agreement observed among the spectral indices in that they reflect locations where disturbance is detected by only one or two spectral indices, respectively.

We analyzed these classes to better understand which indices contributed most to disturbance detection disagreements. Furthermore, we compared the influence of vegetation domain in map agreement. A one-way analysis of variance (ANOVA) was used to test whether agreement classes were significantly different across vegetation domains. If the difference was significant, the test indicated that vegetation domains affect the spatial agreement among vegetation disturbance maps.

2.5.2 Paired Agreement

To evaluate the spatial agreement of an individual disturbance map with those produced using the other six spectral indices and BFAST Monitor, we assessed paired agreement between individual maps. This paired agreement evaluation consisted of analyzing the similarity between two maps by vegetation domain. Similar to the overall agreement, here, we summed pairs of binary disturbance maps, which returned pixel classes of 0 (agreement to undisturbed class), 1 (disagreement), or 2 (agreement to disturbance class).

We calculated the proportion of agreement of a map *i* with a map *j* by summing the agreement of disturbed pixels *Nij* and dividing by the number of disturbed pixels in both maps *Ni* and *Nj*, minus *Nij* (Equation 8). Proportions varied from 0 (total disagreement) to 1 (total agreement). Afterward, we plotted the paired agreement across the vegetation domains in order to produce a comprehensive visual interpretation.

$$Agreement_{i,j} = \frac{\sum N_{ij}}{\sum N_i + \sum N_j - \sum N_{ij}} \quad (8)$$

2.5.3 Accuracy Analysis

For the accuracy analysis, we compared each disturbance map with a reference data set to quantify its accuracy. Reference data were compiled by creating fixed-area plots and then delineating disturbance polygons within the plot by visual interpretation using Landsat images. High-resolution imagery from Google Earth were also used, where available, as auxiliary information to infer land cover changes in ambiguous areas, i.e., non-native vegetation areas

included in the vegetation map mask. Square plots of 120 km^2 were placed across each vegetation domain study area using a systematic point grid of 45 km by 45 km over the scenes. This sampling design represented 5% of each study area and was sufficiently large to contain a suitable number of deforestation observations (OLOFSSON et al., 2014).

In order to balance the number of observations per class, we randomly selected 25 pixels per class (disturbed and undisturbed) in each area plot. A total of 1950 pixels (25 × 2 classes x 13 area plots x 3 scenes) were used to analyze the change maps. We calculated accuracy measures for each map by summing the correctly detected observations and dividing by a) the total number of observations (overall accuracy), b) the proportion of the total number of observations labeled as disturbance in the reference but not labeled by a given map (omission rate), and c) the proportion of the total number of observations labeled as disturbance by a map set but not labeled by the reference (commission rate).

We used ANOVAs to test whether there were significant differences in accuracy statistics across vegetation domains. We performed three separate tests, one for each accuracy statistic: Overall accuracy, producer's accuracy, and user's accuracy. Each test had three groups (vegetation domains) of seven samples (indices). The null hypothesis was that the relevant test statistics all came from the same population.

We also performed McNemar's tests to determine if there were statistically significant differences between the various pairwise map accuracies. McNemar's test is a non-parametric test based on chi-square ($\chi 2$) statistics with 1 degree of freedom, which can be computed from two confusion matrices, and is suitable for assessing distinct mapping performances (SHIMIZU et al., 2019). McNemar's test was applied using the R package 'stats' at a 95% confidence level and included a continuity correction to account for having a discrete statistic in a continuous distribution.

3 RESULTS

3.1 Spatial Agreement Analysis

Overall disturbance map agreement insets are displayed in Figure 3a. These show the visual agreement between the different index-based maps with regard to the disturbed vegetation class. Considering each vegetation domain, the percentage of disturbed pixels in the overall disturbance map, wherein disturbed pixels are those where disturbance was detected by one or more spectral indices, was 13.7% in the Atlantic forest, 13.9% in the savanna, and 16.8% in the semi-arid woodland (Figure 3b).

In general, the agreement analyses returned a similar trend in disturbance agreement classes across the three vegetation domains, indicating that the latter did not influence patterns of spectral-index performance (Figure 3c). These results are reinforced by the ANOVA that revealed no statistically significant differences across vegetation domains with $F_{(2, 18)} = 0.239$ ($p = 0.789$). Mean (standard deviation) F-statistics for Atlantic forest, savanna, and semi-arid woodland were 1.95 (1.36), 1.98 (1.28), and 2.39 (1.37), respectively.

Figure 3 – Overall agreement results. (a) Map insets for Atlantic forest (AF), savanna (SAV), and semi-arid woodland (SAW); (b) percentage of disturbed pixels by vegetation domain; (c) percentage of disturbed pixels by agreement class.

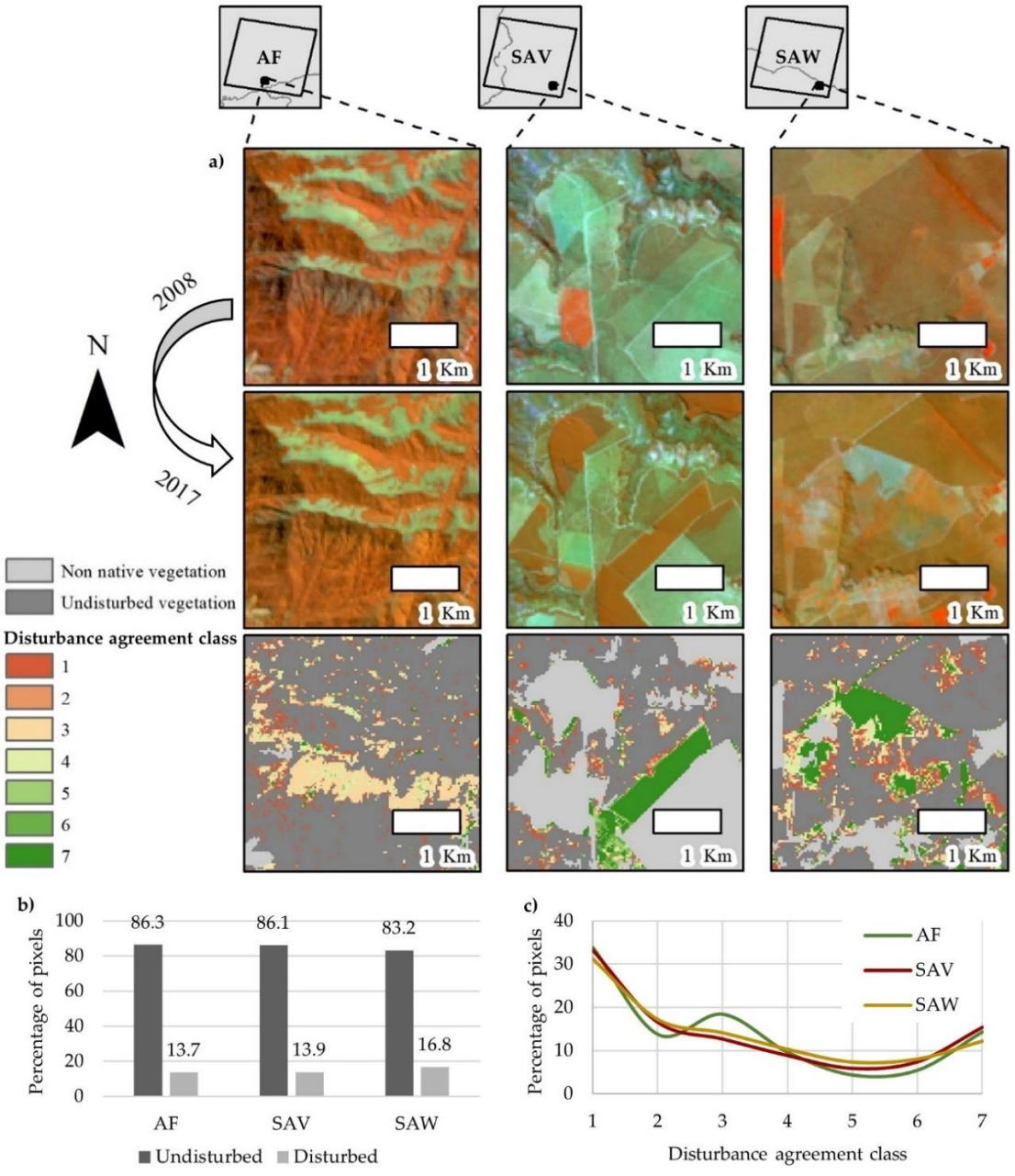

Source: Author (2022).

For savanna and semi-arid woodland, the highest percentages of disturbed pixels were represented by $class_1$ (33.1% and 31.1%, respectively) and $class_2$ (16.6% and 17.2%, respectively). For Atlantic forest, the highest percentage of disturbed pixels was represented by $class_1$ and $class_3$, with 33.8% and 18.4%, respectively (Figure 3c). Table 1 provides the proportion that each spectral index disturbance map contributes to the classes $class_1$ and $class_2$ of the overall agreement map. NBR2 contributed the most to $class_1$ agreement (Atlantic forest = 39.7%, savanna = 43.1%, and semi-arid woodland = 39.5%) followed by NDVI and NDMI. $Class_2$ was very balanced across the spectral indices in the Atlantic forest domain; however, in the savanna and semi-arid woodland domains, moisture indices, represented by NBR, NBR2, NDMI, and NDVI, were responsible for a high proportion of this class.

Table 1 – Summary of proportions each spectral index disturbance map contributes to the classes class1 and class2. Vegetation domains are represented by the following acronyms: Atlantic forest—AF, savanna—SAV, and semi-arid woodland—SAW.

	$Class_1$ (%)			**$Class_2$ (%)**		
	AF	**SAV**	**SAW**	**AF**	**SAV**	**SAW**
EVI	11.4	5.1	6.0	12.0	5.9	6.4
MSAVI	8.6	9.7	6.0	15.9	8.1	9.8
NBR	4.0	5.3	5.1	17.8	26.1	22.6
NBR2	39.7	43.1	39.5	15.2	19.6	21.8
NDMI	9.8	16.2	19.4	13.8	19.7	15.0
NDVI	22.8	18.8	20.7	11.7	13.6	15.7
SAVI	3.6	1.7	3.2	13.7	7.0	8.8
Total	100.0	100.0	100.0	100.0	100.0	100.0

Source: Author (2022).

Exploring the spatial relationships between individual spectral indices, there was an observable pattern in agreement across vegetation domains (Figure 4). Proportions of paired agreement greater than 0.70 (see Equation (8)) were expressed by EVI, MSAVI, SAVI, and their paired combinations, presenting the highest values of spatial agreement for all vegetation types. In addition, NBR and NDMI also presented high values of similarity among the vegetation domains (Atlantic forest = 0.71, savanna = 0.65, and semi-arid woodland = 0.59).

On the other hand, low proportions of agreement were produced by NBR2 and its combinations with EVI, MSAVI, and SAVI (<0.30) for the three vegetation domains as well.

Low values of spatial agreement between the NBR2 index and other indices corroborate our earlier results in Table 1 with regard to the large contribution of this index to class1, at about 40%. Although NBR2 presented very low similarity with most of the indices, exceptions were noticed with NBR (Atlantic forest = 0.48, savanna = 0.45, and semi-arid woodland = 0.46) and NDVI (Atlantic forest = 0.37, savanna = 0.40, and semi-arid woodland = 0.41).

Figure 4 – Paired spatial agreement in detected disturbance between the seven spectral index disturbance maps. Proportions of agreement varied from 0 (total disagreement) to 1 (total agreement) between indices.

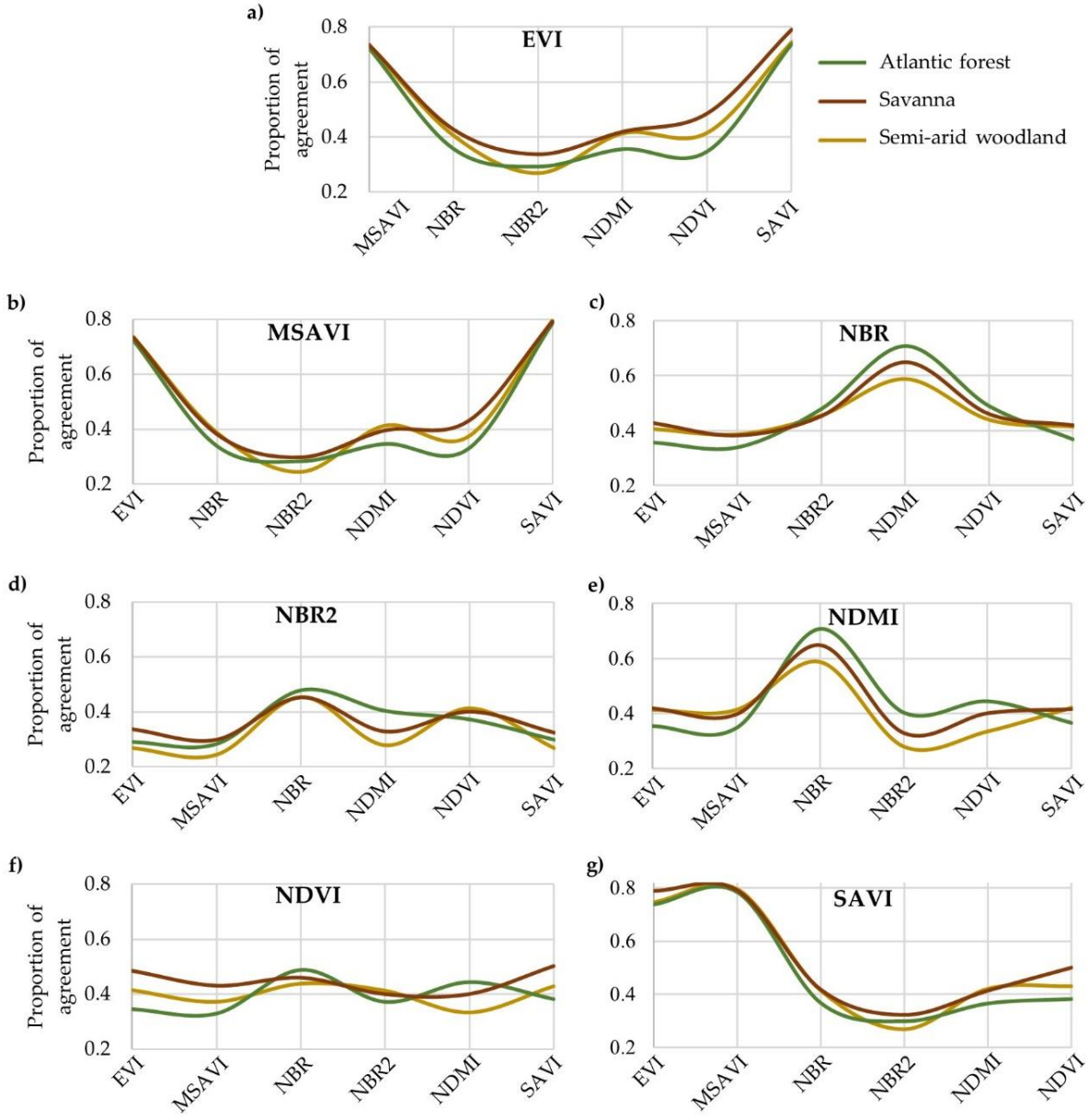

Source: Author (2022).

3.2 Accuracy Analysis and Index Performance

Map accuracies are presented in Table 2. Overall accuracies varied across vegetation domains and varied slightly among indices. Among the study areas, NBR and NDMI indices in the Atlantic forest domain presented the highest overall accuracies of 82.1%, while the lowest result was registered by MSAVI map (78.2%). NDMI presented the poorest results for semi-arid woodland at 54.6% overall accuracy. NDVI produced the highest overall accuracy for both semi-arid woodland (66.0%) and savanna (59.6%). Although savanna accuracies fell between the other two domains, it demonstrated a lower overall accuracy average when compared to semi-arid woodland, 56.6% versus 59.8%, respectively.

Table 2 – Overall accuracy results (in percentage) from all vegetation disturbance maps—Atlantic forest (AF), savanna (SAV), and semi-arid woodland (SAW). Average and standard deviation by vegetation domain are also presented.

	EVI	**MSAVI**	**NBR**	**NBR2**	**NDMI**	**NDVI**	**SAVI**	**Avg.**	**Std.**
AF	78.9	78.2	82.1	81.2	82.1	81.1	78.7	80.3	1.6
SAV	54.9	54.7	58.0	58.0	55.6	59.6	55.4	56.6	1.8
SAW	57.8	57.5	61.1	62.9	54.6	66.0	58.5	59.8	3.5

Source: Author (2022).

Commission error, inversely related to the user's accuracy, was variable among the vegetation types (Figure 5). Atlantic forest commission error rates followed overall accuracy trends across spectral indices, presenting low commission error rates by NDMI and NBR (7.3%), and the highest error rate by MSAVI (13.8%). In the semi-arid woodland vegetation domain, NDMI presented again higher error rates compared to its performance in the Atlantic forest, with the highest commission error for the former vegetation domain at 32.6%. Semi-arid woodland and savanna showed NDVI to produce the lowest commission errors at 10.9% and 13.4%, respectively.

Omission error, inversely related to the producer's accuracy, presented considerable variability throughout the vegetation domains. A spectral index performance hierarchy similar to what was observed in overall accuracies and commission errors was observed in the Atlantic forest, with NDMI and NBR producing the lowest omission error rates (34.2%), and MSAVI producing a 37.9% error rate. Results for the savanna vegetation domain followed a similar pattern.

Finally, semi-arid woodland possessed the highest omission rate among all disturbance maps, represented by 82.2% in the NDMI disturbance map. As in the commission analysis, NDVI produced the lowest errors of omission in semi-arid woodland and savanna, at 62.2% and 67.4%, respectively. Our ANOVA revealed statistically significant differences for the three measures of accuracy across vegetation domains with $F_{(2, 18)} = 165.3$, $p = < 0.0001$ for overall accuracy; $F_{(2, 18)} = 19.02$, $p = < 0.0001$ for commission error; and $F_{(2, 18)} = 140.2$, $p = < 0.0001$ for omission error. Mean and standard deviations for vegetation domains are presented in Table 2.

Figure 5 – Omission and commission rates of the disturbances maps.

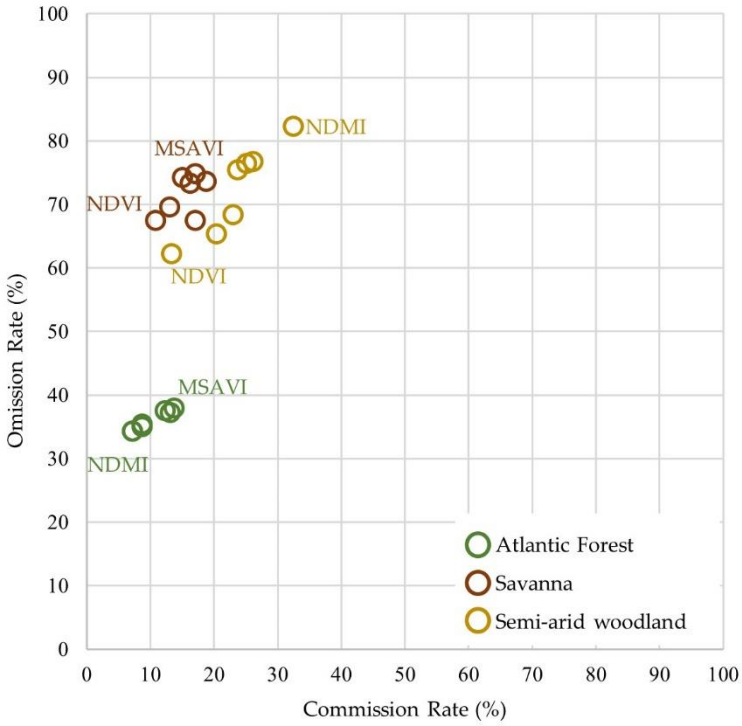

Source: Author (2022).

The McNemar's test showed no statistically significant differences between spectral indices' disturbance map accuracies in either the Atlantic forest or savanna. However, in the semi-arid woodland, there were significant differences between disturbance accuracies. The NDMI disturbance map, which provided the poorest accuracies in this vegetation domain, was statistically different from NBR, NBR2, and NDVI, the top three performing indices. The NDMI also produced the greatest paired difference in accuracies among all map comparisons ($\chi 2 = 16.62$, p-value < 0.0001) when tested against NDVI disturbance map accuracy. NDVI also presented significant differences with other spectral index maps, including EVI, SAVI, and MSAVI (Table 3).

Table 3 – Comparison of spectral indices disturbance accuracies using McNemar's test in semi-arid woodland vegetation domain. The upper number indicates the chi-squared value, the number in parentheses indicates the p-value, and bold values indicate statistical significance.

	EVI	**MSAVI**	**NBR**	**NBR2**	**NDMI**	**NDVI**	**SAVI**
EVI	0.00 (1.0000)						
MSAVI	0.01 (0.9337)	0.00 (1.0000)					
NBR	1.29 (0.2555)	1.56 (0.2120)	0.00 (1.0000)				
NBR2	3.25 (0.0714)	3.66 (0.0557)	0.41 (0.5235)	0.00 (1.0000)			
NDMI	1.29 (0.2555)	1.05 (0.3048)	5.30 (0.0213)	8.81 (0.0030)	0.00 (1.0000)		
NDVI	8.48 (0.0036)	9.14 (0.0025)	3.05 (0.0806)	1.17 (0.2794)	16.62 (<0.0001)	0.00 (1.0000)	
SAVI	0.04 (0.8461)	0.09 (0.7603)	0.84 (0.3601)	2.50 (0.1139)	1.85 (0.1741)	7.24 (0.0071)	0.00 (1.0000)

Source: Author (2022).

4 DISCUSSION

4.1 Vegetation Disturbance Mapping Using BFAST

An initial objective of this study was to identify how maps derived from Landsat based on spectral indices agree in terms of the vegetation change they detect, and how much the vegetation domain impacts their agreement. Vegetation disturbance maps, provided by one change detection algorithm (BFAST Monitor) and seven different spectral indices (EVI, MSAVI, NBR, NBR2, NDMI, NDVI, and SAVI), indicated a low rate of spatial agreement when compared among themselves. This result is consistent with Cohen et al. (2017), who evaluated forest disturbance derived from seven independent Landsat-based algorithms that presented widely varying disturbance rates. However, our observed rates of agreement were higher than those previously reported by Cohen et al. (2017), which can be expected as we exclude the variability by different classification systems associated with land cover, and explored mostly the spectral variation.

In examining our spatial agreement results in more detail, we observed interesting similarities between spectral indices of similar types (i.e., greenness vs. wetness indices) and their disturbance detection maps across the different environments in our three vegetation domains. For instance, the three greenness indices adjusted for signal saturation (i.e., the EVI, SAVI, and MSAVI) increase the dynamic range of the vegetation signal, which induces a higher sensitivity to topographic illuminations effect and leads to significant changes in the observed spectral characteristics of areas with strong topographic relief. This is observed in the unusual trend in the Atlantic forest domain illustrated by a high frequency of agreement pixels in $class_3$ (three spectral indices disturbance detection through the BFAST Monitor in the overall agreement map). In this case, BFAST change detection, based on these three greenness indices adjusted for saturation, detected high rates of disturbance in the Serra da Mantiqueira region (highlighted by the Atlantic forest inset in Figure 3), which represents roughly one quarter of the forested area in the Atlantic forest vegetation domain.

We also observed the two wetness indices that employ NIR in their formulae, i.e., NBR and NDMI showed spatial agreements that reflected the difference in their use of SWIR1 versus SWIR2, respectively. That is, SWIR 2 shows a lower reflectance than SWIR 1 in native vegetation spectral signatures due to higher levels of absorption by leaf water content, which is a contributing factor in the savanna and semi-arid woodland domains. In addition, the agreement of NDMI with other indices (Figure 4e) was influenced by vegetation domains, indicating lower proportions in semi-arid woodland and higher proportions in Atlantic forest domains, with savanna regions lying in between. This suggests an association between NDMI and levels of moisture-related forest seasonality, leading to changes in NDMI performance over dry-deciduous versus evergreen forest.

In contrast to the greenness and wetness spectral indices discussed above, the NBR2 and NDVI showed the lowest rates of spatial agreement with other indices in this study. The first of these—a wetness index—utilizes only shortwave infrared channels in its formula. In part, the low disturbance map agreement produced by this index is clearly demonstrated by $class_1$ in the overall agreement map (Table 1). In this disturbance agreement class, which indicated pixels labeled by only one vegetation disturbance map, NBR2 accounted for 40% of all pixels in the class. In comparison to the other wetness indices, NBR2 presented a higher agreement with NBR (both indices share the SWIR 2 channel in their formulae) than NDMI (indices sharing SWIR 1 channel) in all three vegetation domains (Figure 4d), providing some support for the conceptual premise that both NBR and NBR2 were developed for burn purposes.

The other low-agreement result produced by the NDVI vegetation disturbance map showed an unusual pattern of agreement among the vegetation domains (Figure 4f). This greenness index can be insensitive to high-density vegetation or soil brightness conditions. This may explain the inverse pattern of performance across vegetation domains to what we observed in wetness index disturbance map agreements—a pattern not observed for the other greenness indices that account for signal saturation. That is, we see from NDVI a low spatial agreement with other indices in the Atlantic forest, followed by better agreement in semi-arid woodland and savanna. In the Atlantic forest, this pattern is related to the lower sensitivity of the NDVI to dense vegetation than that of the other greenness indices, leading to a low rate of misclassification due to topographic illumination effects. In the savanna and semi-arid woodland domains, where high-density vegetation is not a typical feature, higher rates of agreement were observed between the NDVI disturbance maps and those from other indices in the semi-arid woodlands due to the presence of mountainous areas comprised mostly of the Serra do Espinhaço mountain range, versus rates of agreement in the savanna domain.

4.2 Vegetation Sensitivity to Spectral Indices

Our second research question was concerned with how accurate forest disturbance maps are based on real change events. In general, previous studies have mapped vegetation disturbance using BFAST and Landsat time series, reaching satisfactory accuracies. For example, in evergreen forested areas, DeVries et al. (2015) estimated an overall accuracy of 78% with commission and omission rates of 17% in southern Ethiopia. In our study, we found similar results in the Atlantic forest domain, with average overall accuracies at 80.3%, and commission and omission rates of 10.2% and 35.9%, respectively. On the other hand, vegetation domains in this study that are more affected by seasonal variations—savanna and semi-arid woodland—presented poor overall accuracy results ranging from 54.7 to 66.0%. Others studies using BFAST in dry regions reached satisfactory accuracies, such as Schultz et al. (2018) who assessed vegetation degradation in Africa savannas, and found a drop in detection performance as vegetation cover decreased. Likewise, Watts and Laffan (2014) using MODIS EVI assessed vegetation greening changes related to known floods in Australia's semi-arid regions, finding a BFAST sensitivity to vegetation cover type and seasonal patterns. However, our study faced broad seasonal vegetation domains encompassing mixed forest landscapes and grassland ranges, without a more detailed vegetation classification.

Similar to spatial agreement results, spectral indices can be grouped by their individual accuracy performances. In general, wetness indices and NDVI presented higher accuracies in

all vegetation types. These results reflect those of Schultz et al. (2016) and DeVries et al. (2016) who also found particular moisture indices highly correlated with disturbances in tropical forests. SWIR-based indices were also highly related to vegetation change detection in seasonal savannas (BUENO et al., 2019) and herbaceous biomass in semi-arid areas (JACQUES et al., 2014). However, the high accuracies presented by NDVI is somewhat surprising given the fact that studies showed low accuracies related to this index in tropical forests (BUENO et al., 2019; SCHULTZ et al., 2016b). This is a particularly useful result indicating why NDVI is still the most frequently used index in remote sensing, and has been presented in forest disturbances detection and monitoring (GAO et al., 2019; WU et al., 2020).

Another particular occurrence observed in our accuracy analysis was related to the NDMI, which presented a distinct accuracy pattern among vegetation domains. In the Atlantic forest domain, this index had the highest accuracies, as highlighted in Figure 5. In savanna, it was the fourth-best performing among the indices, producing the lowest accuracy among the wetness indices but still higher than that of the greenness indices. However, this index had the lowest accuracies in dry forests, which were statistically different from those of other indices when analyzed by McNemar's test. These results confirm the relationship between NDMI and vegetation domains observed in our map agreement results, reinforcing a specific sensitivity to vegetation water content, which is more abundant when more vegetation is present.

Greenness-related indices used in this study that adjusted for signal saturation (EVI, MSAVI, and SAVI) were less successful in our accuracy analysis. They were not able to properly isolate the change signal when run through the BFAST Monitor algorithm, generating disturbance misclassifications. Most of their inaccuracies were due to the topographic illumination artifacts, which were also reported by (TAN et al., 2013) who found a decrease in the accuracy of disturbance detection practices using Landsat imagery.

Vegetation densities were also a source of error for these greenness indices as high densities can increase the dynamic range of the vegetation signal, which renders it more sensitive to topographic illuminations effects, whereas low vegetation densities can be confused with the corrected soil signals, affecting the disturbance detection accuracy. These results are in keeping with previous observational studies, in which EVI and SAVI also proved to be unsuitable for deforestation detection by Schultz et al. (2016a), or in the case of SAVI, unsatisfactory for assessing forest fire disturbances and recovery (HISLOP et al., 2018).

4.3 Consideration and Future Research

Further research on this topic needs to be undertaken before we can clearly understand the relationship between spectral indices using BFAST and their vegetation disturbance detection performances in distinct vegetation types. Some considerations are apparent from this study, such as concerns regarding (1) image preprocessing, (2) algorithm implications, (3) generalization error, and (4) computation timing over large areas.

Image preprocessing is a crucial procedure in disturbance detection studies. The data quality of Landsat products processed at the surface reflectance level by LEDAPS and LaSRC supports time series analysis and data stacking with satisfactory precision (RMSE < 12 m) (ZHU, 2017). In addition, the detection of clouds and cloud shadows is an inevitably required step in time series disturbance detection analysis, particularly in the BFAST Monitor concept that runs on image stacks, not composites. However, Landsat cloud- and cloud shadow-masked products still contribute to misclassifications and may impact disturbance detection analysis as we selected images available with less than 50% of cloud cover detected by the Fmask (ZHU; WOODCOCK, 2012). These misclassifications can be observed in cloudy regions, such the Serra da Mantiqueira. In addition to preprocessing, another source of uncertainty is related to non-native vegetation mask errors, which also influence the analysis. As is the case for the cloud mask, land cover/land use and surface water maps were not perfect and also include misclassifications. Besides commission- and omission-related class errors, mask boundaries and spectrally mixed pixels were sources of commission rates in this study.

Some sources of error regarding deforestation detection using BFAST on Landsat time series were previously reported by Schultz et al. (2016). The authors demonstrated radiometric correction strategies for monitoring change in the tropics in relation to differences resulting from data availability, signal-to-noise ratio, atmospheric contamination, and deforestation type. Grogan et al. (2016) reported the use of filtered MODIS time series in order to improve forest change detection, despite BFAST being able to handle unfiltered data. Although we did not analyze the accuracy outputs as they related to image observation frequency, it is was also described as a methodological challenge by Schultz et al. (2016), who demonstrated improved performance in particular spectral indices as a result of increased observation frequencies.

Additional uncertainty arises from the fact that BFAST Monitor was employed across our vegetation domains without substantive calibration for extant conditions within those particular study areas, such as the order of the harmonic model used to fit the stable land cover history, and the h parameter used to determine the potential number of breaks that can be

detected by the algorithm. This perhaps points to a need for a more thorough examination of the algorithm performance for each new forest system encountered (COHEN et al., 2017).

In our study, single index performances were related to vegetation domains, where a particular spectral variable produced high accuracies in one domain and lower accuracies in another. For example, NDMI was the most successful index in the Atlantic forest with regard to accuracy while producing the poorest results in the semi-arid woodland. This highlights the fact that large-area monitoring programs covering different ecosystems and land cover types therefore require region-specific spectral variables and individual model calibrations (SCHULTZ et al., 2018), as the highly variable and complex spectral response of different types of forest disturbances across diverse ecosystems clearly increase the odds of generalization errors. These results also support the data fusion approach in change detection applications. This particular method proposes the combination of data inputs (in this case, spectral indices) and their distinctive features in order to increase the global performance. Data fusion methods have already been used by some forest change detection studies, i.e., Healey et al. (2018) mapped forest change detection using an ensemble method of eight Landsat-based algorithms and spatial predictors, reaching higher accuracies with all datasets combined. By fusing multiple index-based disturbance maps derived from LandTrendr (COHEN et al., 2018) and BFAST (SCHULTZ et al., 2016b) algorithms, through a random forest scheme, error rates were reduced in comparison to single index outputs. Combining multiple algorithms and spectral indices, Hislop et al. (2019) integrated two algorithms—LandTrendr and a statistical boundary approach—and three spectral indices—NBR, NDVI, and TCW—in order to detect abrupt disturbances in forest environments, which resulted in satisfactory disturbance detection accuracies. Thus, a further study with more focus on data fusion models of different types of forest disturbances across diverse vegetation domains is, therefore, suggested, as feature-level data fusion may produce better results for deforestation disturbance detection than the application of individual spectral indices.

In addition, ancillary data as land cover/land use classifications should be explored in order to mitigate sources of error. Mainly in heterogeneous landscapes, detailed land classes, i.e., classifying woodland from scrublands in savanna regions, are an important approach for avoiding generalization errors and improving BFAST detection accuracies. Another source of uncertainty in this work is related to disturbance types and their magnitudes, as we only assigned disturbances in vegetation as human-induced activities that abruptly remove the native vegetation. Alternative input data are also important as previous studies have reported that canopies can cover sensitive spectral indices such as the NDFI, which demonstrated good

performance in tropical forests disturbance detection, and it is calculated using spectral mixture analysis (SCHULTZ et al., 2016b). However, the decision to conduct our study using easily requested spectral index products available on the USGS website avoided data preprocessing steps.

Finally, further challenges in applying BFAST Monitor for Landsat time series analyses relate to processing time when assessing large-scale vegetation disturbance scenarios. Although high-performance and cloud-computing systems are becoming popular, we used parallel processing capabilities on a desktop computer and experienced considerable computational times while processing our data. Advances in high-performance or cloud computing for vegetation disturbance mapping using BFAST Monitor should be explored. For instance, the establishment of cloud platforms such as Google Earth Engine (GEE) provide many advantages for change detection studies, such as direct access to image time series, the straightforward management of time series stacks, and agile computation through parallel processing (GORELICK et al., 2017). These advances might enable the development of large-scale vegetation disturbance maps, and also a user-friendly format to run the BFAST Monitor algorithm.

5 CONCLUSION

This work contributes to existing knowledge of the performance of vegetation indices from Landsat time series in vegetation disturbance detection by comparing the suitability of spectral indices and their agreement in tropical vegetation domains using BFAST Monitor. We demonstrated that (1) vegetation disturbance maps provided by one change detection algorithm and seven different spectral indices can produce a low rate of spatial agreement when compared, and (2) vegetation domains do not influence this spatial agreement.

With regard to disturbance detection accuracies, wetness indices (NBR, NBR2, and NDMI) outperformed other spectral indices, including greenness-related indices (EVI, MSAVI, and SAVI). NDMI presented the highest accuracy in the Atlantic forest domain while NDVI performed better across savanna and semi-arid woodland domains.

Despite its exploratory nature, this study offered some insight into vegetation disturbance maps and the influence of spectral index choice on the spatial distribution of results, and on detection accuracies. This research has raised many questions in need of further investigation, such as the use of region-specific approaches in order to mitigate the generalization error. Future research should also explore the BFAST Monitor algorithm's computational limitations presented in this study, as well as its expansion to other techniques

and regions across the globe, perhaps with the help of cloud-based processing and analysis platforms.

Acknowledgments: This study was financed in part by the Coordenação de Aperfeiçoamento de Pessoal de Nível Superior – Brasil (CAPES) – Finance Code 001.

6 REFERENCES

ACHARD, F. et al. Determination of tropical deforestation rates and related carbon losses from 1990 to 2010. **Global Change Biology**, v. 20, n. 8, p. 2540–2554, 1 ago. 2014. DOI: 10.1111/gcb.12605.

BARLOW, J. et al. Anthropogenic disturbance in tropical forests can double biodiversity loss from deforestation. **Nature**, v. 535, n. 7610, p. 144–147, 6 jul. 2016. DOI: 10.1038/nature18326.

BELLARD, C. et al. Vulnerability of biodiversity hotspots to global change. **Global Ecology and Biogeography**, v. 23, n. 12, p. 1376–1386, dez. 2014. DOI: 10.1111/geb.12228.

BEUCHLE, R. et al. Land cover changes in the Brazilian Cerrado and Caatinga biomes from 1990 to 2010 based on a systematic remote sensing sampling approach. **Applied Geography**, v. 58, p. 116–127, mar. 2015. DOI: 10.1016/j.apgeog.2015.01.017.

BRIGHT, B. C. et al. Examining post-fire vegetation recovery with Landsat time series analysis in three western North American forest types. **Fire Ecology**, v. 15, n. 1, 1 dez. 2019. DOI: 10.1186/s42408-018-0021-9.

BUENO, I. T. et al. Object-Based Change Detection in the Cerrado Biome Using Landsat Time Series. **Remote Sensing**, v. 11, n. 5, p. 570, 8 mar. 2019. DOI: 10.3390/rs11050570.

COHEN, W. et al. How Similar Are Forest Disturbance Maps Derived from Different Landsat Time Series Algorithms? **Forests**, v. 8, n. 4, p. 98, 26 mar. 2017. DOI: 10.3390/f8040098.

COHEN, W. B. et al. A LandTrendr multispectral ensemble for forest disturbance detection. **Remote Sensing of Environment**, v. 205, p. 131–140, 1 fev. 2018. DOI: 10.1016/J.RSE.2017.11.015.

COLLINS, L. et al. The utility of Random Forests for wildfire severity mapping. **Remote**

Sensing of Environment, v. 216, p. 374–384, 1 out. 2018. DOI: 10.1016/j.rse.2018.07.005.

CURTIS, P. G. et al. Classifying drivers of global forest loss. **Science**, v. 361, n. 6407, p. 1108–1111, 14 set. 2018. DOI: 10.1126/science.aau3445.

DEVRIES, B. et al. Robust monitoring of small-scale forest disturbances in a tropical montane forest using Landsat time series. **Remote Sensing of Environment**, v. 161, p. 107–121, maio 2015. DOI: 10.1016/j.rse.2015.02.012.

DEVRIES, B. et al. Characterizing Forest Change Using Community-Based Monitoring Data and Landsat Time Series. **PLOS ONE**, v. 11, n. 3, p. e0147121, 28 mar. 2016. DOI: 10.1371/journal.pone.0147121.

DUTRIEUX, L. P. et al. Monitoring forest cover loss using multiple data streams, a case study of a tropical dry forest in Bolivia. **ISPRS Journal of Photogrammetry and Remote Sensing**, v. 107, p. 112–125, set. 2015. DOI: 10.1016/j.isprsjprs.2015.03.015.

FERREIRA, L. et al. Seasonal landscape and spectral vegetation index dynamics in the Brazilian Cerrado: An analysis within the Large-Scale Biosphere–Atmosphere Experiment in Amazônia (LBA). **Remote Sensing of Environment**, v. 87, n. 4, p. 534–550, 15 nov. 2003. DOI: 10.1016/j.rse.2002.09.003.

GAO, Y. et al. Monitoring forest disturbance using time-series MODIS NDVI in Michoacán, Mexico. **Geocarto International**, p. 1–17, 9 set. 2019. DOI: 10.1080/10106049.2019.1661032.

GORELICK, N. et al. Google Earth Engine: Planetary-scale geospatial analysis for everyone. **Remote Sensing of Environment**, v. 202, p. 18–27, dez. 2017. DOI: 10.1016/j.rse.2017.06.031.

GRINGS, F.; ROITBERG, E.; BARRAZA, V. EVI Time-Series Breakpoint Detection Using Convolutional Networks for Online Deforestation Monitoring in Chaco Forest. **IEEE Transactions on Geoscience and Remote Sensing**, v. 58, n. 2, p. 1303–1312, fev. 2020. DOI: 10.1109/TGRS.2019.2945719.

GROGAN, K. et al. Mapping Clearances in Tropical Dry Forests Using Breakpoints, Trend, and Seasonal Components from MODIS Time Series: Does Forest Type Matter? **Remote Sensing**, v. 8, n. 8, p. 657, 15 ago. 2016. DOI: 10.3390/rs8080657.

HANSEN, M. C. et al. High-Resolution Global Maps of 21st-Century Forest Cover Change. **Science**, v. 342, n. 6160, p. 850–853, 15 nov. 2013. DOI: 10.1126/science.1244693.

HEALEY, S. P. et al. Mapping forest change using stacked generalization: An ensemble approach. **Remote Sensing of Environment**, v. 204, p. 717–728, 2018. DOI: 10.1016/j.rse.2017.09.029.

HISLOP, S. et al. Using Landsat Spectral Indices in Time-Series to Assess Wildfire Disturbance and Recovery. **Remote Sensing**, v. 10, n. 3, p. 460, 15 mar. 2018. DOI: 10.3390/rs10030460.

HISLOP, S. et al. A fusion approach to forest disturbance mapping using time series ensemble techniques. **Remote Sensing of Environment**, v. 221, p. 188–197, fev. 2019. DOI: 10.1016/j.rse.2018.11.025.

HUETE, A.; JUSTICE, C.; LEEUWEN, W. V. **MODIS Vegetation Index (MOD 13) Algorithm Theoretical Basis Document**. Greenbelt, MD: NASA Goddard Space Flight Center, 1999.

HUETE, A. R. A soil-adjusted vegetation index (SAVI). **Remote Sensing of Environment**, v. 25, n. 3, p. 295–309, 1 ago. 1988. DOI: 10.1016/0034-4257(88)90106-X.

HUSSAIN, M. et al. Change detection from remotely sensed images: From pixel-based to object-based approaches. **ISPRS Journal of Photogrammetry and Remote Sensing**, v. 80, p. 91–106, jun. 2013. DOI: 10.1016/j.isprsjprs.2013.03.006.

JACQUES, D. C. et al. Monitoring dry vegetation masses in semi-arid areas with MODIS SWIR bands. **Remote Sensing of Environment**, v. 153, p. 40–49, 1 out. 2014. DOI: 10.1016/j.rse.2014.07.027.

JIN, S.; SADER, S. A. Comparison of time series tasseled cap wetness and the normalized difference moisture index in detecting forest disturbances. **Remote Sensing of Environment**, v. 94, n. 3, p. 364–372, 15 fev. 2005. DOI: 10.1016/j.rse.2004.10.012.

JUNK, W. J. et al. Brazilian wetlands: their definition, delineation, and classification for research, sustainable management, and protection. **Aquatic Conservation: Marine and Freshwater Ecosystems**, v. 24, n. 1, p. 5–22, fev. 2014. DOI: 10.1002/aqc.2386.

KEY, C. H.; BENSON, N. C. Landscape assessment: ground measure of severity, the composite

burn index; and remote sensing of severity, the normalized burn ratio. In: **FIREMON: Fire effects monitoring and inventory system. Gen. Tech. Rpt. RMRS-GTR-164-CD: LAI-15**. Ogden: USDA Forest Service, Rocky Mountain Research Station, 2006. p. 51.

LAWRENCE, D.; VANDECAR, K. Effects of tropical deforestation on climate and agriculture. **Nature Climate Change**, v. 5, n. 1, p. 27–36, 18 jan. 2015. DOI: 10.1038/nclimate2430.

LI, D. et al. Quantifying annual land-cover change and vegetation greenness variation in a coastal ecosystem using dense time-series Landsat data. **GIScience and Remote Sensing**, v. 56, n. 5, p. 769–793, 4 jul. 2019. DOI: 10.1080/15481603.2019.1565104.

LIU, J. et al. Burned area detection based on Landsat time series in savannas of southern Burkina Faso. **International Journal of Applied Earth Observation and Geoinformation**, v. 64, p. 210–220, 1 fev. 2018. DOI: 10.1016/j.jag.2017.09.011.

MASEK, J. G. et al. A Landsat Surface Reflectance Dataset for North America, 1990–2000. **IEEE Geoscience and Remote Sensing Letters**, v. 3, n. 1, p. 68–72, jan. 2006. DOI: 10.1109/LGRS.2005.857030.

MATRICARDI, E. A. T. et al. Assessment of tropical forest degradation by selective logging and fire using Landsat imagery. **Remote Sensing of Environment**, v. 114, n. 5, p. 1117–1129, 17 maio 2010. DOI: 10.1016/j.rse.2010.01.001.

MIRANDA, P. L. S. et al. Using tree species inventories to map biomes and assess their climatic overlaps in lowland tropical South America. **Global Ecology and Biogeography**, v. 27, n. 8, p. 899–912, ago. 2018. DOI: 10.1111/geb.12749.

MITCHARD, E. T. A. The tropical forest carbon cycle and climate change. **Nature**, v. 559, n. 7715, p. 527–534, 25 jul. 2018. DOI: 10.1038/s41586-018-0300-2.

MURILLO-SANDOVAL, P. et al. Detecting and Attributing Drivers of Forest Disturbance in the Colombian Andes Using Landsat Time-Series. **Forests**, v. 9, n. 5, p. 269, 15 maio 2018. DOI: 10.3390/f9050269.

MYERS, N. et al. Biodiversity hotspots for conservation priorities. **Nature**, v. 403, n. 6772, p. 853–858, 24 fev. 2000. DOI: 10.1038/35002501.

OLOFSSON, P. et al. Good practices for estimating area and assessing accuracy of land change. **Remote Sensing of Environment**, v. 148, n. October, p. 42–57, maio 2014. DOI: 10.1016/j.rse.2014.02.015.

PAN, Y. et al. A large and persistent carbon sink in the world's forests. **Science (New York, N.Y.)**, v. 333, n. 6045, p. 988–93, 19 ago. 2011. DOI: 10.1126/science.1201609.

PEKEL, J. F. et al. High-resolution mapping of global surface water and its long-term changes. **Nature**, v. 540, n. 7633, p. 418–422, 15 dez. 2016. DOI: 10.1038/nature20584.

QI, J. et al. A Modified Soil Adjusted Vegetation Index. **Remote Sensing of Environment**, v. 48, p. 119–126, 1994. DOI: 10.1016/0034-4257(94)90134-1.

RIBEIRO, M. C. et al. The Brazilian Atlantic Forest: How much is left, and how is the remaining forest distributed? Implications for conservation. **Biological Conservation**, v. 142, n. 6, p. 1141–1153, jun. 2009. DOI: 10.1016/j.biocon.2009.02.021.

SCHULTZ, M. et al. Error Sources in Deforestation Detection Using BFAST Monitor on Landsat Time Series Across Three Tropical Sites. **IEEE Journal of Selected Topics in Applied Earth Observations and Remote Sensing**, v. 9, n. 8, p. 3667–3679, 1 ago. 2016a. DOI: 10.1109/JSTARS.2015.2477473.

SCHULTZ, M. et al. Performance of vegetation indices from Landsat time series in deforestation monitoring. **International Journal of Applied Earth Observation and Geoinformation**, v. 52, p. 318–327, out. 2016b. DOI: 10.1016/j.jag.2016.06.020.

SCHULTZ, M. et al. Forest Cover and Vegetation Degradation Detection in the Kavango Zambezi Transfrontier Conservation Area Using BFAST Monitor. **Remote Sensing**, v. 10, n. 11, p. 1850, 21 nov. 2018. DOI: 10.3390/rs10111850.

SHIMIZU, K. et al. A comprehensive evaluation of disturbance agent classification approaches: Strengths of ensemble classification, multiple indices, spatio-temporal variables, and direct prediction. **ISPRS Journal of Photogrammetry and Remote Sensing**, v. 158, p. 99–112, dez. 2019. DOI: 10.1016/j.isprsjprs.2019.10.004.

SMITH, V. et al. Assessing the accuracy of detected breaks in Landsat time series as predictors of small scale deforestation in tropical dry forests of Mexico and Costa Rica. **Remote Sensing**

of Environment, v. 221, p. 707–721, 1 fev. 2019. DOI: 10.1016/j.rse.2018.12.020.

TAN, B. et al. Improved forest change detection with terrain illumination corrected Landsat images. **Remote Sensing of Environment**, v. 136, p. 469–483, 1 set. 2013. DOI: 10.1016/j.rse.2013.05.013.

TOVO, A. et al. Upscaling species richness and abundances in tropical forests. **Science Advances**, v. 3, n. 10, p. e1701438, 1 out. 2017. DOI: 10.1126/sciadv.1701438.

TUCKER, C. J. Red and photographic infrared linear combinations for monitoring vegetation. **Remote Sensing of Environment**, v. 8, n. 2, p. 127–150, maio 1979. DOI: 10.1016/0034-4257(79)90013-0.

USGS. **Landsat 4-7 Collection 1 (C1) Surface Reflectance (LEDAPS) Product Guide (Version 3.0).** U.S. Geological Survey, 2020. Disponível em: https://www.usgs.gov/media/files/landsat-4-7-collection-1-surface-reflectance-code-ledaps-product-guide. Acesso em: 20 out. 2020.

VAN DER WERF, G. R. et al. CO2 emissions from forest loss. **Nature Geoscience**, v. 2, n. 11, p. 737–738, nov. 2009. DOI: 10.1038/ngeo671.

VERBESSELT, J. et al. Detecting trend and seasonal changes in satellite image time series. **Remote Sensing of Environment**, v. 114, n. 1, p. 106–115, jan. 2010. DOI: 10.1016/j.rse.2009.08.014.

VERBESSELT, J.; ZEILEIS, A.; HEROLD, M. Near real-time disturbance detection using satellite image time series. **Remote Sensing of Environment**, v. 123, p. 98–108, ago. 2012. DOI: 10.1016/j.rse.2012.02.022.

VERMOTE, E. F. et al. Preliminary analysis of the performance of the Landsat 8/OLI land surface reflectance product. **Remote Sensing of Environment**, v. 185, p. 46–56, nov. 2016. DOI: 10.1016/j.rse.2016.04.008.

WALLER, E. K. et al. Landsat time series analysis of fractional plant cover changes on abandoned energy development sites. **International Journal of Applied Earth Observation and Geoinformation**, v. 73, p. 407–419, 1 dez. 2018. DOI: 10.1016/j.jag.2018.07.008.

WATTS, L. M.; LAFFAN, S. W. Effectiveness of the BFAST algorithm for detecting

vegetation response patterns in a semi-arid region. **Remote Sensing of Environment**, v. 154, n. 1, p. 234–245, 1 nov. 2014. DOI: 10.1016/j.rse.2014.08.023.

WILSON, E. H.; SADER, S. A. Detection of forest harvest type using multiple dates of Landsat TM imagery. **Remote Sensing of Environment**, v. 80, n. 3, p. 385–396, 1 jun. 2002. DOI: 10.1016/S0034-4257(01)00318-2.

WU, L. et al. Multi-Type Forest Change Detection Using BFAST and Monthly Landsat Time Series for Monitoring Spatiotemporal Dynamics of Forests in Subtropical Wetland. **Remote Sensing**, v. 12, n. 2, p. 341, 20 jan. 2020. DOI: 10.3390/rs12020341.

WULDER, M. A. et al. Current status of Landsat program, science, and applications. **Remote Sensing of Environment**, v. 225, p. 127–147, 1 maio 2019. DOI: 10.1016/j.rse.2019.02.015.

ZHU, Z. Change detection using landsat time series: A review of frequencies, preprocessing, algorithms, and applications. **ISPRS Journal of Photogrammetry and Remote Sensing**, v. 130, p. 370–384, ago. 2017. DOI: 10.1016/j.isprsjprs.2017.06.013.

ZHU, Z.; WOODCOCK, C. E. Object-based cloud and cloud shadow detection in Landsat imagery. **Remote Sensing of Environment**, v. 118, p. 83–94, mar. 2012. DOI: 10.1016/j.rse.2011.10.028.

ARTICLE 2 – A LARGE-SCALE DISTURBANCE MAPPING ENSEMBLE THROUGH DATA-DRIVEN REGIONALIZATION

Inacio Thomaz Bueno[1*], Jennifer Hird[2], Greg McDermid[2], Lênio Soares Galvão[3], Fausto Weimar Acerbi Júnior[1]

[1] *Department of Forest Science, Federal University of Lavras, Lavras 37200-000, Brazil;*
[2] *Department of Geography, University of Calgary, Calgary T2N 1N4, Canada;*
[3] *Department of Remote Sensing, National Institute for Space Research, São José dos Campos, 3037, Brazil.*

***** Corresponding author email: inaciotbueno@gmail.com

Publication status: Submitted in the **International Journal of Applied Earth Observation and Geoinformation**

Abstract: Mapping and monitoring disturbances in vegetation over large areas demand reliable approaches and accurate end-user maps. Methods and algorithms have been developed to meet satisfactory disturbance map accuracies, and the combination of multiple approaches has shown promise as a reliable alternative to any single method. However, extracting meaningful disturbance information from these combined methods is still challenging. Data variance from environmental conditions and disturbance drivers leads to spatial-temporal heterogeneity in land surfaces over large areas, which results in mapping errors. We evaluate the effectiveness of ensemble classification and data-driven regionalization for mapping vegetation disturbances at a broad scale. Our ensemble approach combines multispectral LandTrendr outputs reflecting preliminary disturbance information in a Random Forest model to map disturbances in the state of Minas Gerais, Brazil, using the Google Earth Engine cloud computing platform. We then applied an unsupervised clustering technique to perform data-driven regionalization of our study area using several sources of environmental and anthropogenic information, and analyzed gains and losses in map accuracies. Our results indicated gains in accuracy by the ensemble method compared to non-ensemble methods of disturbance mapping. Data-driven regionalization addressed complexities arising from variability in vegetation types, local climate, and topography across our study area, identifying climate and seasonal metrics as important variables for reducing uncertainties in vegetation disturbance maps. The integration of these techniques has revealed great potential for the increase of map accuracy and has provided important insights into the development of disturbance mapping methods in heterogeneous environments.

Keywords: Remote sensing; Landsat time series; LandTrendr; Random Forest.

1 INTRODUCTION

In the era of free, open-source satellite data streams, large-scale disturbance maps provide support for developing management strategies, implementing policy initiatives, and providing inputs for modeling ecological and environmental processes (HERMOSILLA et al., 2018).

The opening of the Landsat archive in 2008 allowed the development of new disturbance-mapping approaches. Free global mid-resolution (30 m) remote sensing imagery and a long-term record of observations have enabled more accurate land change analysis, the characterization of disturbance drivers, and the monitoring of post-disturbance conditions (WULDER et al., 2012). Methods and algorithms to detect and monitor vegetation disturbances

have been developed to exploit the Landsat data archive and to examine long-term vegetation trends. An example that uses Landsat time series is the Landsat-based detection of Trends in Disturbance and Recovery, or LandTrendr (KENNEDY; YANG; COHEN, 2010). LandTrendr uses a pixel-based segmentation method to investigate land trajectories by modeling time series and computing straight-line segments, returning outputs as the magnitude, duration, and timing of a land disturbance. Although first developed to detect disturbance in forest environments (KENNEDY et al., 2012), LandTrendr has become popular for other vegetation analyses, such as changes in cropland patterns (ZHU et al., 2019a), natural disturbances in mangrove areas (DE JONG et al., 2021), and post-fire vegetation recovery (BRIGHT et al., 2019).

There is an increasing need for methods and algorithms that exploit open-access Landsat time series data to provide greater disturbance map accuracies in complex, heterogeneous environments. However, most authors recognize that an optimal disturbance mapping technique does not yet exist since a single method might be not sensitive to the spatio-temporal heterogeneity of varied and continuous landscapes (HUSSAIN et al., 2013). An alternative to choosing a single method or algorithm for mapping disturbances is utilizing multiple classifier systems or a multi-algorithm ensemble. The ensemble technique for classification systems is based on multiple or committee classifiers combining their predictions. The objective is to exclude individual weakness and to benefit from particular advantages of each individual algorithm, reducing the generalization error (OZA; TUMER, 2008). In remote sensing studies, ensemble classification has produced better results than individual systems (Bruzzone et al., 2004; Rodriguez-Galiano et al., 2012; Shimizu et al., 2019; Cohen et al., 2020).

Previous research has established two varieties of ensemble architectures (also described as fusion rules by Healey et al., 2018). The first uses outputs from multiple runs of a single classifier and combines them into a final classification, and is called a homogeneous ensemble method. Random Forests (RF; Breiman, 2001) is a popular example of the homogeneous ensemble approach because it uses different instantiations of the same classifier, and combines the results to produce a final classification (BELGIU; DRĂGUŢ, 2016). Homogeneous ensemble classifiers have been widely used in many forest-related applications such as land cover classification (Gessner et al., 2013; Zhang and Yang, 2020; Schulz et al., 2021), disturbance mapping (Collins et al., 2018; Silveira et al., 2018; Bueno et al., 2019), and tree parameter modeling (Chrysafis et al., 2017; Bour et al., 2021; Jevšenak and Skudnik, 2021). The second – the heterogeneous ensemble approach, uses outputs from different classifiers and a secondary model to reclassify these outputs according to their performance in relation to a set of reference data. These heterogeneous ensembles have received more attention recently in the

disturbance mapping of vegetation, varying in the number of algorithms, vegetation indices, and spatial predictors used in the approach. Healey et al. (2018) presented a method using 'stacked generalization' with a variety of change detection algorithms and spatial predictors to map forest changes. Using two disturbance detection algorithms and three spectral indices, Hislop et al. (2019) accounted for abrupt disturbances in forested areas. Bullock et al. (2019) used three algorithms for detecting breaks in Landsat time series, while Hu et al. (2021) detected human-induced disturbances at fine scales using a heterogeneous ensemble algorithm that combines numerous time series decomposition models.

Despite their success, heterogeneous ensemble approaches have shown some practical restraints for broader implementations. These restraints include access to code for multiple algorithms, image acquisition and pre-processing costs for those requiring massive system demands, and computational power. To overcome these problems, the multispectral heterogeneous ensemble strategy combines single band/index outputs of a single algorithm into a secondary classification, reducing pre-processing costs. Some authors have demonstrated that an efficient multispectral heterogeneous ensemble using a single algorithm may provide comparable or even improved performance. For instance, Cohen et al. (2018) combined single band/index outputs of LandTrendr to map forest disturbances across the conterminous United States, while Schultz et al. (2016a) took a similar approach to fuse BFAST outputs to map deforestation in tropical areas. Both studies found that combining output maps based on different band/index increased overall mapping accuracy and consequently reduced the overestimation of disturbances.

In addition, the challenge of computational power has been met through cloud computing services such as those available on the Google Earth Engine (GEE) platform. By allowing a planetary-scale analysis of big data, GEE not only facilitates computation through parallel processing, but also enables straightforward access and management to the entire Landsat archive, alongside many other datasets (GORELICK et al., 2017). Besides a broad range of algorithms available in code editor-GEE, some methods for forest disturbance detection have been implemented recently (Kennedy et al., 2018; Hamunyela et al., 2020). These methods are supported by an extensive number of interactive applications, allowing the development of a user-friendly graphical user interface backed by Earth Engine's resources. Recent studies have shown the ability to handle big earth observation data in forest change mapping studies in national (White et al., 2017; Sebald et al., 2021), continental (MIDEKISA et al., 2017; SENF; SEIDL, 2021), and global scales (HANSEN et al., 2013).

In spite of recent advances in tools and technologies, extracting reliable and meaningful data from disturbance detection methods remains challenging. Landsat time series contain noise, even after processing, from residual clouds and cloud shadows (ZHU; WOODCOCK, 2012), variation in frequency of the satellite observations (SCHULTZ et al., 2016b), and radiometric uncertainties (SCHULTZ et al., 2016a). In addition, significant variability in environmental conditions and disturbance drivers over large areas leads to spatial-temporal heterogeneity in land surfaces and related disturbances, which results in mapping errors (SCHULTZ et al., 2016a).

The process of land regionalization into ecosystem units, also known as ecoregions, may overcome limitations on vegetation disturbance mapping imposed by spatio-temporal heterogeneity. According to Bailey (2014), land regionalization is defined as the geographical grouping of units of the Earth's surface that have common ecosystem characteristics, and can be considered a form of spatial stratification. This concept appears to be an effective way of grouping the spatial variability of the land surface since it involves a simplification of the heterogeneity in landscapes, into spatial units suitable for communication in management and research. For instance, Powers et al. (2012) revealed that the regionalization of the indicators of the physical environment explains much of the variance in many species richness. In land cover-based regionalization applications, vegetation patterns in a region can be identified as favorable or problematic for a specific management goal. Likewise, other areas can be also identified for the same purpose based on their similar spatial conditions (LONG; NELSON; WULDER, 2010).

Recently, the characterization and regionalization of vegetation has gained considerable attention in the scientific literature since agile computation (e.g., cloud-based platforms) and more accurate datasets have become available (SIMENSEN; HALVORSEN; ERIKSTAD, 2018). With regards to the regionalization of vegetation dynamics in large areas, spatial regions can be reflected by the influence of anthropogenic factors, such as fragmentation and deforestation (KUPFER; GAO; GUO, 2012). In a study by Bourbonnais et al. (2017), vegetation disturbances were modeled over time, and characterized as temporal trajectories of specific natural and anthropogenic disturbance types. There is still uncertainty, however, whether regionalization can improve the accuracy of thematic maps since no previous study has employed such procedure to map disturbances in large areas.

The objective of our study was to evaluate the effectiveness of a heterogeneous ensemble classification and data-driven regionalization for improving vegetation disturbance mapping accuracies over large areas. This paper first evaluates the performance of an ensemble

method on mapping disturbances in a heterogenous vegetated area, investigating the benefit of using multiple classifiers by exploring their particular advantages. In this case, we investigated whether a multispectral heterogeneous ensemble was significantly different against individual bands and indices. Second, we tested a land regionalization scheme based on environmental and anthropogenic information. We hypothesized that the grouping of land units and their respective variability will significantly improve the performance of disturbance mapping algorithms over traditional methods because these algorithms will be customized to each individual unit and their respectively disturbance observations, returning gains in accuracy.

This study addresses the following research questions: (1) How does a vegetation disturbance mapping method based on an ensemble premise perform over a large and heterogeneous area? (2) How does a data-driven regionalization scheme, based on environmental and anthropogenic information, affect disturbance map accuracies? (3) Can the integration of regionalization with ensemble techniques optimize the disturbance mapping over large areas?

To answer these research questions, we combined multispectral LandTrendr outputs in a RF model to map disturbances in the state of Minas Gerais (MG), southeastern Brazil. We applied an unsupervised clustering technique to perform data-driven regionalization using several datasets containing environmental and anthropogenic information. We analyze gains and losses in map accuracies produced by these approaches.

2 METHODS

Figure 1 illustrates the major methodological steps of this study. First, to perform regionalization, we created eight datasets of the entire study area that included environmental and anthropogenic information. These datasets were used to conduct data-driven regionalization that generated regions of greater homogeneity in the study area (Section 2.3 and Figure 1a). Second, after regionalization, we performed a two-stage mapping procedure (Section 2.4) using the LandTrendr and Random Forest algorithms (Figure 1b). We applied this mapping to the various regionalizations, and evaluated the performance of the ensemble method over the regionalized study area. Finally, we computed classification accuracies for all data regions, analyzing gains and losses in metrics of accuracy (Section 2.5 and Figure 1c).

Figure 1 – Flowchart of the proposed ensemble mapping approach.

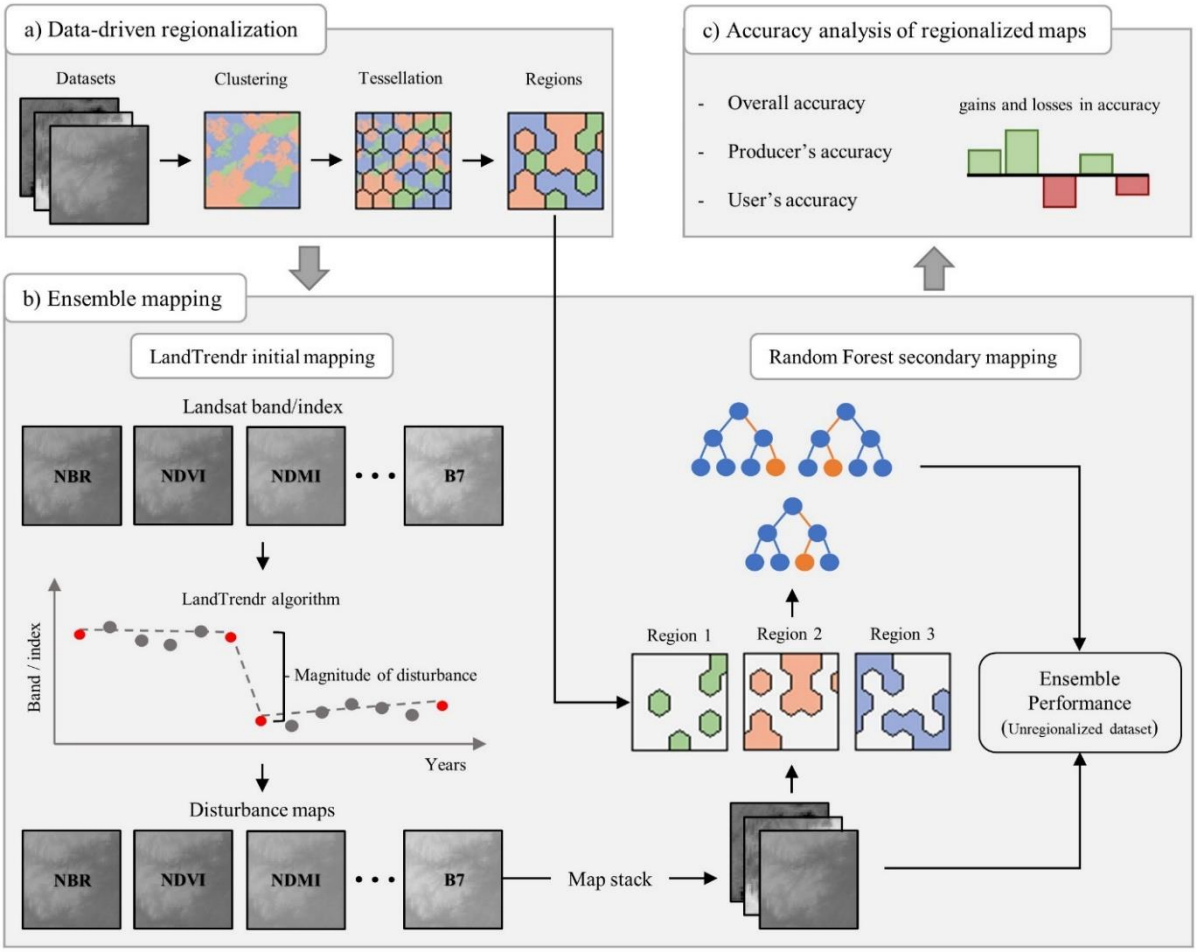

Source: Author (2022).

2.1 Study Area

The study area is the state of *Minas Gerais*, which is the fourth largest state in Brazil (Figure 2). The current anthropic scenario, combined with high levels of spatial heterogeneity over vegetation domains of Atlantic forest, savanna, and semi-arid woodland, makes this state an important area for disturbance detection studies. Its 586,528 km² are comparable in area to countries such as France and Spain. It is also the second most populous state of the country with the third largest gross domestic product (IBGE, 2010). This large area has a high heterogeneity of land covers, climatic conditions and topography. The region has three warm temperate classes of climate (Köppen-type *Cwa*, *Cwb* and *Cfa*) concentrated in the south and west of the state with dry winters and warm summers, as well as two predominant tropical classes (Köppen-type *Aw* and *Am*) (Peel et al., 2007). *Aw* predominates at the central and north regions, while *Am* occurs at the eastern region having a severe dry winter followed by a rainy summer.

The study area is represented by a mix of plains and mountain ranges (Figure 2a), with elevation largely varying from 300 to 1,200 meters above sea level. Some exceptions are visible in eastern regions exhibiting altitudes of around 100 meters, and in high mountain ranges reaching 2,891 meters in the *Pico da Bandeira* – the second highest location in Brazil. Annual rainfall (Figure 2b) and mean temperature (Figure 2c) have a gradient from southwest to northeast of the state. Southern regions receive around 2000 mm annual precipitation with higher values found at the mountain range *Serra da Mantiqueira*. Northern regions have distinct rainy periods where nearly all of their annual precipitation is accumulated in summer and ranges from 1,200 to 1,800 mm. Semi-arid regions receive the lowest amount of rainfall in the state, reaching zero mm of monthly precipitation in winter.

The high spatial variability found in *Minas Gerais* can be categorized into the three main vegetation domains: Atlantic forest, savanna, and semi-arid woodland (OLIVEIRA-FILHO et al., 2006). The Atlantic forest encompasses a large variety of tropical vegetation formations, mostly including rainforests, semi-deciduous forests, and high-altitude rangelands. This vegetation domain is a global biodiversity hotspot due its outstanding levels of species endemism (MYERS et al., 2000), thus playing an important ecological role at continental scales. The Brazilian savanna (also known as *Cerrado*) is also considered a biodiversity hotspot. These savannas present a particular combination of plant formations, compared to other savannas around the world. They range from woodland formations with high canopy density to grasslands and shrublands composed of sparse and short twisted trees (FURLEY, 1999). The third vegetation domain – semi-arid woodland – occurs in a small area in northern *Minas Gerais* (Figure 2), with vegetation characterized by a mixture of deciduous woodland formations and herbaceous understory.

A long history of deforestation has considerably changed the landscape across *Minas Gerais*. The Atlantic forest was subjected to considerable deforestation in the past, which reduced its occurrence to approximately 14% of its original area (RIBEIRO et al., 2009). Savannas and semi-arid woodlands have been subjected to more recent disturbance scenario with increasing rates of land conversion. From 1990 to 2010, 266,000 km^2 and 90,000 km^2 of vegetation was cleared in savanna and semi-arid woodland areas, respectively (Beuchle et al., 2015).

Figure 2 – The state of *Minas Gerais* and its spatial heterogeneity with regards to a) topography, b) annual precipitation (AP), and c) mean annual temperature (AMT). d) Reference dataset inset detailing an area plot and its disturbance polygons. The predominant vegetation domains are indicated in the upper portion of the figure.

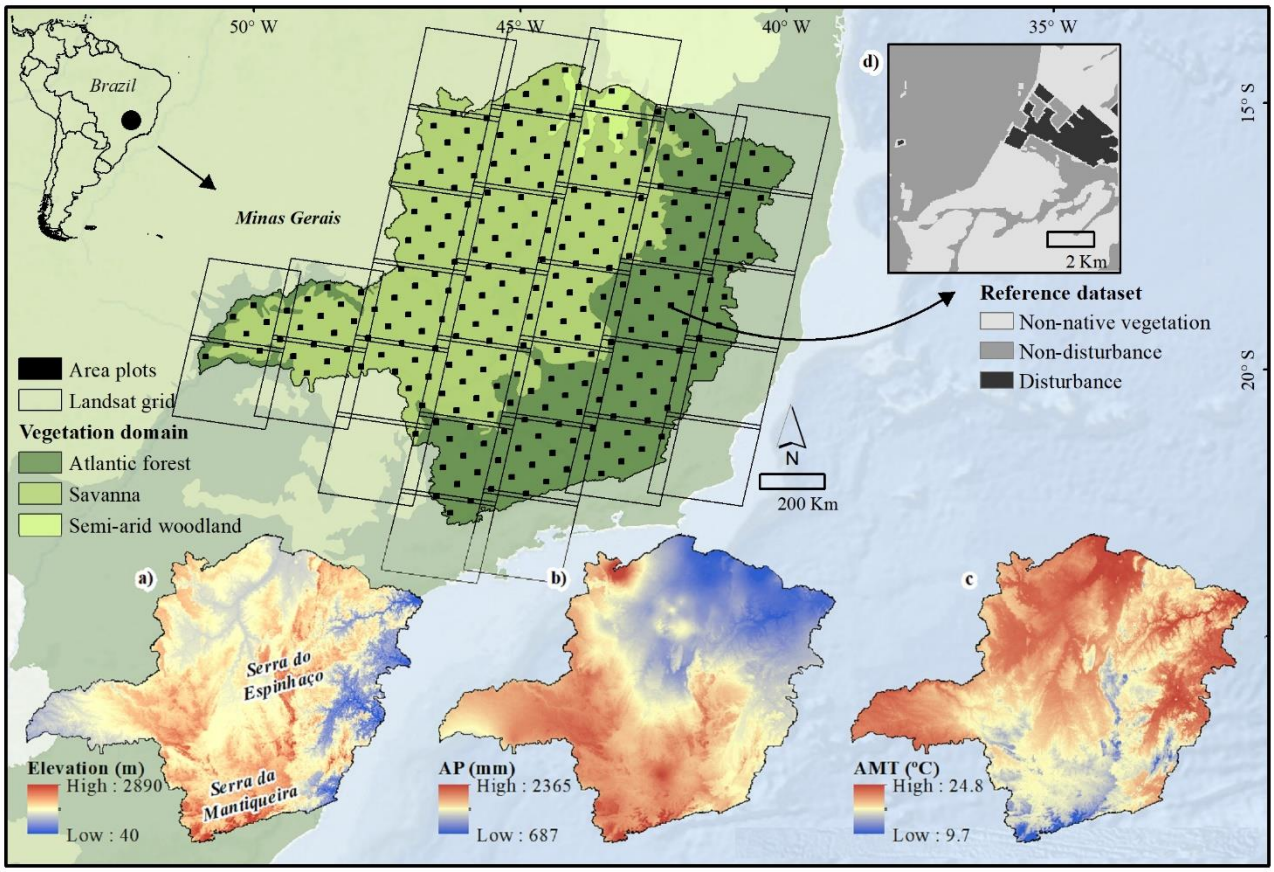

Source: Author (2022).

2.2 Reference Data

Reference data were obtained from disturbance and non-disturbance areas from 2008 to 2017. In this study, we defined disturbance as the complete removal of native vegetation at the Landsat pixel scale and its conversion into bare soil, crops, planted forests, or natural regeneration. Disturbance by fire was not considered in the data analysis. Non-disturbance areas were defined as stable vegetation covers although disturbed by seasonal differences. We delineated disturbance and non-disturbance polygons using fixed sample plots (Figure 2d). Our procedure included sample design creation, native vegetation masking, and disturbance polygon delineation.

We first used a systematic sampling grid to create fixed area plots. A total of 278 square plots of 100 km² (10 x 10 km) were placed across the entire state of *Minas Gerais*. Our sampling design represented 5% of the state and was sufficiently large to contain a suitable number of

disturbance observations (OLOFSSON et al., 2014), and dispersed enough to capture the study area's spatial heterogeneity.

Our second step was to mask the area plots with a native/non-native vegetation layer, limiting further disturbance mapping efforts to native vegetation areas only. We used the land use/land cover map of the *Cadastro Ambiental Rural* (CAR), Brazil's Rural Environmental Registry. CAR's land use/land cover classification is from 2008 and was generated using Landsat and RapidEye imagery (30-m and 5-m spatial resolution, respectively). Another important feature of the CAR's product is the native vegetation class, which encompasses forested areas as well as non-forested areas (e.g., grasslands). In addition to masking non-native vegetation, we also extracted masked water bodies from our area plots using the Global Surface Water product (PEKEL et al., 2016).

We created disturbance polygons through visual interpretation using Landsat images on the GEE platform. For each masked plot, we selected one Landsat image per year during the local dry season (June to September). By fixing this period of observation in the dry season, we increase the chances of obtaining cloud-free data and reduce the effects of vegetation phenology on disturbance detection (SILVEIRA et al., 2018b; SOUZA et al., 2020a). As auxiliary image information, we used high-resolution imagery from Google Earth, when available. Finally, area plots were systematically split into 50% for training and 50% for validation where alternate rows of plots were offset of each other. In this sampling design, we prevented training and validation observation occurring in the same area, which can overestimate mapping models. We randomly sampled 1400 pixels (700 of disturbance and 700 of non-disturbance) inside training area plots, and 600 pixels (300 per class) in validation area plots. Training pixels were used to fit further models, and validation pixels assessed the generalization error of fitted models.

2.3 Data-Driven Regionalization

We grouped the study area into regions using a data-driven method. A total of 54 numerical interval-scale variables representing climate information, terrain attributes, landscape metrics, seasonal variations, and human-related layers were acquired as multiple input combinations for the regionalization. These variables were accessed and processed in GEE and grouped into eight datasets, which included:

I. Unregionalized – This is an empty and hypothetical dataset, resulting in no further regionalization. Its purpose was for comparison with other datasets and their performances.

II. Climate – A broad-scale factor directly related to global vegetation dynamics, and an important discriminating input for ecological regionalization (METZGER et al., 2013). We obtained climate variables from WorldClim-1 database at 30-second resolution or ~ 1 km^2 (HIJMANS et al., 2005). Nineteen variables, including mean annual temperature and mean annual precipitation, represent interpolated weather data from 1950 to 2000. Climate variables were subsequently resampled to the 30 m Landsat pixel cells. For detailed information about WorldClim bioclimatic layers, consult Hijmans et al. (2005) or Table 2S in the Supplementary material.

III. Terrain – From the Shuttle Radar Topography Mission (SRTM) elevation model, we acquired version 4.0 that is hosted on GEE (JARVIS et al., 2008) and derived four terrain products: elevation, slope, aspect and hillshade. The elevation of a pixel is its height above sea level and the slope identifies the maximum change in z-value from each elevation pixel to the next. Aspect is the slope direction, which identifies the downslope direction of the maximum rate of change in value from each pixel to its neighbors. Hillshade is the shaded relief from the elevation layer by considering the illumination source angle and shadows.

IV. Seasonal – This dataset represented the seasonal response expressed by vegetation phenology. It is useful to define the distinct domains of more seasonal (savannas and semi-arid woodlands) and less seasonal (Atlantic Forest) vegetation types, which also have very different canopy characteristics for vegetation disturbance detection. We captured the inter-annual and seasonal response of vegetation using thirteen Landsat-based bands and indices (Table 1). We created two seasonal pixel-based image composites per year: one representing the wet season and another the dry season. The vegetation indices selected in Table 1 are adequate to represent canopy structure (e.g., NDVI), the strong seasonality of the savannas and semi-arid woodland vegetation of the study area (e.g., NDVI and NDMI), and the occurrence of fire in these vegetation domains (e.g., NBR). Composite images included the first cloud-free pixel available in an appropriate period to represent the season. The wet season encompasses the months of January through May, and the dry season from June through September. Annual seasonal response values were calculated as a ratio between the seasonal difference and the dry season (Equation 1), and were then reduced to the average of the study period.

$$SeasonalResponse_i = \frac{1}{n}\sum_{j=1}^{n}\left(\frac{WetSeason_{i,j} - DrySeason_{i,j}}{DrySeason_{i,j}}\right) \quad (1)$$

Where *i* indicates an individual band/index, and *j* indicates the numeric position of a year in a total of *n* years in the study period.

Table 1 – Bands and indices used in the dataset acquisition.

Band/ Index	Equation	Reference
Blue	N/A	(USGS, 2020)
Green	N/A	(USGS, 2020)
Red	N/A	(USGS, 2020)
NIR	N/A	(USGS, 2020)
SWIR1	N/A	(USGS, 2020)
SWIR2	N/A	(USGS, 2020)
NBR	(NIR - SWIR2)/(NIR + SWIR2)	(KEY; BENSON, 2006)
NDVI	(NIR - Red)/(NIR + Red)	(TUCKER, 1979)
NDMI	(NIR - SWIR1)/(NIR + SWIR1)	(WILSON; SADER, 2002)
TCB	0.2043 × B1 + 0.4158 × B2 + 0.5524 × B3 + 0.5741 × B4 + 0.3124 × B5 + 0.2303 × B7	(CRIST, 1985)
TCG	-0.1603 × Blue + -0.2819 × Green + -0.4934 × Red + 0.7940 × NIR + -0.0002 × SWIR1 + 0.1446 × SWIR2	(CRIST, 1985)
TCW	0.0315 × B1 + 0.2021 × B2 + 0.3102 × B3 + 0.1594 × B4 + -0.6806 × B5 + -0.6109 × B7	(CRIST, 1985)
TCA	Arctan(TCG/TCB)	(POWELL et al., 2010)

Source: Author (2022).

V. Landscape – We created three variables to represent some of the spatial properties of the forested landscape, which were the forest canopy density, area of forest, and forest patch density. We set as forest canopy density, the percent of tree cover from Global Forest Change (HANSEN et al., 2013), which is defined as canopy closure of vegetation taller than 5 m in height. This layer represents forest information from 2000 and we used CAR's mask to clip pixels that are established as vegetation at the beginning of the study period. Area of forest represented the forest canopy density layer accounted per area units. We set a regular hexagonal grid over the study area where each hexagon cell corresponded an area unit of 10,000 ha. This unit's shape and size were previously assessed by Ferreira et al. (2010) in order to detect forest disturbances. The forest patch density represented the number of forest patches per area unit, serving as a general index of forest fragmentation of the entire landscape mosaic. We counted isolated forest patches in each hexagon cell before generating the density of patches. Although this metric may be important to a number of ecological processes, we did not explore the area or distribution of patches.

VI. Variability – The standard deviation of band/index values for each pixel for a given date over the study period quantified the interannual variability. It reflected vegetation changes on a per year basis in the Landsat time series. To account for variability, we used annual cloud-free composite images of the dry season to calculate per-pixel standard deviation. We also calculated the variability from the thirteen band/index of Table 1.

VII. Human-related – Two variables were used to characterize human-related activities. The first variable was computed using the nighttime lights layer (NTL) from the Defense Meteorological Satellite Program – Operational Lines System, which is an indicator of infrastructure activity. We generated a 30-meter pixel size cumulative cost layer by calculating the distance from each non-zero NTL pixel. In this layer, every non-zero pixel gets a value (cost) according to the distance of the respectively target, where the higher the value, the farther the distance. The second human-related variable was created using the Brazilian roads network, extracted from OpenStreetMap data. We also calculated the cumulative cost layer for this variable by extracting distance from the main roads in the study area.

VIII. Blended – Finally, a dataset containing all previous variables. The Blended dataset has a total of 54 variables: 19 climate, 4 terrain, 13 seasonal, 3 landscape, 13 variability, and 2 human-related.

The initial pool of variables was screened to limit the potential effects of multicollinearity by calculating correlations between pairs of variables using the Pearson's correlation coefficient. We removed those with R values greater than 0.80. Following the removal of correlated variables, we performed our regionalization of the study area using each of these sets of variables, and k-means clustering. The k-means clustering algorithm identified clusters of pixels with similar data values, based on a particular set of input variables. We asset the number of clusters to three in our analysis, which divided our study area into three regions. This was based on preliminary tests, to ensure that regions created by the process were suitable for mapping disturbances. We performed our preliminary tests with various numbers of clusters, and found that the greater the number of clusters, the greater the odds that any particular region does not contain disturbances. We found three clusters that performed best in our study area. The clustering analysis itself was performed individually for each of the datasets listed above, but the Unregionalized, and only for pixels masked as native vegetation in the beginning of the period.

We performed a post-processing step on the clustering outputs to improve spatial cohesiveness across the final regions. We used a tessellation process into a regular hexagonal grid to filter small regions of pixels into larger hexagonal-based units. After summing the number of pixels allocated to the three regions inside each hexagon, we assigned these hexagons to their respective region of majority. This tessellation step reduced the "salt and pepper" speckle effects caused by small or spurious groups of pixels found in the resulting maps, which is a prominent feature of pixel-based classifications (HUSSAIN et al., 2013). This step therefore built blocks of regions rather than agglomerating pixels, creating a more unified pattern for each dataset (NOWOSAD; STEPINSKI, 2018).

Finally, we compared the regionalized maps by pairs to analyze their similarities. In this case, we considered a hexagon as the unit of analysis, combined hexagon cells of a pair of maps and computed the proportion of identical cells. This proportion returned similarity values close to 0 that represented a pair of maps fully distinct with each other while values close to 1 were considered fully similar.

2.4 Ensemble Mapping

Disturbance mapping was accomplished with a two-stage mapping step. An initial application of LandTrendr produced multiple disturbance maps from a variety of Landsat bands and indices. A secondary mapping then applied RF to the LandTrendr outputs. This is an example of a heterogeneous ensemble classification in which classifiers were pooled before a final classification decision, or a secondary classification. We tested a strategy similar to that used by Cohen et al. (2018), and assessed both algorithms in GEE.

The LandTrendr output used in this study comprised magnitude of disturbance, which reflects a significant spectral change in the yearly trajectory of a pixel. The magnitude of disturbance is an integer number that varies from 'no data' (a non-significant change not detected by the algorithm, and thereafter assigned to a zero value) to large values of magnitude. We chose to use this non-binary value to infer about disturbance profiles since we are analyzing high levels of spatial heterogeneity over vegetation domains. Algorithm parameters (e.g. max number of segments, recovery threshold, and best model proportion) were left at their default values (KENNEDY et al., 2018). Rather than optimizing parameters for the study area, our goal was to produce initial maps for a secondary classification and to simplify the workflow. In addition, recent studies have shown the insensitivity of LandTrendr parameters (RODMAN et al., 2021; YI et al., 2021). Since LandTrendr runs on a single band or spectral index, we generated thirteen distinct disturbance maps using the bands and indices listed in Table 1. While

we did not optimize LandTrendr parameter settings, neither with reference to the study area nor to the individual input bands or indices used, the expression of vegetation disturbances is itself band-dependent and is expected to cause different disturbance maps (COHEN et al., 2017). We integrated the results from all LandTrendr runs as a multispectral ensemble into a secondary classification in RF, wherein LandTrendr outputs became RF input variables. We chose RF in this study because it has become one of the most popular homogeneous ensemble classification technique (different instantiations of the same classifier) in remote sensing studies (BELGIU; DRĂGUŢ, 2016). We used training observations collected in the reference data to fit the RF model, and validation to assess the generalization error of the fitted model. We set the number of decision trees (*Ntree*) in the RF model to 500 and the number of predictors sampled at each tree node (*Mtry)* to 4.

Secondary classification allowed us to test whether an integration of LandTrendr outputs based on various Landsat bands and vegetation indices improves final disturbances mapping accuracies. To assess the performance of this ensemble strategy, we compared the method with a non-ensemble procedure or a single algorithm output. In this case, the non-ensemble method consisted of each LandTrendr disturbance map previously created, which were validated individually by confusion matrices. We assessed all thirteen disturbance maps of Table 1 against the ensemble method. All methods were applied in the Unregionalized dataset, preventing the regionalization effect.

2.5 Accuracy Analysis of Regionalized Maps

For each region created through clustering, a different RF model was computed in the secondary map step. Almost all model specs remained the same between regions, but the locations of sampled pixels varied among regions due to their dimensions and boundaries. To evaluate the performance of regionalized maps against the Unregionalized dataset (e.g., where no regionalization was performed), we analyzed gains and losses in accuracy between these maps. Since we generated three regions per dataset, we merged the respective accuracies by computing their weighted average by area, then returning a single accuracy per dataset.

We created individual confusion matrices using the validation dataset and computed overall accuracy, producer's accuracy of the disturbance class (observations characterized as disturbance in the reference dataset, but not assigned as such by the model), and user's accuracy of the disturbance class (observations detected as disturbance by the model, but not identified as such in the reference dataset).

2.6 Statistical Test

To test for statistical significance, the accuracy analysis for both ensemble performance and regionalized maps was repeated 100 times, such that each accuracy output was estimated based on a random pixel selection. In the first test, paired t-tests were performed on the individual methods against the ensemble, while in the second, tests were performed on the regionalized maps against the Unregionalized. We assessed whether the differences in accuracy averages were significant at the 5% level. The null hypothesis in the paired tests stated that the mean difference in the population equals zero. In addition, this massive repetition of accuracy analysis allowed us to obtain a more representative performance evaluation of the mapping methods.

3 RESULTS

3.1 Performance of the Ensemble Method

Accuracy results of the ensemble and non-ensemble disturbance mapping approaches are displayed in Figure 3. The ensemble method significantly outperformed the individual methods of disturbance mapping (LandTrendr bands and indices) in overall accuracy measures at the 5% level of significance. For instance, compared to the best average in individual accuracy obtained for B2 (81.0±1.7%), the ensemble method was superior (88.3±1.3%). This improvement was also expressed in producer's accuracy of the disturbance class (92.1±1.7% with the ensemble method versus 75.6±2.5% with just B2). Considering the 300 disturbance observations sampled in the reference dataset, only 24 in average were omitted (7.9% of omission error of the disturbance class) by the ensemble model. On the other hand, the rate of omission in LandTrendr ranged from 15±4 (TCB) to 168±7 (NDMI) observations. High producer's accuracy, as expressed by TCB, were related to a high area mapped as disturbance, which also caused a low user's accuracy of the disturbance class (see TCB in Figure 3c), and a high user's accuracy of the non-disturbance class (see Table 2S of the Supplementary material for details).

Our method returned a user's accuracy of the disturbance class in 85.6±1.6%, with an average of 46 non-disturbance observations included in the disturbance class. However, a few LandTrendr maps presented very high user's accuracy values as well (e.g., NDVI with 90.3±2.0%). These results were related to a small number of observations mapped as disturbance, which also caused a low producer's accuracy of the disturbance class, and a high producer's accuracy of the non-disturbance class.

Figure 3 – Comparison of accuracy measures between ensemble and non-ensemble methods.

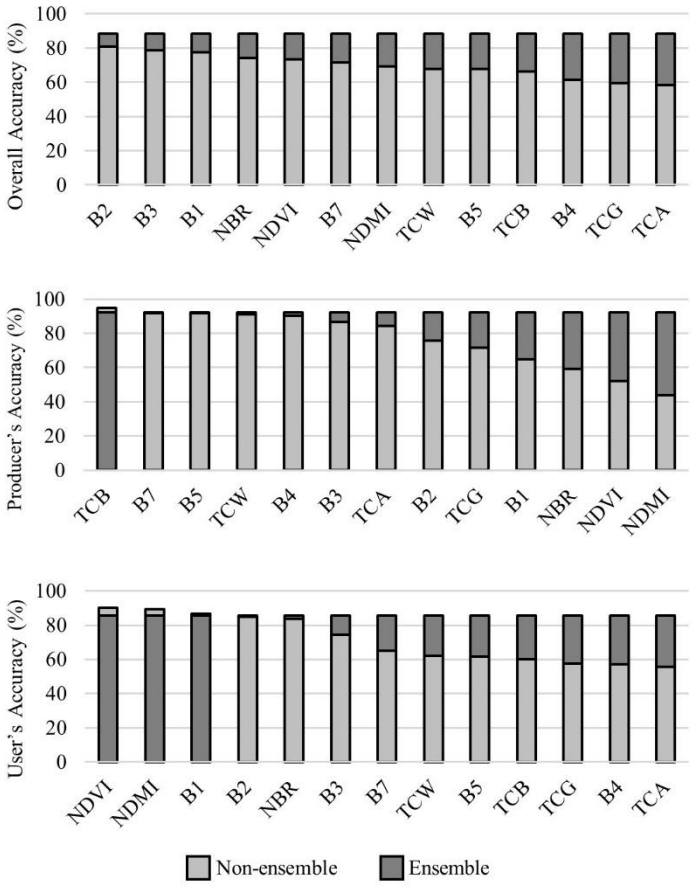

Source: Author (2022).

3.2 Regionalization

The Pearson's correlation results for the 54 numerical interval-scale variables are presented in the correlation matrix of Figure 1S (Supplementary material). There was a high correlation among variables within individual datasets, but we did not find considerable correlation between datasets. A total of 19 variables were removed from the Blended dataset by this multicollinearity screening: 10 variables from Climate and 8 from Variability.

Data-driven regionalization created seven regionalized maps of the study area (Figure 4), and the k-means algorithm seemed to return a suitable spatial clustering for analysis in this study. The tessellation process into the hexagonal grid did reduce salt and pepper effects in most of the final regionalized maps. However, the Terrain map still presented a large number of isolated hexagon units, which maintained a salt and pepper effect and resulted in smaller blocks of regions than is seen in the other regionalizations.

Similarity between maps suggests that values close to 0 represent a pair of maps fully distinct to each other while values close to 1 indicate fully similar maps (Table 2). Analyzing

the similarity among final maps, we found similarities between Blended and Climate. These results were expected because these datasets shared a considerable number of variables. The lowest similarities were observed for the Terrain map, due to the presence of residual salt and pepper effects in this map.

Table 2 – Similarity among final regionalized maps ranging from 0 to 1. (Cli = Climate, Ter = Terrain, Szn = Seasonal, Lnd = Landscape, Var = Variability, Hr = Human related, Bld = Blended).

	Cli	**Ter**	**Szn**	**Lnd**	**Var**	**Hr**
Ter	0.29					
Szn	0.43	0.17				
Lnd	0.24	0.16	0.32			
Var	0.41	0.11	0.23	0.25		
Hr	0.31	0.15	0.11	0.25	0.13	
Bld	0.61	0.35	0.46	0.49	0.32	0.33

Source: Author (2022).

Figure 4 – Regionalized maps of the study area.

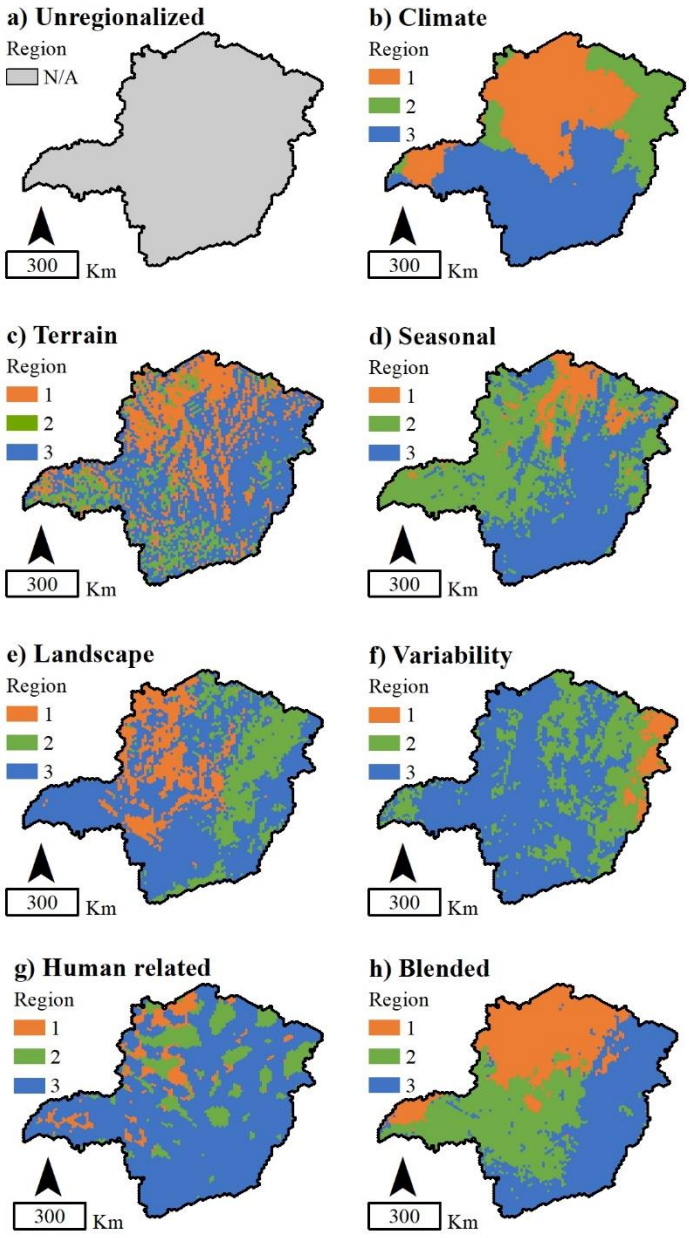

Source: Author (2022).

3.3 Accuracy Analysis of Regionalized Maps

RF modelled disturbances in eight regionalized datasets and we accounted for gains and losses in accuracy between these and the Unregionalized disturbance map (Figure 5). Climate, Seasonal, Blended, and Landscape datasets achieved the greatest overall accuracy measures in comparison to the Unregionalized dataset, as expressed by the green wedges in Figure 5a. However, no significant differences were found between overall accuracies of Landscape and Unbounded datasets. The Climate dataset had the highest overall accuracy among the datasets

(89.7±0.7% versus 88.3±1.3% for Unregionalized), while the Landscape dataset showed the lowest gain over the Unregionalized dataset (0.1%).

Figure 5b showed that producer's accuracies of the disturbance class were significantly reduced compared to the Unregionalized layer (92.1±1.7%). Nevertheless, regionalizations that produced superior overall accuracy results are worth of some attention since they still returned producer's accuracies greater than 90%. Contrary to producer's accuracies, most regionalizations surpassed the Unregionalized condition in their user's accuracies by a significant amount, with the exception of the Human-related layer that returned a loss of 0.3% in user's accuracy (red wedge in Figure 5c).

Figure 5 – Percentage of gains and losses in the data-driven regionalizations in comparison to the Unregionalized map, in (a) overall accuracy, (b) producer's accuracy, and (c) user's accuracy. Green wedges indicate a gain in accuracy, and red wedges indicate loss.

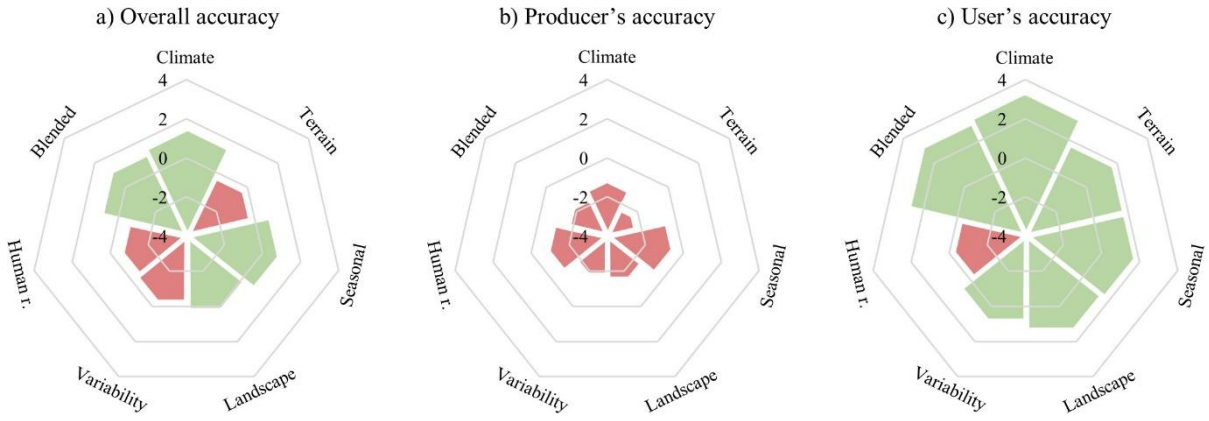

Source: Author (2022).

The top three regionalizations for improving vegetation disturbance maps were Climate, Seasonal and Blended, in terms of both overall and user's accuracies. In general, the Terrain, Human-related, and Variability regionalizations presented unsatisfactory accuracies in comparison to the others. The Human-related dataset had the poorest performance in terms of all accuracy measures. A complete accuracy analysis of regionalized maps is displayed in Table 3S of the Supplementary Material.

4 DISCUSSION

In this research, we evaluated the effectiveness of an ensemble classification and data-driven regionalization for vegetation disturbance mapping over a large area (state of *Minas Gerais*), covering portions of three distinct vegetation domains in Brazil (Atlantic forest,

savanna, and semi-arid woodland). The ensemble techniques used in this study produced very satisfactory results and the adopted data-driven regionalization increased map accuracies. In addition, our results exemplify the importance of cloud-based geospatial services like the GEE platform for optimizing analyses of large areas.

4.1 Ensemble Mapping in Large Areas

Our results showed that ensemble methods using the LandTrendr disturbance algorithm and the RF classifier produced more accurate vegetation disturbance maps than regular methods that use a single algorithm. By using a similar LandTrendr multispectral ensemble disturbance mapping to what is described here, Cohen et al. (2018) also found gains in accuracy when using multiple indices or bands, relative to secondary classification based on individual indices or bands, revealing the importance of a multispectral approach to forest disturbance detection. In that study, balanced error rates were substantively reduced while individual bands or indices produced error rates ranging from 47% to 76%, depending on the spectral band or vegetation index being used. Multispectral secondary classification produced a 30% error rate. Others have also demonstrated the value of secondary classification for forest disturbance mapping. For instance, in a study by Healey et al. (2018) using multiple classifiers and RF, error rates for ensemble approaches were reduced by 32% compared to single-algorithm approaches. Elsewhere, Hislop et al. (2019) used RF models to fuse forest change maps, raster information and pixel-based time series metrics, outperforming single algorithm/index derived maps. Schultz et al. (2016a) performed a secondary classification using a variety of vegetation indices and the BFAST Monitor algorithm. They also observed a reduction in error rates compared to those obtained from single index algorithm outputs. However, Shultz et al. (2016a) who performed disturbance mapping over tropical evergreen forests in Brazil, did not observe an improvement in overall classification accuracies. This contrasts with our results, which showed an improved overall accuracy (88.3±1.3%) in spite of the mix of very different vegetation types across three distinct vegetation domains in our study area. This heterogeneity can impact disturbance map accuracies (BUENO et al., 2020). Another important finding from our study was the low omission error of 7.9±1.7% for the disturbance class. This result is somewhat significant given the fact that the omission error is often correlated to disturbances with low magnitude as they might be associated with noise in Landsat time series. Thus, the low omission error may be taken to indicate that our ensemble method adequately mapped low magnitude disturbances. In our study, individual LandTrendr disturbance maps presented overall accuracies ranging from 58.4±1.3 to 81.0±1.7%, while their combination returned 88.3±1.3%

of accuracy. These results also support the evidence that an ensemble method, combining the prediction of a multispectral classifier, excludes individual weakness and incorporates the particular advantages of each output.

Our findings reveal the potential of ensemble methods for mapping large tropical areas, independent of the vegetation types and climate or landscape attributes. Our study area has significant variability in all these factors, and yet was mapped successfully with a multispectral, multi-algorithm secondary classification approach. One unique feature of our method was the use of both decreases and increases in spectral bands or indices as reflected in the LandTrendr magnitude of change outputs. In general, a vegetation disturbance causes band or index values to decrease, and for this reason, disturbance mapping parameters are standardized to display these as negative changes. However, positive spectral changes were essential to mapping vegetation disturbance in the non-forested portions of our study area, since disturbances in these environments commonly cause a conversion from low band or index values (e.g., native grassland) to higher values (e.g., agriculture or planted forests). Another important feature of our method was the use of the magnitude of change of disturbed pixels as RF input variables. Disturbance observations had a broad range of band/index magnitudes that can often include false or low magnitude detections, especially in non-forested areas (e.g., grasslands to bare soil). Nevertheless, by exploring the full range of disturbance magnitudes of thirteen band/index, RF better inferred about disturbance and non-disturbance observations in the training dataset.

4.2 Regionalized Maps: What do They Represent?

The regionalization process produced seven distinct vegetation disturbance maps. Some sets of regionalization variables showed within-dataset multicollinearity such as that we observed for the Climate and Variability datasets. However, the lack of strong correlations between the different regionalization datasets supports their suitability for this study. Another important component in our regionalization procedure was the tessellation of the output regions into a regular hexagonal grid, which produced blocks of regions. A similar procedure was attempted by Nowosad and Stepinski (2018) to access ecophysiographic regions over a land surface. The authors also considered the agglomeration of sites instead of pixels.

Regionalized disturbance maps that outperformed the Unregionalized map also presented patterns of homogeneity in their regionalizations. For instance, the Climate regionalization generated homogeneous blocks of regions: a distinctive region in northern state defined by high temperatures and low precipitations (Figure 4b, region one), a south region opposing the north with mid to low temperature and higher precipitation (Figure 4b, region

three), and a middle term with diverse climate variations. This regionalization produced the highest overall accuracy among our disturbance maps. The second highest overall accuracy was presented by Blended regionalization (Figure 4h), which compared to Climate, also showed the highest similarity between regionalizations. These results seem to be consistent since one quarter of Blended variables were derived from Climate dataset. Other regionalization that outperformed the Unregionalized map (Figure 4a) was the Seasonal (Figure 4d), which reflected the boundaries of vegetation domains in the state, showing the relationship between seasonality and spatial distribution of vegetation types (ADAMI et al., 2018). The last regionalization with gains in overall accuracy was the Human-related (Figure 4g), which presented patches of low human intensity across the state of *Minas Gerais*. Low intensity of these patches is expected in the southern region due to the high population density.

Our regionalized vegetation disturbance maps that produced low accuracies also showed observable and meaningful patterns in their regions. The Landscape regionalization clustered pixels according to canopy and patch density. It grouped large extensions of homogeneous savannas (Figure 4e, region one) because of their low canopy and patch density. Another distinctive region was created upon the *Serra da Mantiqueira* and *Serra do Espinhaço* mountain complexes (Figure 4e, region two). These mountains have a high canopy density while having a low number of patches. This reflects the presence of protected areas, which prevents forest fragmentation by anthropic activities. Finally, the Variability regionalization (Figure 4f) is based on standard deviations of pixel spectral trajectories over the period of study. An intriguing region created by this clustering is displayed in the eastern portion of our study area, close to the coastal zones of Brazil. This small area may be affected by cloud and resulting shadows, an intrinsic characteristic of this region. Since we only masked clouds and cloud shadows without filtering the time signature, pixel values in this region can differ through time even though not representing an anthropic disturbance.

Several factors could explain the gains in accuracy by the regionalization process. With regards to Climate regionalization (the most accurate map), region one encompassed the majority of the disturbed area accounted in the reference data. These results are in line with those of previous studies by Beuchle et al. (2015), which showed a recent disturbance scenario with increasing rates of land conversion in savanna and semi-arid woodland areas. On the other hand, region three was the largest region created while presented the lowest disturbed area of the reference data. There were a few reference plots that have not shown disturbance observations during the study period since this region encompasses a considerable number of protected areas. These observations may support the hypothesis about the relationship between

accuracy measures and disturbance frequency. Considering environmental variables, region one was mostly defined by a savanna vegetation domain, high temperatures and low precipitations, while region three grouped areas with high annual precipitation as high altitudes as well. Such conditions lead to a gradient of seasonality between those regions, which might be associated with noise in disturbance mapping procedures. Therefore, such factors grouped related disturbances in the study area, confirming our hypothesis that the grouping of land units improved the performance of disturbance mapping.

4.3 Google Earth Engine on Large-Scale Disturbance Mapping

Effective and efficient large-scale analysis using Landsat time series requires the use of high-performance computing systems and analysis-ready data. Both are made available through the GEE platform. Several studies have shown the utility of GEE to map disturbances in native vegetation such as forests (WANG et al., 2019), rangelands (XIE et al., 2019), savannas (Souza et al., 2020), and mangroves (THOMAS et al., 2017). In this study, we further exemplify the importance of GEE for big geospatial data analysis. The method applied in this study efficiently analyzed 35 Landsat scenes over a 10-year period in a short amount of processing time. The total amount of image data comprised 3,904 images, or approximately 2.2 terabytes of data, which demands a high cost of processing and time that would be unfeasible for a single desktop computer. In addition, our method not only mapped disturbances over a large area, but also performed multiple rounds of mapping, totalling 100 trials of 225 maps by one remote sensing analyst in a couple of hours (after code implementation). It should also be noted that ancillary variables were already available, whether from external sources or originally developed on the GEE platform, including climate, topographic and Global Forest Change products. These are easily accessible within the GEE environment. We also generated large amounts of data ourselves, e.g. Seasonal and Variability datasets corresponding approximately to 25 gigabytes each. Finally, a crucial GEE product for this study was the LandTrendr code implemented by Kennedy et al. (2018), which enabled a quick approach for mapping vegetation disturbances from Landsat images.

4.4 Method Limitations

There are limitations of our method that should be considered in further research, and that are largely related to the image pre-processing, algorithm calibration, and reference data. With regard to image preprocessing, Landsat pixels are filtered using two sources of information: the presence of native vegetation and the absence of clouds and cloud shadows.

Our vegetation mask was extracted from CAR land cover maps dated from 2008, which provided a valuable high-resolution, large-scale product for this study. However, it limited the start date of analysis. In future, we propose creating a reliable, custom vegetation mask within GEE, which would enable us to expand the period of analysis. With regard to the second masking step, cloud and cloud shadow contamination was reduced by the application of LandTrendr on image composites of the dry season, since the temporal segmentation it performs removes some shorter-term fluctuations that likely reflect this sort of contamination. However, cloud is still a source of noise in regions often experiencing overcast conditions such as the eastern regions of *Minas Gerais*, which are close to the coastal zones of Brazil. This source of noise was clearly influential in region one produced by the Variability regionalization, which created a particular cluster related to the frequent presence of clouds in that region.

Algorithm calibration is important for successful mapping. However, in this study, LandTrendr parameters were left at their default values regardless of the band or index used. The defaults were derived after thorough testing with NBR index in a forested area in western United States (KENNEDY et al., 2012). This parameter configuration would likely affect mapping accuracies when using other bands and indices, especially in non-forested areas. In spite of these anticipated effects, some studies have found LandTrendr to be robust to changes in parameter settings, identifying only slight differences when used in mapping mangrove dynamics (DE JONG et al., 2021). Nevertheless, we suggest a detailed parameter evaluation for disturbance mapping over such a large and heterogeneous area should be undertaken in future investigations.

Another source of uncertainty is the limited consideration of vegetation disturbances as only the complete removal of native vegetation at the Landsat pixel scale. Therefore, commission errors in the disturbance class may be related to other drivers of disturbance not accounted in the reference dataset. For instance, disturbance by fire is a very important landscape process in our study area, but it is sometimes difficult to detect, depending on the vegetation type where the event occurs and on fire frequency and severity.

5 CONCLUSION

The increasing attention on mapping and monitoring changes in vegetation over large scales has demanded reliable approaches for producing accurate disturbance maps. The present study investigated the effectiveness of ensemble classification and data-driven regionalization for the accurate mapping of vegetation disturbance at a broad scale, over a heterogeneous landscape. In a large study area based in the state of Minas Gerais, we examined the hypothesis

that data-driven regionalized maps derived from an ensemble procedure would return higher disturbance map accuracies than non-regionalized and non-ensemble maps. Results showed that our ensemble method, combining the LandTrendr algorithm and the RF classifier, outperformed non-ensemble or individual approaches for mapping vegetation disturbances. Data-driven regionalization divided the study area into regions based on seven sets of input variables, which addressed the complexity and variability of vegetation types, local climate, and topography found in the area. These regionalizations created spatial arrangements with particular ecological and anthropic characteristics, reducing the uncertainty in mapping the vegetation loss. Regionalized maps based on climate and seasonal information returned gains in accuracy and are important environmental variables when mapping disturbance with high levels of spatial heterogeneity. The integration of ensemble classification and clustering techniques has revealed great potential for the increase of end-user map accuracy and has provided important insights into the development of disturbance mapping methods in heterogeneous environments.

In order for countries to implement more effective deforestation policies, there is a need to improve the accuracy of thematic maps produced through the process of disturbance mapping, especially in areas with ongoing anthropic activities and related disturbances. The accuracies achieved with this approach represent promising opportunities toward the sufficiently accurate mapping and monitoring of vegetation disturbances. Further work could assess a more detailed LandTrendr evaluation with respect to parameter calibration, especially in areas having a large range of vegetation types and disturbances. In addition, a broader GEE implementation should be carried out to establish a fully automated approach to map disturbances accurately over the long term and large areas.

Acknowledgments: This study was financed in part by the Coordenação de Aperfeiçoamento de Pessoal de Nível Superior – Brasil (CAPES) – Finance Code 001.

6 REFERENCES

ADAMI, M. et al. Seasonality of vegetation types of South America depicted by moderate resolution imaging spectroradiometer (MODIS) time series. **International Journal of Applied Earth Observation and Geoinformation**, v. 69, p. 148–163, jul. 2018. DOI: 10.1016/j.jag.2018.02.010.

BAILEY, R. G. **Ecoregions: The Ecosystem Geography of the Oceans and Continents**. Second ed. New York: Springer New York, 2014.

BELGIU, M.; DRĂGUŢ, L. Random forest in remote sensing: A review of applications and future directions. **ISPRS Journal of Photogrammetry and Remote Sensing**, v. 114, p. 24–31, abr. 2016. DOI: 10.1016/j.isprsjprs.2016.01.011.

BEUCHLE, R. et al. Land cover changes in the Brazilian Cerrado and Caatinga biomes from 1990 to 2010 based on a systematic remote sensing sampling approach. **Applied Geography**, v. 58, p. 116–127, mar. 2015. DOI: 10.1016/j.apgeog.2015.01.017.

BOUR, B. et al. Modeling post-logging height growth of black spruce-dominated boreal forests by combining airborne LiDAR and time since harvest maps. **Forest Ecology and Management**, v. 502, p. 119697, 15 dez. 2021. DOI: 10.1016/J.FORECO.2021.119697.

BOURBONNAIS, M. L. et al. Characterizing spatial-temporal patterns of landscape disturbance and recovery in western Alberta, Canada using a functional data analysis approach and remotely sensed data. **Ecological Informatics**, v. 39, p. 140–150, 1 maio 2017. DOI: 10.1016/J.ECOINF.2017.04.010.

BREIMAN, L. Random forests. **Machine Learning**, v. 45, n. 1, p. 5–32, out. 2001. DOI: 10.1023/A:1010933404324.

BRIGHT, B. C. et al. Examining post-fire vegetation recovery with Landsat time series analysis in three western North American forest types. **Fire Ecology**, v. 15, n. 1, 1 dez. 2019. DOI: 10.1186/s42408-018-0021-9.

BRUZZONE, L.; COSSU, R.; VERNAZZA, G. Detection of land-cover transitions by combining multidate classifiers. **Pattern Recognition Letters**, v. 25, n. 13, p. 1491–1500, 1 out. 2004. DOI: 10.1016/j.patrec.2004.06.002.

BUENO, I. T. et al. Object-Based Change Detection in the Cerrado Biome Using Landsat Time Series. **Remote Sensing**, v. 11, n. 5, p. 570, 8 mar. 2019. DOI: 10.3390/rs11050570.

BUENO, I. T. et al. Spatial Agreement among Vegetation Disturbance Maps in Tropical Domains Using Landsat Time Series. **Remote Sensing**, v. 12, n. 18, p. 2948, 11 set. 2020. DOI: 10.3390/rs12182948.

BULLOCK, E. L.; WOODCOCK, C. E.; HOLDEN, C. E. Improved change monitoring using an ensemble of time series algorithms. **Remote Sensing of Environment**, n. March 2018, p.

111165, 2019. DOI: 10.1016/j.rse.2019.04.018.

CHRYSAFIS, I. et al. Estimating Mediterranean forest parameters using multi seasonal Landsat 8 OLI imagery and an ensemble learning method. **Remote Sensing of Environment**, v. 199, p. 154–166, 15 set. 2017. DOI: 10.1016/J.RSE.2017.07.018.

COHEN, W. et al. How Similar Are Forest Disturbance Maps Derived from Different Landsat Time Series Algorithms? **Forests**, v. 8, n. 4, p. 98, 26 mar. 2017. DOI: 10.3390/f8040098.

COHEN, W. B. et al. A LandTrendr multispectral ensemble for forest disturbance detection. **Remote Sensing of Environment**, v. 205, p. 131–140, 1 fev. 2018. DOI: 10.1016/J.RSE.2017.11.015.

COHEN, W. B. et al. Diversity of Algorithm and Spectral Band Inputs Improves Landsat Monitoring of Forest Disturbance. **Remote Sensing**, v. 12, n. 10, p. 1673, 23 maio 2020. DOI: 10.3390/rs12101673.

COLLINS, L. et al. The utility of Random Forests for wildfire severity mapping. **Remote Sensing of Environment**, v. 216, p. 374–384, 1 out. 2018. DOI: 10.1016/j.rse.2018.07.005.

CRIST, E. P. A TM Tasseled Cap equivalent transformation for reflectance factor data. **Remote Sensing of Environment**, v. 17, n. 3, p. 301–306, 1 jun. 1985. DOI: 10.1016/0034-4257(85)90102-6.

DE JONG, S. M. et al. Mapping mangrove dynamics and colonization patterns at the Suriname coast using historic satellite data and the LandTrendr algorithm. **International Journal of Applied Earth Observation and Geoinformation**, v. 97, p. 102293, 1 maio 2021. DOI: 10.1016/j.jag.2020.102293.

FERREIRA, N. C.; FERREIRA, L. G.; HUETE, A. R. Assessing the response of the MODIS vegetation indices to landscape disturbance in the forested areas of the legal Brazilian Amazon. **International Journal of Remote Sensing**, v. 31, n. 3, p. 745–759, 17 fev. 2010. DOI: 10.1080/01431160902897817.

FURLEY, P. A. The nature and diversity of neotropical savanna vegetation with particular reference to the Brazilian cerrados. **Global Ecology and Biogeography**, v. 8, n. 3–4, p. 223–241, 1 maio 1999. DOI: 10.1046/j.1466-822X.1999.00142.x.

GESSNER, U. et al. Estimating the fractional cover of growth forms and bare surface in savannas. A multi-resolution approach based on regression tree ensembles. **Remote Sensing of Environment**, v. 129, p. 90–102, 15 fev. 2013. DOI: 10.1016/J.RSE.2012.10.026.

GORELICK, N. et al. Google Earth Engine: Planetary-scale geospatial analysis for everyone. **Remote Sensing of Environment**, v. 202, p. 18–27, dez. 2017. DOI: 10.1016/j.rse.2017.06.031.

HAMUNYELA, E. et al. Implementation of BFASTmonitor Algorithm on Google Earth Engine to support large-area and sub-annual change monitoring using earth observation data. **Remote Sensing**, v. 12, n. 18, p. 2953, 11 set. 2020. DOI: 10.3390/RS12182953.

HANSEN, M. C. et al. High-Resolution Global Maps of 21st-Century Forest Cover Change. **Science**, v. 342, n. 6160, p. 850–853, 15 nov. 2013. DOI: 10.1126/science.1244693.

HEALEY, S. P. et al. Mapping forest change using stacked generalization: An ensemble approach. **Remote Sensing of Environment**, v. 204, p. 717–728, 2018. DOI: 10.1016/j.rse.2017.09.029.

HERMOSILLA, T. et al. Disturbance-Informed Annual Land Cover Classification Maps of Canada's Forested Ecosystems for a 29-Year Landsat Time Series. **Canadian Journal of Remote Sensing**, v. 44, n. 1, p. 67–87, 2 jan. 2018. DOI: 10.1080/07038992.2018.1437719.

HIJMANS, R. J. et al. Very high resolution interpolated climate surfaces for global land areas. **International Journal of Climatology**, v. 25, n. 15, p. 1965–1978, 1 dez. 2005. DOI: 10.1002/joc.1276.

HISLOP, S. et al. A fusion approach to forest disturbance mapping using time series ensemble techniques. **Remote Sensing of Environment**, v. 221, p. 188–197, fev. 2019. DOI: 10.1016/j.rse.2018.11.025.

HU, T. et al. Mapping fine-scale human disturbances in a working landscape with Landsat time series on Google Earth Engine. **ISPRS Journal of Photogrammetry and Remote Sensing**, v. 176, p. 250–261, 1 jun. 2021. DOI: 10.1016/J.ISPRSJPRS.2021.04.008.

HUSSAIN, M. et al. Change detection from remotely sensed images: From pixel-based to object-based approaches. **ISPRS Journal of Photogrammetry and Remote Sensing**, v. 80, p.

91–106, jun. 2013. DOI: 10.1016/j.isprsjprs.2013.03.006.

INSTITUTO BRASILEIRO DE GEOGRAFIA E ESTATÍSTICA. Censo demográfico. Rio de Janeiro, 2010. Disponível em: https://censo2010.ibge.gov.br/sinopse/. Acesso em: 20 out. 2020.

JARVIS, A. et al. **Hole-filled SRTM for the globe version 4.** CGIAR Consortium for Spatial Information, 2008. Disponível em: http://srtm.csi.cgiar.org. Acesso em 20 out. 2020.

JEVŠENAK, J.; SKUDNIK, M. A random forest model for basal area increment predictions from national forest inventory data. **Forest Ecology and Management**, v. 479, p. 118601, 1 jan. 2021. DOI: 10.1016/J.FORECO.2020.118601.

KENNEDY, R. et al. Implementation of the LandTrendr Algorithm on Google Earth Engine. **Remote Sensing**, v. 10, n. 5, p. 691, 1 maio 2018. DOI: 10.3390/rs10050691.

KENNEDY, R. E. et al. Spatial and temporal patterns of forest disturbance and regrowth within the area of the Northwest Forest Plan. **Remote Sensing of Environment**, v. 122, p. 117–133, 1 jul. 2012. DOI: 10.1016/j.rse.2011.09.024.

KENNEDY, R. E.; YANG, Z.; COHEN, W. B. Detecting trends in forest disturbance and recovery using yearly Landsat time series: 1. LandTrendr — Temporal segmentation algorithms. **Remote Sensing of Environment**, v. 114, n. 12, p. 2897–2910, 15 dez. 2010. DOI: 10.1016/j.rse.2010.07.008.

KEY, C. H.; BENSON, N. C. Landscape assessment: ground measure of severity, the composite burn index; and remote sensing of severity, the normalized burn ratio. In: **FIREMON: Fire effects monitoring and inventory system. Gen. Tech. Rpt. RMRS-GTR-164-CD: LAI-15**. Ogden: USDA Forest Service, Rocky Mountain Research Station, 2006. p. 51.

KUPFER, J. A.; GAO, P.; GUO, D. Regionalization of forest pattern metrics for the continental United States using contiguity constrained clustering and partitioning. **Ecological Informatics**, v. 9, p. 11–18, 1 maio 2012. DOI: 10.1016/J.ECOINF.2012.02.001.

LONG, J.; NELSON, T.; WULDER, M. Regionalization of landscape pattern indices using multivariate cluster analysis. **Environmental management**, v. 46, n. 1, p. 134–142, jul. 2010. DOI: 10.1007/S00267-010-9510-6.

METZGER, M. J. et al. A high-resolution bioclimate map of the world: a unifying framework

for global biodiversity research and monitoring. **Global Ecology and Biogeography**, v. 22, n. 5, p. 630–638, maio 2013. DOI: 10.1111/geb.12022.

MIDEKISA, A. et al. Mapping land cover change over continental Africa using Landsat and Google Earth Engine cloud computing. **PLOS ONE**, v. 12, n. 9, p. e0184926, 27 set. 2017. DOI: 10.1371/journal.pone.0184926.

MYERS, N. et al. Biodiversity hotspots for conservation priorities. **Nature**, v. 403, n. 6772, p. 853–858, 24 fev. 2000. DOI: 10.1038/35002501.

NOWOSAD, J.; STEPINSKI, T. F. Towards machine ecoregionalization of Earth's landmass using pattern segmentation method. **International Journal of Applied Earth Observation and Geoinformation**, v. 69, p. 110–118, jul. 2018. DOI: 10.1016/j.jag.2018.03.004.

OLIVEIRA-FILHO, A. T. et al. Workshop: Definição e delimitação de domínios e subdomínios das paisagens naturais do Estado de Minas Gerais. In: **Mapeamento e inventário da flora nativa e dos reflorestamentos de Minas Gerais**. Lavras: Editora UFLA, 2006. p. 21–35.

OLOFSSON, P. et al. Good practices for estimating area and assessing accuracy of land change. **Remote Sensing of Environment**, v. 148, n. October, p. 42–57, maio 2014. DOI: 10.1016/j.rse.2014.02.015.

OZA, N. C.; TUMER, K. Classifier ensembles: Select real-world applications. **Information Fusion**, v. 9, n. 1, p. 4–20, jan. 2008. DOI: 10.1016/j.inffus.2007.07.002.

PEEL, M. C.; FINLAYSON, B. L.; MCMAHON, T. A. Updated world map of the Köppen-Geiger climate classification. **Hydrology and Earth System Sciences**, v. 11, n. 5, p. 1633–1644, 11 out. 2007. DOI: 10.5194/hess-11-1633-2007.

PEKEL, J. F. et al. High-resolution mapping of global surface water and its long-term changes. **Nature**, v. 540, n. 7633, p. 418–422, 15 dez. 2016. DOI: 10.1038/nature20584.

POWELL, S. L. et al. Quantification of live aboveground forest biomass dynamics with Landsat time-series and field inventory data: A comparison of empirical modeling approaches. **Remote Sensing of Environment**, v. 114, n. 5, p. 1053–1068, 17 maio 2010. DOI: 10.1016/j.rse.2009.12.018.

POWERS, R. P. et al. A remote sensing approach to biodiversity assessment and regionalization

of the Canadian boreal forest. **Progress in Physical Geography**, v. 37, n. 1, p. 36–62, 24 ago. 2013. DOI: 10.1177/0309133312457405.

RIBEIRO, M. C. et al. The Brazilian Atlantic Forest: How much is left, and how is the remaining forest distributed? Implications for conservation. **Biological Conservation**, v. 142, n. 6, p. 1141–1153, jun. 2009. DOI: 10.1016/j.biocon.2009.02.021.

RODMAN, K. C. et al. Disturbance detection in landsat time series is influenced by tree mortality agent and severity, not by prior disturbance. **Remote Sensing of Environment**, v. 254, p. 112244, 1 mar. 2021. DOI: 10.1016/J.RSE.2020.112244.

RODRIGUEZ-GALIANO, V. F. et al. An assessment of the effectiveness of a random forest classifier for land-cover classification. **ISPRS Journal of Photogrammetry and Remote Sensing**, v. 67, n. 1, p. 93–104, 1 jan. 2012. DOI: 10.1016/j.isprsjprs.2011.11.002.

SCHULTZ, M. et al. Error Sources in Deforestation Detection Using BFAST Monitor on Landsat Time Series Across Three Tropical Sites. **IEEE Journal of Selected Topics in Applied Earth Observations and Remote Sensing**, v. 9, n. 8, p. 3667–3679, 1 ago. 2016a. DOI: 10.1109/JSTARS.2015.2477473.

SCHULTZ, M. et al. Performance of vegetation indices from Landsat time series in deforestation monitoring. **International Journal of Applied Earth Observation and Geoinformation**, v. 52, p. 318–327, out. 2016b. DOI: 10.1016/j.jag.2016.06.020.

SCHULZ, D. et al. Land use mapping using Sentinel-1 and Sentinel-2 time series in a heterogeneous landscape in Niger, Sahel. **ISPRS Journal of Photogrammetry and Remote Sensing**, v. 178, p. 97–111, 1 ago. 2021. DOI: 10.1016/J.ISPRSJPRS.2021.06.005.

SEBALD, J.; SENF, C.; SEIDL, R. Human or natural? Landscape context improves the attribution of forest disturbances mapped from Landsat in Central Europe. **Remote Sensing of Environment**, v. 262, p. 112502, 1 set. 2021. DOI: 10.1016/j.rse.2021.112502.

SENF, C.; SEIDL, R. Mapping the forest disturbance regimes of Europe. **Nature Sustainability**, v. 4, n. 1, p. 63–70, 1 jan. 2021. DOI: 10.1038/s41893-020-00609-y.

SHIMIZU, K. et al. A comprehensive evaluation of disturbance agent classification approaches: Strengths of ensemble classification, multiple indices, spatio-temporal variables, and direct

prediction. **ISPRS Journal of Photogrammetry and Remote Sensing**, v. 158, p. 99–112, dez. 2019. DOI: 10.1016/j.isprsjprs.2019.10.004.

SILVEIRA, E. M. O. et al. Using spatial features to reduce the impact of seasonality for detecting tropical forest changes from landsat time series. **Remote Sensing**, v. 10, n. 6, p. 808, 23 maio 2018b. DOI: 10.3390/rs10060808.

SIMENSEN, T.; HALVORSEN, R.; ERIKSTAD, L. Methods for landscape characterisation and mapping: A systematic review. **Land Use Policy**, v. 75, p. 557–569, jun. 2018. DOI: 10.1016/j.landusepol.2018.04.022.

SOUZA, A. A. et al. Dynamics of savanna clearing and land degradation in the newest agricultural frontier in Brazil. **GIScience and Remote Sensing**, v. 57, n. 7, p. 965–984, 2 out. 2020a. DOI: 10.1080/15481603.2020.1835080.

THOMAS, N. et al. Distribution and drivers of global mangrove forest change, 1996–2010. **PLOS ONE**, v. 12, n. 6, p. e0179302, 8 jun. 2017. DOI: 10.1371/journal.pone.0179302.

TUCKER, C. J. Red and photographic infrared linear combinations for monitoring vegetation. **Remote Sensing of Environment**, v. 8, n. 2, p. 127–150, maio 1979. DOI: 10.1016/0034-4257(79)90013-0.

USGS. **Landsat 4-7 Collection 1 (C1) Surface Reflectance (LEDAPS) Product Guide (Version 3.0)**U.S. Geological Survey, 2020. Disponível em: https://www.usgs.gov/media/files/landsat-4-7-collection-1-surface-reflectance-code-ledaps-product-guide. Acesso em: 20 out. 2020.

WANG, Y. et al. Mapping tropical disturbed forests using multi-decadal 30 m optical satellite imagery. **Remote Sensing of Environment**, v. 221, n. April 2018, p. 474–488, 1 fev. 2019. DOI: 10.1016/j.rse.2018.11.028.

WHITE, J. C. et al. A nationwide annual characterization of 25 years of forest disturbance and recovery for Canada using Landsat time series. **Remote Sensing of Environment**, v. 194, p. 303–321, jun. 2017. DOI: 10.1016/j.rse.2017.03.035.

WILSON, E. H.; SADER, S. A. Detection of forest harvest type using multiple dates of Landsat TM imagery. **Remote Sensing of Environment**, v. 80, n. 3, p. 385–396, 1 jun. 2002. DOI:

10.1016/S0034-4257(01)00318-2.

WULDER, M. A. et al. Opening the archive: How free data has enabled the science and monitoring promise of Landsat. **Remote Sensing of Environment**, v. 122, p. 2–10, jul. 2012. DOI: 10.1016/j.rse.2012.01.010.

XIE, Z. et al. Using Landsat observations (1988–2017) and Google Earth Engine to detect vegetation cover changes in rangelands - A first step towards identifying degraded lands for conservation. **Remote Sensing of Environment**, v. 232, p. 111317, 1 out. 2019. DOI: 10.1016/j.rse.2019.111317.

YI, Z. et al. Long-term Landsat monitoring of mining subsidence based on spatiotemporal variations in soil moisture: A case study of Shanxi Province, China. **International Journal of Applied Earth Observation and Geoinformation**, v. 102, p. 102447, 1 out. 2021. DOI: 10.1016/J.JAG.2021.102447.

ZHANG, F.; YANG, X. Improving land cover classification in an urbanized coastal area by random forests: The role of variable selection. **Remote Sensing of Environment**, v. 251, p. 112105, 15 dez. 2020. DOI: 10.1016/j.rse.2020.112105.

ZHU, L. et al. Long-Term Monitoring of Cropland Change near Dongting Lake, China, Using the LandTrendr Algorithm with Landsat Imagery. **Remote Sensing**, v. 11, n. 10, p. 1234, 24 maio 2019a. DOI: 10.3390/rs11101234.

ZHU, Z.; WOODCOCK, C. E. Object-based cloud and cloud shadow detection in Landsat imagery. **Remote Sensing of Environment**, v. 118, p. 83–94, mar. 2012. DOI: 10.1016/j.rse.2011.10.028.

7 SUPPLEMENTARY MATERIAL

Figure 1S – Correlation matrix of the 54 variables and their respectively datasets. See Table 1S for legend details.

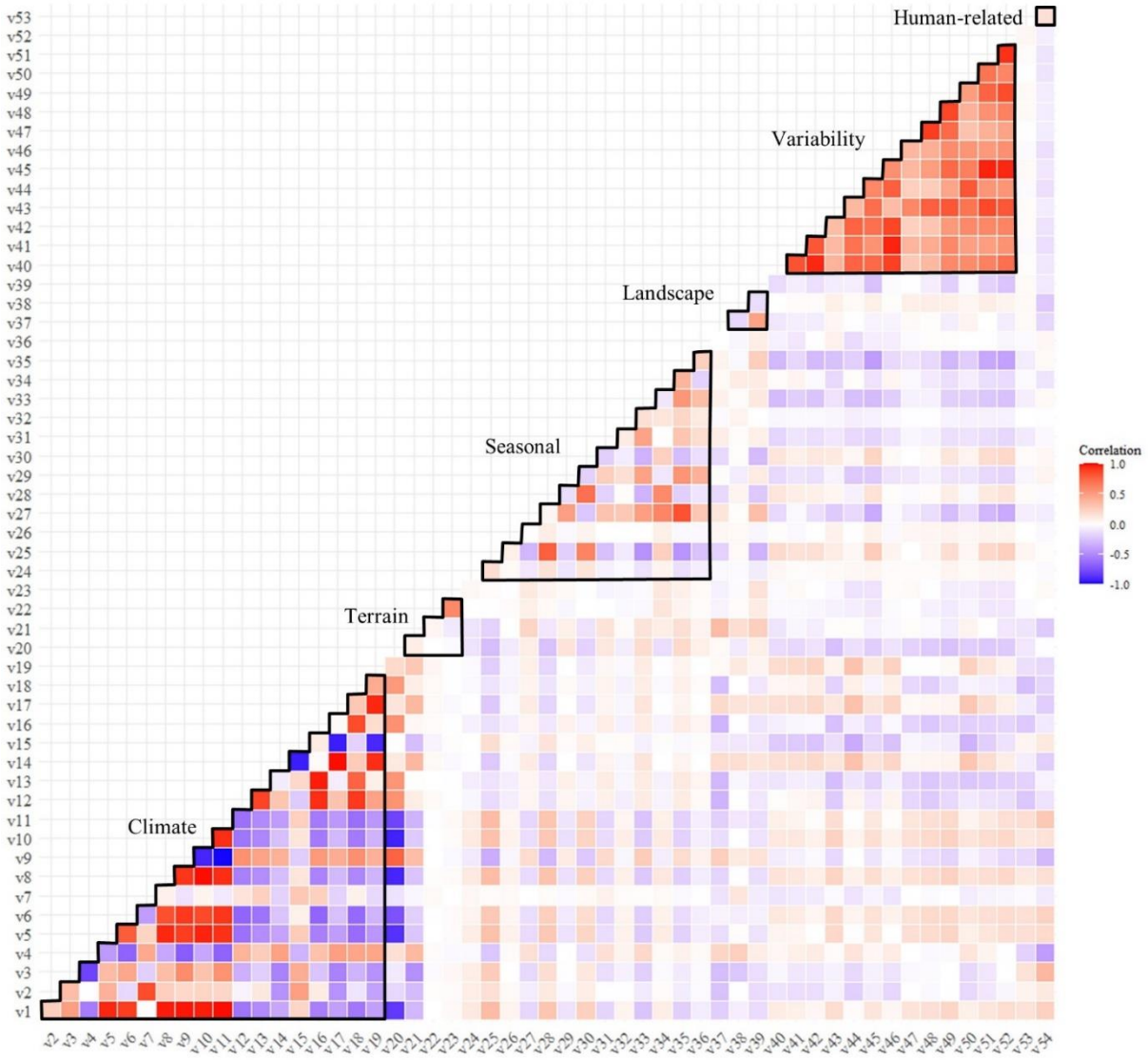

Source: Author (2022).

Table 1S – The 54 variables and their respectively codes used in dataset acquisition.

Code	Variable	Code	Variable
	Climate		*Seasonal*
v1	Annual Mean Temperature	v29	TCB
v2	Mean Diurnal Range (Mean of monthly (max temp - min temp))	v30	TCW
v3	Isothermality (v2/v7 * 100)	v31	B1
v4	Temperature Seasonality (std * 100)	v32	B2
v5	Max Temperature of Warmest Month	v33	B3
v6	Min Temperature of Coldest Month	v34	B4
v7	Temperature Annual Range (v5 - v6)	v35	B5
v8	Mean Temperature of Wettest Quarter	v36	B7
v9	Mean Temperature of Driest Quarter		*Landscape*
v10	Mean Temperature of Warmest Quarter	v37	Area of forest
v11	Mean Temperature of Coldest Quarter	v38	Patch density
v12	Annual Precipitation	v39	Canopy density
v13	Precipitation of Wettest Month		*Variability*
v14	Precipitation of Driest Month	v40	NBR
v15	Precipitation Seasonality (Coefficient of Variation)	v41	NDVI
v16	Precipitation of Wettest Quarter	v42	NDSI
v17	Precipitation of Driest Quarter	v43	NDMI
v18	Precipitation of Warmest Quarter	v44	TCG
v19	Precipitation of Coldest Quarter	v45	TCB
	Terrain	v46	TCW
v20	Elevation	v47	B1
v21	Slope	v48	B2
v22	Aspect	v49	B3
v23	Hillshade	v50	B4
	Seasonal (seasonal response)	v51	B5
v24	NBR	v52	B7
v25	NDVI		*Human related*
v26	NDSI	v53	NTL
v27	NDMI	v54	Roads
v28	TCG		

Source: Author (2022).

Table 2S – Complete accuracy averages individuals and ensemble method. TP = true positive; FP = false positive; FN = false negative; TN = true negative; OA = overall accuracy; OE* = overall error; PA = producer's accuracy; OE = omission error; UA = user's accuracy; and CE = commission error.

Method (Rank)	Observation averages				OA (%)	OE* (%)	Disturbance (%)				Non-disturbance (%)			
	TP	FN	FP	TN			PA	OE	UA	CE	PA	OE	UA	CE
Ensemble (1º)	254±6	46±6	24±5	276±5	88.3±1.3	11.7±1.3	92.1±1.7	7.9±1.7	85.6±1.6	14.4±1.6	84.5±2.0	15.5±2.0	91.5±1.6	8.5±1.6
NBR (5º)	266±6	34±6	122±8	178±8	74.0±1.6	26.0±1.6	59.4±2.5	40.6±2.5	83.9±2.4	16.1±2.4	88.6±1.9	11.4±1.9	68.6±1.4	31.4±1.4
NDVI (6º)	283±4	17±4	143±7	157±7	73.3±1.4	26.7±1.4	52.3±2.5	47.7±2.5	90.3±2.0	9.7±2.0	94.3±1.2	5.7±1.2	66.4±1.2	33.6±1.2
NDMI (8º)	284±3	16±3	168±7	132±7	69.3±1.3	30.7±1.3	43.9±2.4	56.1±2.4	89.2±2.2	10.8±2.2	94.7±1.1	5.3±1.1	62.8±1.0	37.2±1.0
TCB (11º)	112±7	188±7	15±4	285±4	66.1±1.4	33.9±1.4	94.9±1.3	5.1±1.3	60.2±1.0	39.8±1.0	37.4±2.3	62.6±2.3	88.0±2.8	12.0±2.8
TCG (13º)	142±7	158±7	86±8	215±8	59.3±1.7	40.7±1.7	71.5±2.7	28.5±2.7	57.5±1.4	42.5±1.4	47.2±2.5	52.8±2.5	62.4±2.4	37.6±2.4
TCW (9º)	133±10	167±10	27±5	273±5	67.7±1.8	32.3±1.8	91.1±1.8	8.9±1.8	62.1±1.4	37.9±1.4	44.3±3.3	55.7±3.3	83.3±3.0	16.7±3.0
TCA (14º)	98±6	202±6	48±5	253±5	58.4±1.3	41.6±1.3	84.2±1.7	15.8±1.7	55.6±0.9	44.4±0.9	32.7±2.1	67.3±2.1	67.4±2.7	32.6±2.7
B1 (4º)	270±5	30±5	106±8	194±8	77.4±1.6	22.6±1.6	64.8±2.7	35.2±2.7	86.7±2.2	13.3±2.2	90.0±1.8	10.0±1.8	71.9±1.5	28.1±1.5
B2 (2º)	259±6	41±6	73±7	227±7	81.0±1.7	19.0±1.7	75.6±2.5	24.4±2.5	84.8±2.2	15.2±2.2	86.4±2.1	13.6±2.1	78.0±1.8	22.0±1.8
B3 (3º)	211±9	89±9	40±6	260±6	78.4±1.6	21.6±1.6	86.6±1.9	13.4±1.9	74.5±1.8	25.5±1.8	70.2±2.9	29.8±2.9	84.0±1.9	16.0±1.9
B4 (12º)	98±7	202±7	29±5	271±5	61.5±1.6	38.5±1.6	90.2±1.7	9.8±1.7	57.3±1.1	42.7±1.1	32.7±2.5	67.3±2.5	77.0±3.4	23.0±3.4
B5 (10º)	130±10	170±10	25±5	275±5	67.5±1.9	32.5±1.9	91.7±1.6	8.3±1.6	61.9±1.5	38.1±1.5	43.4±3.5	56.6±3.5	84.0±2.9	16.0±2.9
B7 (7º)	153±9	147±9	24±5	276±5	71.4±1.8	28.6±1.8	91.9±1.7	8.1±1.7	65.2±1.6	34.8±1.6	51.0±3.1	49.0±3.1	86.3±2.7	13.7±2.7

Source: Author (2022).

Table 3S – Complete accuracy averages of regionalized maps and their respectively standard deviations. TP = true positive; FP = false positive; FN = false negative; TN = true negative; OA = overall accuracy; OE* = overall error; PA = producer's accuracy; OE = omission error; UA = user's accuracy; and CE = commission error.

	Observation averages						Disturbance (%)				Non-disturbance (%)			
Method (rank)	**TP**	**FN**	**FP**	**TN**	**OA (%)**	**OE* (%)**	**PA**	**OE**	**UA**	**CE**	**PA**	**OE**	**UA**	**CE**
Unbounded (5º)	254±6	46±6	24±5	276±5	88.3±1.3	11.7±1.3	92.1±1.7	7.9±1.7	85.6±1.6	14.4±1.6	84.5±2.0	15.5±2.0	91.5±1.6	8.5±1.6
Climate (1º)	266±4	34±4	27±3	273±3	89.7±0.7	10.3±0.7	90.8±1.1	9.2±1.1	89.0±1.0	11.0±1.0	88.6±1.2	11.4±1.2	90.6±1.0	9.4±1.0
Terrain (6º)	260±4	40±4	31±4	269±4	88.1±0.8	11.9±0.8	89.6±1.4	10.4±1.4	87.3±1.0	12.7±1.0	86.7±1.2	13.3±1.2	89.3±1.2	10.7±1.2
Seasonal (3º)	261±4	39±4	26±3	274±3	89.2±0.7	10.8±0.7	91.5±0.9	8.5±0.9	87.6±1.1	12.4±1.1	87.0±1.4	13.0±1.4	91.1±0.8	8.9±0.5
Landscape (4º)	259±5	41±5	29±4	271±4	88.4±0.8	11.6±0.8	90.4±1.2	9.6±1.2	87.0±1.3	13.0±1.3	86.4±1.5	13.6±1.5	90.0±1.1	10.0±1.1
Variability (7º)	257±5	43±5	29±4	271±4	88.0±0.8	12.0±0.8	90.2±1.2	9.8±1.2	86.4±1.2	13.6±1.2	85.7±1.5	14.3±1.5	89.8±1.1	10.2±1.1
Human r. (8º)	253±5	47±5	27±4	273±4	87.7±1.1	12.3±1.1	91.1±1.3	8.9±1.3	85.3±1.4	14.7±1.4	84.3±1.7	15.7±1.7	90.5±1.3	9.5±1.3
Blended (2º)	265±4	35±4	29±4	271±4	89.3±0.7	10.7±0.7	90.2±1.3	9.8±1.3	88.7±1.0	11.3±1.0	88.4±1.2	11.6±1.2	88.6±1.1	11.4±1.1

Source: Author (2022).

ARTICLE 3 – USING SPATIAL PREDICTOR VARIABLES TO IMPROVE LAND COVER CHANGE DETECTION FROM LANDTRENDR

Inacio Thomaz Bueno [1*], Eduarda Martiniano de Oliveira Silveira [2], José Márcio de Mello [1], Marcelo Ângelo Cirillo [3], Fausto Weimar Acerbi Junior [1]

[1] *Department of Forest Science, Federal University of Lavras, Lavras 37200-000, Brazil;*
[2] *SILVIS Lab, Department of Forest and Wildlife Ecology, University of Wisconsin-Madison, Madison WI 53706, USA.*
[3] *Department of Statistics, Federal University of Lavras, Lavras 37200-000, Brazil;*

***** Corresponding author email: inaciotbueno@gmail.com

Publication status: In preparation to submission in the **GIScience and Remote Sensing**

Abstract: Mapping the land-use and land-cover changes in seasonal biomes is of vital importance for both environmental monitoring and economic activities. Remote sensing techniques and algorithms, such as the LandTrendr have become increasingly indispensable for mapping and monitoring changes in vegetation; however, they are still sensitive to time series noise and changes caused by phenology in vegetation that are erroneous detected as change. Spatial predictors have the advantage of reducing seasonal variations; thus, this study evaluated the accuracy of predictor variables derived from the LandTrendr algorithm and semivariogram parameters for mapping and characterizing land cover changes in seasonal areas of Brazilian savannas and semi-arid woodland biomes. We defined three land cover change classes: non-change, vegetation loss, and post-change, then created three datasets: LandTrendr, Semivariogram, and a combination set Blended. Object-based image analysis defined image-objects, which were classified and have their accuracies assessed based on datasets and classification designs. A qualitative method through visual interpretation of semivariogram variables was used to infer patterns of land cover change. Results showed that LandTrendr significantly outperformed Semivariogram predictor variables for mapping land cover changes, reaching 12.0% of gain in overall accuracy. Therefore, using a blend set of these datasets, we found a significant increase ranging from 2.8 to 4.0% in map accuracies. Our study also indicated that the semivariogram variables faithfully captured patterns of vegetation loss and recovery. The knowledge of these relationships provided important insights into the role of predictor variables for mapping and monitoring vegetation change in seasonal biomes.

Keywords: remote sensing, NDVI, vegetation phenology, semivariogram, object-based image analysis.

1 INTRODUCTION

Land-use and land-cover changes in vegetation ecosystems, whether natural or human-induced, affect the spatial and temporal availability of natural resources (PITTOCK et al., 2015). The identification of land-use and land-cover changes areas is of vital importance as they are linked to economic activities, such as employment, governmental investments and funding, the construction of irrigation infrastructure, or product supply for local or international markets (TRUMBORE; BRANDO; HARTMANN, 2015).

The Brazilian savanna (also known as Cerrado) and semi-arid woodland (also known as Caatinga), which both together cover approximately 35% of the Brazilian territory, are among the most threatened ecoregions in the world due to high rates of conversion and few protected

areas (HOEKSTRA et al., 2004). Nevertheless, the current understanding of land-use and land-cover changes in Cerrado and Caatinga biomes is still limited, due to few researches and conservation efforts focusing on these seasonal areas (ACERBI JÚNIOR et al., 2015; BEUCHLE et al., 2015; RIBEIRO et al., 2011).

Due to spatial, spectral, and temporal characteristics, the advantageous application of satellite images has become increasingly indispensable for mapping and monitoring land-use and land-cover changes in vegetation, such as selective logging and wildfires (WULDER et al., 2020). A key challenge in remote sensing change detection is accurately map land-use and land-cover changes while not accounting those associated with phenological differences, which is an intrinsic characteristic of Cerrado and Caatinga biomes (TRANCOSO; SANO; MENESES, 2015). When images from different seasons are acquired, changes caused by phenology in vegetation are inevitable and can easily be confused with forest change (LU et al., 2016).

With the Landsat archive opened for free access, techniques and algorithms using time series imagery and de-seasoning models have been developed (ZHU, 2017) on the assumption that seasonal variations among images can be modeled and extracted from the dataset (VERBESSELT et al., 2010b). For example, the Landsat-based detection of Trends in Disturbance and Recovery, or LandTrendr, uses a pixel-based segmentation method to investigate land trajectories by modeling time series and computing straight-line segments (KENNEDY; YANG; COHEN, 2010). Trajectory-based segments are further used for identifying forest disturbance events and capturing the associated information such as the year of event, duration, and magnitude of change. LandTrendr has become a well-recognized and widely used algorithm for detecting and monitoring land cover dynamics since its implementation on the Google Earth Engine platform (KENNEDY et al., 2018), which provided straightforward access and management of the Landsat archive and computation through parallel processing (GORELICK et al., 2017).

However, noise modeling and detection are usually sensitive to time series properties such as the regular interval between images and gaps caused by clouds and cloud shadows (BUENO et al., 2019). In addition, non-forested areas as Cerrado grasslands, are still affected by seasonal noise and may return poor accuracies in disturbance mapping studies (SCHWIEDER et al., 2016). In this context, researchers have proposed methods to detect land cover changes by exploiting the spatial information and variability of spectral indices using geostatistical functions (BALAGUER-BESER et al., 2013). In the remote sensing context, the semivariogram is a geostatistical function that describes textural and spatial features of remote sensing images. The semivariogram also relates the semivariance of a regionalized variable

with spatial intervals, providing a straightforward description of its spatial variability (CURRAN, 1988). Recent studies have been designed to determine whether semivariogram can reduce the noise caused by vegetation phenology in change detection (POWERS et al., 2015; SILVEIRA et al., 2018a) and classification applications (SILVEIRA et al., 2017a; YUE et al., 2013).

Furthermore, the integration of spatial information with time-series features to mapping and monitoring vegetation changes has also been reported. For instance, in a study by Wu et al. (2015), better results were found in land cover classification by combining semivariogram features and spectral information with respect to the texture features derived from the gray level co-occurrence matrix and spectral information. Gil-Yepes et al. (2016) explored the geostatistical functions of codispersion and cross-semivariogram to derive temporal features and detect land cover changes in agricultural areas. Others have also explored the geostatistical information of remote sensing images to detect changes in forested landscapes affected by vegetation phenology. Hamunyela et al. (2016) demonstrated the inclusion of pixel-based neighborhood information in a seasonal model, while Silveira et al. (2019) integrated NDVI-derived semivariogram and spectral features to reduce seasonal variations in Landsat data. Their results indicated a reduction of seasonal noise from vegetation phenology when integrating spatial and spectral features.

Despite these promising results, questions still remain. No previous study has inferred the spatial information of post-disturbance recovery or has integrated it with change detection algorithms. Thus, this study evaluated the accuracy of LandTrendr algorithm and the semivariogram features derived from NDVI images to map and characterize land-use and land-cover changes in Brazilian seasonal biomes. Specifically, we aimed at (1) to evaluate the accuracy of LandTrendr, semivariogram, and their combination as predictor variables to classify changes in seasonal areas; (2) to evaluate gains and losses in map accuracies by analyzing the relationship between classification accuracies and the number of classes plus land-use and land-cover change types; and (3) to analyze patterns of change in accordance to the temporal behavior of the semivariogram parameters to infer about vegetation loss and recovery. With regards to the first two objectives, we investigated whether a combination of both LandTrendr and semivariogram was significantly different against individual datasets. We hypothesized that the grouping of predictor variables from different methods will significantly improve the performance of change mapping because the blended set may exclude individual weakness and benefit from particular advantages of each predictor variable, reducing the generalization error.

The study presented here used object-based image analysis to extract information from LandTrendr algorithm and semivariogram predictor variables. We classified land-use and land-cover changes and analyzed the accuracies derived from the sets of variables and their combination. We also analyzed accuracies with regards to change classes, hereafter presented as the classification design. Finally, a qualitative method based on visual interpretation of important spatial variables was adopted to infer patterns of land cover change.

2 MATERIAL AND METHODS

Figure 1 illustrates the major steps of this study. The preprocessing of data included the segmentation of Landsat images and the assignment of image-objects to reference land-use and land-cover changes classes. We then created three sets of predictor variables by extracting spatial and disturbance information inside the image-objects, which were LandTrendr, Semivariogram, and the combination of both previous sets (hereafter labeled as Blended). We mapped land cover changes and evaluated the performance of datasets and classification designs. Finally, a qualitative method based on visual interpretation of important spatial variables was adopted to infer about patterns of land cover change.

Figure 1 – Method flowchart and the steps detailed to provide mapping accuracy and patterns of change. Land cover classes: NC – Non-change; VL – Vegetation loss; and PC – Post-change.

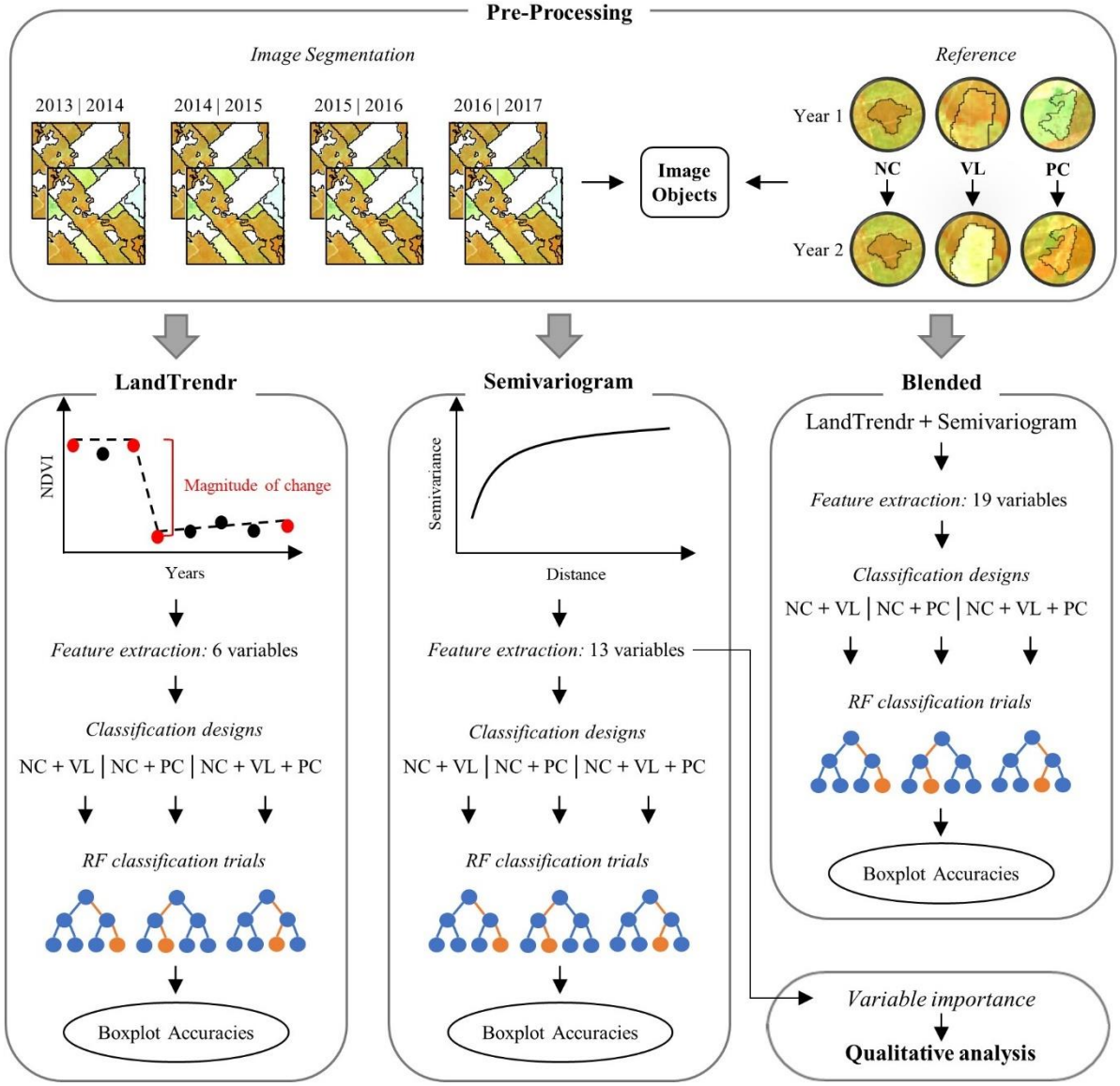

Source: Author (2022).

2.1 Study Area and Sample Design

The study area is inserted in the north of Minas Gerais state, Brazil, between the coordinates 14º 00' to 16º 30' south latitude and 43º 00' to 46º 00' west longitude and comprises the Rio Pandeiros Water Resources Planning and Management Unit (Figure 2a). Two main biomes are presented in the area: savanna or *Cerrado*, and the semi-arid woodland, also known as *Caatinga*. A variety of vegetation types are presented in both biomes such as open grasslands (*Cerrado* grassland), open grassland with sparse shrubs (*Cerrado sensu stricto)*, deciduous

forest, and palm swamps (*veredas*) (OLIVEIRA-FILHO et al., 2006). These vegetation types encompass many endemic and rare species; however, they are also situated within a biodiversity hotspot representing the most endangered ecosystems in the world (MYERS et al., 2000).

The climate is classified as *Aw*, characterized by dry winters and rainy summers (PEEL; FINLAYSON; MCMAHON, 2007). Annual precipitation is accumulated on summer ranging from 1,200 to 1,800 mm, while dry season can reach zero mm of monthly precipitation, displaying a high variation in precipitation during the year (Figure 2b). Such variation is also presented in temperature, varying from 15º C to 35º C according to seasons (Figure 2c). Eventually, the seasonal effect also impacts the photosynthetic activity of vegetation. Values of the normalized vegetation difference index (NDVI), which is related to vegetation greenness, are strongly affected by climate seasonality and differ across the area (Figure 2d).

In order to perform the analyses presented in this study, we created 16 plots of 100 km² (10 x 10 km) distributed in the study area. These plots display multiple vegetation types and change events as human-induced and natural phenological changes. Area plots were sufficiently large to contain a suitable number of change events observations and suitable dispersed to attend the spatial heterogeneity in the area (OLOFSSON et al., 2014).

Figure 2 – (a) Location of the study area; (b) The seasonal effect on precipitation, expressed by the difference between the wettest and the driest quarter; (c) temperature difference between the warmest and the coldest month; (d) inter-annual vegetation seasonal response of NDVI; (e) image segmentation and image-objects.

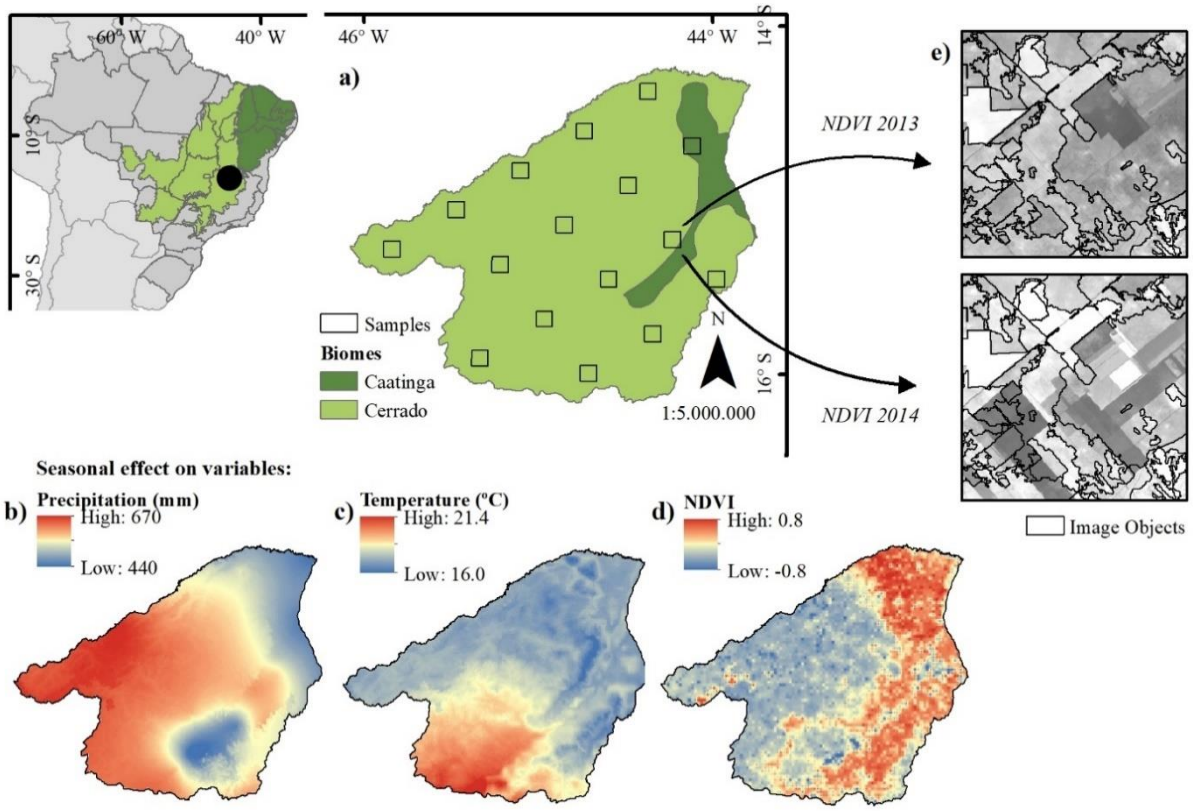

Source: Author (2022).

2.2 Data Acquisition

To accomplish this research, we selected one cloud free Landsat OLI image per year from 2013 to 2017, and downloaded from the U.S. Geological Survey's Earth Resources Observation and Science (USGS EROS) (See Table 1S of the Supplementary material for details). All scenes were pre-processed to surface reflectance levels using the Land Surface Reflectance Code (LaSRC) atmospheric and topographic correction algorithm (VERMOTE et al., 2016). From each corrected Landsat image, we calculated the NDVI inside each area plot. Besides being the most frequently used index in remote sensing science, previous studies indicated NDVI as an adequate index in change detection applications when used across cerrado and caatinga biomes (BUENO et al., 2020). We masked NDVI images with the *Cadastro Ambiental Rural* land use/land cover classification in order to obtain only native vegetation areas. The map of *Cadastro Ambiental Rural* encompasses forested areas as well as non-

forested areas, such as native grasslands, which makes a suitable dataset for the analysis in this study.

As reference data, we created change polygons by visual interpretation using Landsat images. We selected one image per year (usually on the dry season – June to September – to avoid cloud contamination), and accounted for vegetation changes in consecutive images. We accounted as changes in vegetation, only the conversion of native vegetation cover at the Landsat pixel scale to a non-native class, e.g., bare soil, agriculture, or pastures. To infer about inconclusive change areas, we used high-resolution imagery from Google Earth (where available) as auxiliary information. Finally, change polygons were double-checked by different analyst experts in order to remove uncertainty regions. The reference data collection step was performed in Envi software (Exelis Visual Information Solutions, Boulder, Colorado).

2.3 Image Segmentation

Image segmentation is a crucial step in OBIA and divides an image into groups of pixels spatially continuous and spectrally homogeneous, also known as image objects (Figure 2e). The segmentation of a remote sensing image minimizes the within-object variability compared to the between-object variability (DESCLÉE; BOGAERT; DEFOURNY, 2006). We used the multiresolution segmentation algorithm (BAATZ; SCHAPE, 2000) implemented in the eCognition software (DEFINIES AG, 2009). We selected all 30-m OLI bands from two consecutive years during the 2013-2017 period. Therefore, we ran the segmentation four times (2013-2014, 2014-2015, 2015-2016, 2016-2017) then merged all objects into a single dataset. The image segmentation using multiple year intervals is particularly useful since it increases the number of image-objects, and therefore the change observations. Another advantage of considering all images during object formation is that it minimizes sliver errors and potentially honoring key multi-temporal boundaries.

Three important segmentation parameters: scale, compactness, and shape, control the size and shape of the image objects. We set 200 for scale, 0.5 for compactness, and 0.1 for shape. The most critical step is the selection of the scale parameter, which controls the size of the image objects. This parameter is crucial when analyzing spatial features of image objects, since their size or number of pixels is directly related to the semivariogram criterion lag distance (SILVEIRA et al., 2018a). We adopted a trial and error approach to find an appropriate value for the scale parameter (DURO; FRANKLIN; DUBÉ, 2012). We ensured a minimum number of samples (25 pixels) inside the objects and an adequate size to allow further geostatistical analysis.

We assigned image-objects to change events and defined three classes of land-use and land-cover change:

- Non-change: image objects comprising the same land cover in both years, although seasonal changes due to phenological effects might be common;
- Vegetation loss: the complete removal of native vegetation at the Landsat pixel scale and its conversion into bare soil;
- Post-change: the spectral change after the loss of vegetation, which is mainly characterized by the land conversion into areas with higher NDVI values (e.g., crops, planted forests, and natural regeneration.

Representative image-objects of change classes were identified from visual inspection using Landsat images and high-resolution imagery from Google Earth, when available. We assigned a total of 4,250 image-objects representing the non-change class, 99 representing vegetation loss, and 56 representing post-change.

2.4 Feature Extraction

From image-objects, we extracted disturbance information and spatial features based on the NDVI values inside the objects. We then created three sets of predictor variables generated from 1) LandTrendr algorithm, 2) Semivariogram parameters, and 3) Blended. The initial pool of variables was screened to limit the potential effects of multicollinearity by calculating correlations between pairs of variables using the Pearson's correlation coefficient (R). We removed those with R values greater than 0.80.

2.4.1 LandTrendr

Instead of using LandTrendr change maps, we chose to use an ensemble mapping approach, integrating LandTrendr change map with further classification. The ensemble technique for classification systems is based on multiple or committee algorithms combining their predictions, then excluding individual weakness.

To extract LandTrendr information from NDVI time series, we followed three steps: algorithm tunning, magnitude of change extraction, and calculation of final predictor variables. We first tuned three LandTrendr parameters *p* related to the trajectory segmentation fitting: the maximum number of segments $p = \{4, 6, 12\}$, the recovery threshold $p = \{0.25, 0.50, 0.75\}$, and the best model proportion $p = \{0.50, 1.00, 1.25\}$. Each parameter value was varied according to their respectively attempts and the change map was evaluated for 1000 reference points equally sampled over the study area. The most accurate change map was selected for

further analysis. Applying the best parameter configuration (lowest overall error), we extracted the magnitude of change in each year. The magnitude of change reflected a significant spectral change in the yearly trajectory of a pixel, and varied from negative values (magnitude of vegetation loss) to positive values (magnitude of vegetation gain). Pixels with zero values represented a non-significant change not detected by the algorithm. We included the magnitude of gain once it can also indicate a loss in vegetation. The magnitude of change with regards to gain in vegetation is an important role in mapping non-forested changes since they are usually converted from low NDVI values, as native grasslands, to higher values such as agriculture and planted forests. Finally, we computed six predictor variables from the magnitude of change inside each image-object: minimum, maximum, range, mean, standard deviation, and sum (Table 1). LandTrendr-related analysis were undertaken in Google Earth Engine platform.

Table 1 – LandTrendr predictor variables calculated from the magnitude of change of image-objects.

Variable	Description
MIN	Minimum value of change magnitude computed by LandTrendr inside an image-object.
MAX	Maximum value of change magnitude computed by LandTrendr inside an image-object.
RANGE	Difference between the lowest and highest values of change inside an image-object.
MEAN	Mean value of change magnitude inside an image-object.
STD	Standard deviation of change magnitudes an image-object.
SUM	The total of change magnitudes values inside an image-object.

Source: Author (2022).

2.4.2 Semivariogram

We calculated the semivariance $\gamma(h)$ from experimental semivariograms, defined from the spatial variance of measures performed in samples from a determined distance h being the sum of the squares' difference between the sampled values $Z(x)$ separated by a distance h, divided by two times the number of possible pairs on each distance $N(h)$ (Equation 1). For each image-object, the final experimental semivariogram was obtained by computing the mean of the semivariograms calculated in six directions. The graphical representation of the experimental semivariogram illustrates the spatial variance and distance h illustrates, which permits obtaining the estimative of the variance for the different combinations of pairs of observations. For further details, please refer to Curran (1988).

$$\gamma(h) = \frac{1}{2N(h)} \sum_{i=1}^{N(h)} [Z(x) - Z(x+h)]^2 \quad (1)$$

The semivariance is characterized by three parameters: sill (γ_{max_1} or σ^2), range (h_{max_1} or φ), and nugget effect (τ^2). The sill is the semivariance value when the model reaches the plateau, commonly displayed on the y-axis, and represents the amount of variation explained by the spatial design of the data. The range is the distance *h* at which the semivariogram reaches the sill, commonly displayed on the x-axis, and illustrates the distance until the data is spatially correlated. The nugget effect is the non-spatial component of the variance composed of random sensor noise or sampling errors.

Based on the semivariogram standard parameters – sill, range, and nugget – we computed a set of eleven indices (Table 2). Semivariogram indices were firstly calculated by Balaguer et al. (2010) and describe the shape of the semivariogram and, therefore, the properties that characterize the spatial patterns of the image-objects. To ensure that semivariogram parameters would provide a reliable description of the semivariogram shape and data variability, we attempted to set a satisfactory lag distance. We set the number of lags as 30 Landsat pixels scale, resulting in a lag distance of 900 m. This lag distance was previously defined as a good value for related analysis (SILVEIRA et al., 2018b). We used FETEX 2.0 to compute and extract semivariogram parameters of image-objects (RUIZ et al., 2011). Finally, we computed predictor variables based on the parameters of the difference between two consecutive years.

Table 2 – Semivariogram variables calculated from the NDVI values inside the objects, where the semivariogram features $\{(h_1, \gamma_1), (h_2, \gamma_2) \ldots (h_{max\_1}, \gamma_{max\_1})\}$ are the points of the experimental semivariogram until the first local maximum. Variance is the value of the total variance of the pixels belonging to the image-object. Delta symbol represents the parameter difference between two consecutive years.

Variable	Description	Formula
ΔRVF	Ratio between the values of the total variance and the semivariance at first lag	$\frac{variance}{\gamma_1}$
ΔRSF	Ratio between semivariance values at second and first lag	$\frac{\gamma_2}{\gamma_1}$
ΔFDO	First derivative near the origin	$\frac{\gamma_2 - \gamma_1}{h}$
ΔSDT	Second derivative at third lag	$\frac{\gamma_4 - 2\gamma_3 + \gamma_{12}}{h^2}$
ΔFML	First maximum lag value	
ΔMFM	Mean of the semivariogram values up to the first maximum	$\frac{1}{max\_1} \sum_{i=1}^{max\_1} \gamma_i$

ΔVFM	Variance of the semivariogram values up to the first maximum	$\frac{1}{max\_1}\sum_{i=1}^{\max\_1}\left(\gamma_i - \gamma_{\max\_1}^{mean}\right)^2$
ΔDMF	Difference between the mean of the semivariogram values up to the first maximum and the semivariance at first lag	$MFM - \gamma_i$
ΔRMM	Ratio between the semivariance at first local maximum and the mean semivariogram values up to this maximum	$\frac{\gamma_{\max\_1}}{\gamma_{\max\_1}^{mean}}$
ΔSDF	Second-order difference between first lag and first maximum	$\gamma_{\max\_1} - 2\gamma_{\frac{\max\_1}{2}} + \gamma_1$
ΔAFM	Semivariance curvature	$\frac{h}{2}\left(\gamma_1 + 2\left(\sum_{i=2}^{\max\_1-1}\gamma_1\right) + \gamma_{\max\_1}\right) - \left(\gamma_1\left(h_{\max\_1} - h_1\right)\right)$

Source: Author (2022).

2.4.3 Blended

Blended dataset encompassed all predictor variables previously described: six from LandTrendr and thirteen from semivariogram. We combined the spatial information of the semivariogram with the change output of LandTrendr, assessing gains and losses in accuracy.

2.5 Change Mapping

We used The Random Forest algorithm (RF; Breiman, 2001) to classify the land-use and land-cover changes. RF consists of many decision trees voting the best model's prediction and has become one of the most popular classifiers presenting easy learning and very satisfactory outputs (BELGIU; DRĂGUŢ, 2016). RF involves several parameters controlling the structure of the algorithm. In this study, we tunned three of those parameters: the number of trees to grow, or *Ntree*; the number of predictors sampled at each tree node, or *Mtry*; and the minimum size of terminal nodes, or node size. The control of node size parameter defines the minimum number of observations in a terminal node, where a lower number defines trees with a larger depth, which means that more splits are performed until the terminal nodes. We used the following parameter values in the RF tunning: *Ntree* = {250, 500, 750, 1000}; *Mtry* = {*p*/4, *p*/3, *p*/2, *p*} with *p* the total number of variables; and node size = {2, 4, 6, 8}.

For each RF classification, we balanced the observations according to the class with fewer image-objects. We split the data into 70% for training to fit the RF model, while 30% was used for the validation set, assessing the generalization error of the RF model. We repeated 100 RF trials per classification design to capture a possible variation in accuracies resulting from random sampling of training samples (especially in ND class, the most numerous class). In addition, multiple trials allowed us to obtain a more representative classification performance

of the datasets and classification designs. Accuracy analysis consisted in the creation of confusion matrices for each RF trial. The overall accuracy, omission (inversely related to producer's accuracy), and commission error rate (inversely related to user's accuracy) were obtained for all the trials. Accuracy analysis were graphically presented using boxplots. RF analysis and tunning were undertaken using the *mlr* package (BISCHL et al., 2016), while confusion matrices were derived using the *caret* package (KUHN, 2008) in R v 4.1.0 (R CORE TEAM, 2016)

The change mapping step was performed based on two analyses: the first evaluating the dataset, and the second the classification designs.

2.5.1 Dataset Evaluation

The dataset evaluation consisted of comparing accuracies of the three sets of prediction variables: 6 LandTrendr, 13 semivariogram, and 19 Blended. To test for statistical significance, we tested whether there were differences in overall accuracies between datasets. We performed paired t-tests for each dataset (comparing each of them with each other) to assess if the differences in accuracy were significant at the 5% level. The null hypothesis in the paired tests stated that the mean difference in the population equals zero.

2.5.2 Classification Design Evaluation

Classification designs mainly analyzed the relationship between classification accuracies and the number of classes plus major land-use and land-cover change types of the study area. We evaluated three classification designs based on the selection of the change classes. The first design used only non-change and vegetation loss observations, which is a common vegetation change analysis. Second, we selected non-change and post-change, which allowed us to investigate the performance of mapping areas of vegetation recovery and other types of land conversion. Third, we used all change classes – non-change, vegetation loss and, post-change to determine accuracies, and to analyze loss and gains in accuracy compared with the other two designs. Paired t-tests were also performed to analyze whether there were differences in overall accuracies between classification designs at 5% level.

2.6 Qualitative Analysis

A qualitative analysis through visual interpretation of Semivariogram variables and classification designs was also done. We calculated the variable importance of each RF model using the mean decrease in Gini index, which measures the difference in out-of-bag accuracy

with respect to the rest of the variables. The two most important variables considering all RF runs were selected. We then separately plotted the three classification designs and their respective variables in a 2-d plot to infer patterns of change.

3 RESULTS

3.1 Change Mapping Evaluation

The overall accuracies for the 100 RF trials using boxplots allowed us to evaluate the overall performance among datasets and classifications designs (Figure 3). The overall accuracy median of Blended significantly outperformed the other datasets in all classification designs. For instance, the Blended median of the first classification design was 84.0%, while LandTrendr and Semivariogram had 80.0% and 68.0%, respectively. With regards to the maximum accuracy, LandTrendr had the highest value in the same classification design, 94.0%, while Blended and Semivariogram had 92.0% and 88.0%, respectively. Semivariogram dataset had the lowest overall accuracies considering the median, maximum, and minimum values. According to the paired t-test, overall accuracies of datasets were significantly different in almost all classification designs (Table 3). However, we did not find statistical difference at 5% level between LandTrendr and Blended overall accuracies in the classification design that used only non-change and post-change observations.

Figure 3 – Boxplots of overall accuracies displaying datasets (SV – Semivariogram; LT – LandTrendr; BL – Blended) and classification designs (NC – Non-change; VL – Vegetation loss; PC – Post-change).

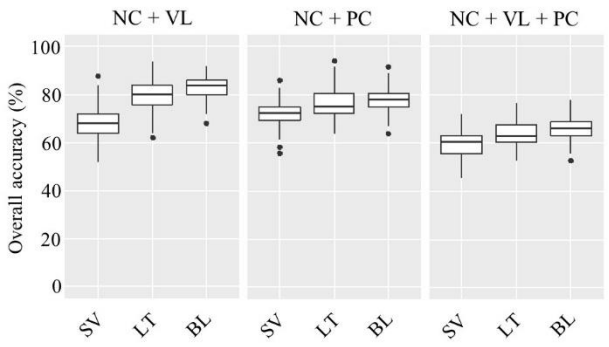

Source: Author (2022).

Table 3 – Comparison of datasets overall accuracies (SV – Semivariogram; LT – LandTrendr; BL – Blended) using a paired t-test. The upper number indicates the t-value, the number in parentheses indicates the p-value, and bold values indicate no statistical significance at 5% level. (NC – Non-change; VL – Vegetation loss; PC – Post-change).

	NC + VL			**NC + PC**			**NC + VL + PC**		
	SV	**LT**	**BL**	**SV**	**LT**	**BL**	**SV**	**LT**	**BL**
SV	0.00 (1.000)			0.00 (1.000)			0.00 (1.000)		
LT	12.75 (<0.001)	0.00 (1.000)		5.54 (<0.001)	0.00 (1.000)		5.93 (<0.001)	0.00 (1.000)	
BL	21.14 (<0.001)	5.27 (<0.001)	0.00 (1.000)	7.05 (<0.001)	**1.45 (0.1502)**	0.00 (1.000)	10.08 (<0.001)	2.70 (0.008)	0.00 (1.000)

Source: Author (2022).

Regarding the classification designs, all overall accuracies were significantly different (Table 4). An important result can be shown when analyzing classifications that used two change classes (non-change + vegetation loss and non-change + post-change), and the classification design with three classes (non-change, vegetation loss, and post-change). A comparison of both results reveals a decrease in accuracies when adding the third class. For instance, the overall accuracy median of Blended decreased 17.8% when adding the post-change class in the first classification design, while 11.6% decreased in the second design when adding vegetation loss class. Other datasets also showed a decrease of accuracies close to 10% when adding the additional change class. The decrease of accuracy can also be represented by t values of paired t-test, where the comparisons with the third classification design had higher t-values (large difference existed between the two sample sets). In addition, the third classification design returned no accuracies higher than 80%, which suggests that the more the land cover change classes, the lower the overall accuracy values.

Table 4 – Comparison of classification designs overall accuracies using a paired t-test (classification design 1 – CD1: non-change + vegetation loss; classification design 2 – CD2: non-change + post-change; classification design 3 – CD3: non-change + vegetation loss + post-change). The upper number indicates the t value, the number in parentheses indicates the p-value. All comparisons were statistically significant at 5% level.

	Semivariogram			**LandTrendr**			**Blended**		
	CD1	**CD2**	**CD3**	**CD1**	**CD2**	**CD3**	**CD1**	**CD2**	**CD3**
CD1	0.00 1.0000			0.00 1.0000			0.00 1.0000		
CD2	4.77 <0.0001	0.00 1.0000		2.97 0.0038	0.00 1.0000		6.49 <0.0001	0.00 1.0000	
CD3	9.51 <0.0001	14.47 <0.0001	0.00 1.0000	17.15 <0.0001	14.27 <0.0001	0.00 1.0000	24.33 <0.0001	15.43 <0.0001	0.00 1.0000

Source: Author (2022).

Omission and commission error rates for the 100 RF trials followed a similar trend compared to overall accuracies, where LandTrendr outperformed Semivariogram, and their combination returned the lowest error rates (Figure 4). It is also noticeable that error rates presented a higher range of output values. Considering all classifications designs, the omission error rate of NC, which were the non-change observations wrongly classified as land cover change, roughly ranged from 60% to 0%. These results suggest that vegetation seasonality affected the internal structure of image-objects regardless the dataset. The error rate increase when adding a third change class was also seen in omission and commission outputs. The error increase is even more apparent in post-change omission error rate where error rates reached an increase of 28.0% in Semivariogram dataset.

Figure 4 – Omission and commission error rates of classification designs (NC – Non-change; VL – Vegetation loss; PC – Post-change) and their respectively datasets (SV – Semivariogram, LT – LandTrendr, BL – Blended).

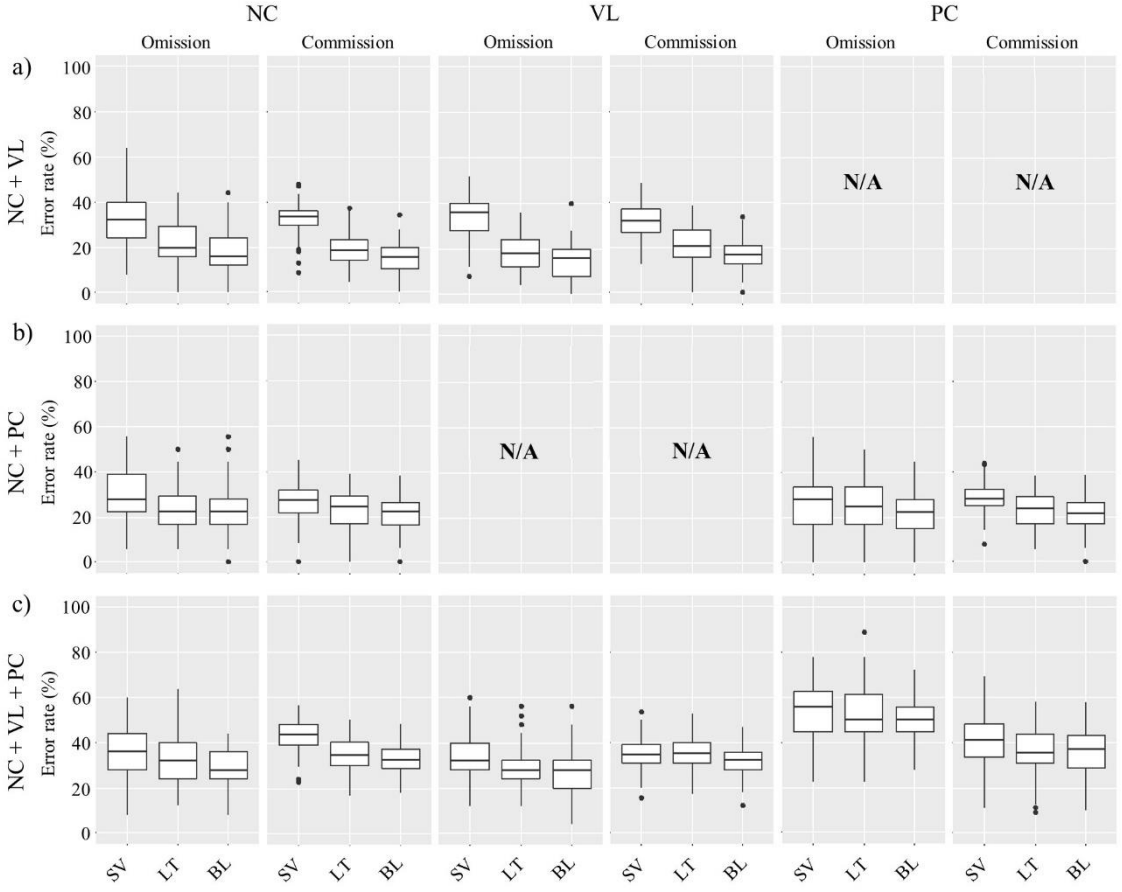

Source: Author (2022).

3.2 Qualitative Analysis

Three Semivariogram variables were selected as the most important ones in RF classifications. In the first classification design, ΔRVF was the most important variable in the majority of RF trials, while ΔAFM was the second most important variable selected. In the second and third designs, ΔRVF was maintained as the most important variable, and ΔRSF turned into the second most important variable.

Two-dimensional plots display land cover change image-objects in classification designs based on the most important Semivariogram variables (Figure 5). We found patterns of changes by analyzing individual image-objects. The first pattern can be seen in the first classification design, when vegetation loss image-objects presented an increase of both ΔRVF and ΔAFM, while values of non-change remained constant (Figure 5a). In Year 1, objects covered by native vegetation are composed of homogeneous pixels (low internal NDVI

variability) with low values of total variance. After change (e.g., deforestation), there was an increase in internal variability of NDVI values due to the conversion to bare soil, evidenced by higher variance values (Figure 5b).

The classification design that investigated only post-change along with stable areas (Figure 5c), indicated three main patterns of change, which were: (i) both ΔRVF and ΔRSF increase; (ii) both ΔRVF and ΔRSF decrease; and (iii) both ΔRVF and ΔRSF remain constant. The first pattern was opposite of loss of vegetation, where heterogenous image-objects mostly covered by bare soil in Year 1 presented a vegetation recovery in Year 2, which stabilizes the textural variation and decreases the total variance (Figure 5d). In the second pattern, Year 2 presented an uneven recovery inside the image-object, where part of the pixels recovered and part remained constant, then increasing its variance (Figure 5e). Finally, the third pattern presented the same land use in both Years 1 and 2 (Figure 5f). The classification design that combined non-change, vegetation loss, and post-change did not present a particular pattern although combines all patterns previously described (Figure 5g).

Figure 5 – The qualitative analysis through visual interpretation of Semivariogram most important variables, and classification designs using (a) non-change and vegetation loss; (c) non-change and post-change; and (g) non-change, vegetation loss, and post-change classes. The vegetation loss pattern of change is represented in (b); while post-change patterns were represented in (d), (e) and (f).

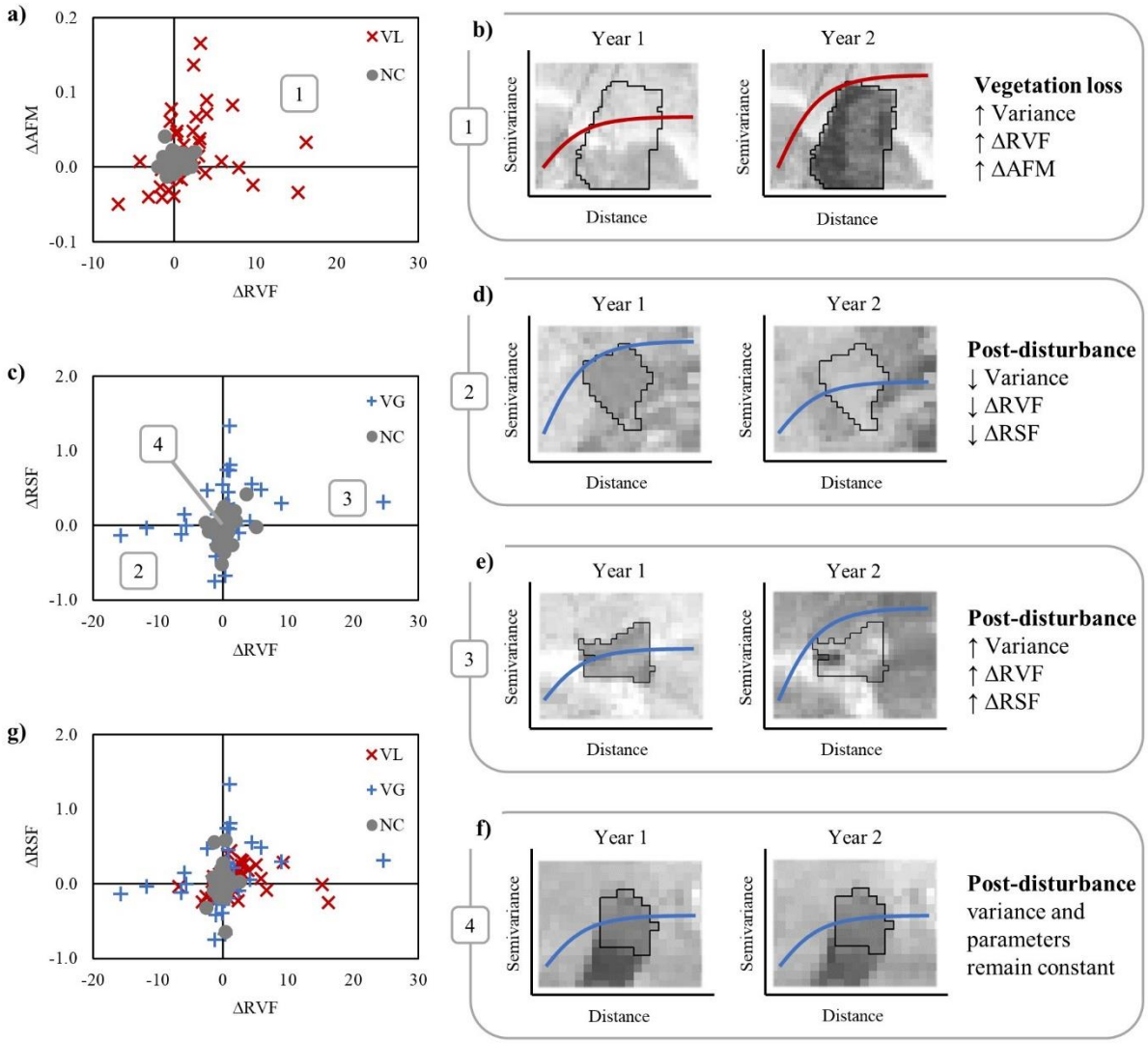

Source: Author (2022).

4 DISCUSSION

In this research, we evaluated the accuracy of LandTrendr algorithm and semivariogram parameters to detect and to characterize land-use and land-cover changes in seasonal areas. LandTrendr and semivariogram were also evaluated as a unique dataset by combining both sets of variables, which increased map accuracies. In addition, our results infer about patterns of change in accordance to the temporal behavior of the semivariogram parameters.

4.1 Change Mapping Evaluation

The first objective in this study sought to evaluate the accuracy of LandTrendr algorithm, semivariogram, and their combination to map vegetation changes in seasonal areas. Our results showed that variables generated from a LandTrendr map returned, on average, more accurate land-use and land-cover changes maps than semivariogram parameters. These results mirror those of the previous studies that have evaluated the potential of LandTrendr in mapping vegetation changes and dynamics in tropical dry forests (DE MARZO et al., 2021), savannas (SOUZA et al., 2020a), and mangroves (DE JONG et al., 2021). Using LandTrendr resulted in overall accuracies high enough detecting changes under the first two classification designs. A total of 44% in LandTrendr trials returned overall accuracy higher than 80% in the first classification design, and 33% in the second. Despite those potential errors, the low omission and commission error rates for both designs imply that the LandTrendr approach used in this research was robust.

One unanticipated finding was the unsatisfactory performance of semivariogram predictor variables. This finding is contrary to previous studies that have suggested the spatial context may be not affected by vegetation seasonality (HAMUNYELA; VERBESSELT; HEROLD, 2016; SILVEIRA et al., 2018b). The concept of mapping land cover changes using spatial information was also evaluated by Silveira et al. (2019) in a location near our study area. In that study, the spatial context reduced the seasonal variations in the data and increased accuracies. However, this rather contradictory result may be explained by several factors. We used a full and repeated random selection of training and validation image-objects, which allowed us to explore a larger number of image-objects throughout the area and to obtain a more representative mapping analysis. However, some image-objects can be misclassified by RF. For instance, the random selection might have selected image-objects representing more than one vegetation type (e.g., deciduous forest and riparian forest), which might have different spectral responses to the seasonal noise; therefore, different internal variances. Another factor might be the selection of image-objects with mask errors from the *Cadastro Ambiental Rural* classification. In addition, we used a different period of analysis and image date acquisition from those previous studies, which might affect the seasonal noise captured by the analysis in this study.

The combination of both sets of variables revealed more accurate land-use and land-cover changes maps than assessing them individually. By investigating a similar hypothesis to what is described here, Silveira et al. (2019) also found gains in accuracy when combining

semivariogram indices and descriptive statistics of NDVI. In that study, semivariogram indices outperformed spectral features, while their combination returned a gain of 5% in overall accuracy. Others have also demonstrated the value of combining predictor variables for forest disturbance mapping. For instance, in a study by Hislop et al. (2019), disturbance mapping models based on a set of forest change maps, raster information and time series predictor variables, had higher accuracies than models with fewer variables. The combination of sets based on spatial and spectral information was also demonstrated to classify agriculture areas (AKAR; GÜNGÖR, 2015).

Our study produced results that verify the findings of the previous work in land cover change mapping. One important feature of our method was the use of predictor variables from distinct methods. Besides the spatial context, semivariogram and LandTrendr differed with regards to the image frequency. The Semivariogram method analyzes changes in bitemporal NDVI images, which is a common change detection method based on image differencing (or, in this case, variance differencing). In image differencing studies, changes are defined by image-objects that show large differences. Some authors have demonstrated that a bi-temporal set of features shows high rates of accuracy in change detection classification and reduced vegetation phenology when used along with the spatial context (GIL-YEPES et al., 2016). On the other hand, the LandTrendr algorithm models time trajectories and demands historical time series data available at the same time. By constraining the image selection to the dry season, we also reduced the vegetation-phenology and view-illumination effects on clearing detection. Therefore, such a variety of predictor variables provided to our method the capability to exclude individual weakness and to benefit from particular advantages of each predictor variable, reducing the generalization error.

With respect to the second objective, it was revealed that accuracies decreased when adding the third change class. A strong relationship between classification accuracies and the number of classes has been reported in the literature, where the classification accuracy decreases with an increase in the number of classes (MA et al., 2017). Others have also reported that the occurrence of accuracies below 85% in wetland classification studies increased after the number of classes exceeded four (DRONOVA, 2015). Our study demonstrated that accuracies can decrease based on a very low number of land-use and land-cover change classes. However, a possible explanation for this high decrease in accuracies may be the presence of observation uncertainties that are discussed in the next sections.

4.2 Post-Change Uncertainty

The third objective in this research was to analyze patterns of change in accordance with the temporal behavior of the semivariogram variables to infer vegetation loss and recovery. The most important variables of Semivariogram, ΔRVF, ΔRSF, and ΔAFM were directly related to the difference of variance between consecutive years. The first two use semivariogram values near the origin and basically differ in their lag distances. ΔRVF is an indicator of the relationship between the spatial correlation at long and short distances. Its value increases when high variability at long distances and low variability at short distances occurs. ΔRSF provides information about changes in the variability of data at short distances. If we now turn to ΔAFM, this variable uses the semivariogram values ranging from the first lag up to the first local maximum of the experimental semivariogram. ΔAFM provides information about the semivariogram curvature and is also related to the variability of the data.

However, we found different patterns when analyzing the second classification design, which used information of post-change image-objects. In general, the classification design using non-change and post-change classes performed well. For instance, 45% of Blended classification trials had an overall accuracy higher than 80.0%. Nevertheless, by adding the vegetation loss class, accuracies considerably decreased and the highest overall accuracy of Blended turned to 78.0%. On the question of these results, we found post-change uncertainties due to the variance similarity of post-change with vegetation loss and non-change image-objects. Post-change uncertainties patterns were the main cause of poor accuracies in the classification designs that selected all land cover change classes.

Some post-change image-objects did not follow the pattern of vegetation recovery in Year 2, which could be expected by an increase of NDVI pixels values and a decrease in the total variance. Nevertheless, the increase of variance inside post-change image-objects can easily be confused with vegetation loss observations, which decreases the overall accuracy and increases the omission error rate of the post-change class. Even though our image segmentation method considers both years during object formation and intends to capture the heterogeneity in Year 2, it may present some boundary errors in small objects. Boundary errors can be explained by the fixed minimum number of pixels inside the objects to allow the calculation of the semivariogram, which may create large image-objects. In addition, those errors raise intriguing questions regarding the optimal image segmentation and the suitable image objects for change mapping analysis. The second post-change uncertainty, the variance regularity in Year 2, also leads to a decrease in the overall accuracy and increase of the omission error rate

of the post-change class. The similarity of NDVI values in both years can be confused with non-change image-objects less affected by vegetation phenology.

The uncertainties of post-change class support the importance of modeling change dynamics to improve mapping accuracies. Prior studies also have noted the importance of assessing post-change areas to infer land cover classes (ARÉVALO; OLOFSSON; WOODCOCK, 2020; HERMOSILLA et al., 2018) and to monitor forest dynamics (BARTELS et al., 2016). However, the poor accuracies caused by post-change uncertainties need to be interpreted with caution. The present study was limited by a low number of post-change observations, which might be unrepresentative for the study area. In future investigations, a straightforward analysis of a representative land cover change database should be considered as it can provide a trustful background of post-change information and its accuracy.

4.3 Non-Change Variability

Another important finding was the high variability of accuracies outputs, graphically presented by the boxplots. The high variability may be explained by the fact that non-change image-objects were more numerous than other classes, and their random selection was affected by vegetation phenology in some RF trials. The vegetation phenology has been reported as noise by several authors with regard to change mapping and monitoring, requiring appropriate methodologies to deal with such complexity (VENKATAPPA et al., 2019). There are comparable methods to what is described here that intended to capture spectrally complex and heterogeneous land change processes. For instance, in a study by De Marzo et al. (2021), LandTrendr along with RF had been reported as a valuable ensemble technique to map disturbances in tropical dry forests strongly affected by vegetation phenology.

The results of our study indicate that vegetation phenology might be prevalent in some image-objects. It is possible that these results were influenced by the lack of vegetation classes since we considered forested (e.g., cerrado woodlands, deciduous forest, and riparian forest) and non-forested areas (e.g., cerrado grasslands, wetlands) as a unique vegetation class.

Another interesting finding based on the high variability of accuracy outputs was the high omission error rate of non-change class in Semivariogram classifications. For instance, the highest non-change omission error reached 64% in the first classification design, which means 19 out of 30 non-change image-objects from the validation set were wrongly classified as vegetation loss. Such unsatisfactory finding is contrary to previous studies that have suggested that the spatial variability of NDVI and semivariogram indices might be not affected by vegetation seasonality (SILVEIRA et al., 2019). However, the reader must be cautioned since

Semivariogram classifications also returned 8% of omission error rate of non-change and 88% of overall accuracy (highest accuracy), which was in line with those of previous studies.

The observed accuracy variability can be attributed to a unique feature of our method that was the repeated random selection of non-change observations. A few training samples of non-change image-objects might be more affected by vegetation phenology than others, returning higher omission error rates and vice-versa. There were efforts in the remote sensing community to improve continuous land cover classification accuracy with regards to training samples. Large samples of training pixels was suggested to classify land cover changes in large areas (ZHOU; TROY; GROVE, 2008; ZHU et al., 2016). However, there is difficulty in collecting large sets of samples through traditional approaches including manual interpretation or from high-resolution imagery. Others have used multiple existing databases to mitigate the uncertainties of training samples selection (LI et al., 2021). There are still unanswered questions about the effect of vegetation phenology on change mapping. Further research is required to evaluate the effect of training data selection, especially stable vegetated areas affected by phenology.

5 CONCLUSION

We evaluated the accuracy of LandTrendr algorithm and semivariogram parameters to map and to characterize land-use and land-cover changes in Brazilian seasonal biomes. LandTrendr predictor variables outperformed semivariogram features to map land-use and land-cover changes; however, the combination of the two datasets produced the best result. Our findings provide important insights into the role of predictor variables for mapping and monitoring land cover changes in tropical seasonal biomes. Our study also indicated that predictor variables extracted from semivariogram faithfully captured patterns of vegetation loss and recovery. The knowledge of these relationships allows the analyst not only to detect change events, but also to infer the type of change, whether caused by deforestation or by areas in regeneration. In addition, we reinforced the importance of post-change characterization to improve map accuracies, and the evaluation of training data selection, especially stable areas affected by vegetation phenology.

Acknowledgments: This study was financed in part by the Coordenação de Aperfeiçoamento de Pessoal de Nível Superior – Brasil (CAPES) – Finance Code 001.

6 REFERENCES

ACERBI JÚNIOR, F. W. et al. Change Detection in Brazilian Savannas Using Semivariograms Derived from NDVI Images. **Ciência e Agrotecnologia**, v. 39, n. 2, p. 103–109, abr. 2015. DOI: 10.1590/S1413-70542015000200001.

AKAR, Ö.; GÜNGÖR, O. Integrating multiple texture methods and NDVI to the Random Forest classification algorithm to detect tea and hazelnut plantation areas in northeast Turkey. **International Journal of Remote Sensing**, v. 36, n. 2, p. 442–464, 17 jan. 2015. DOI: 10.1080/01431161.2014.995276.

ARÉVALO, P.; OLOFSSON, P.; WOODCOCK, C. E. Continuous monitoring of land change activities and post-disturbance dynamics from Landsat time series: A test methodology for REDD+ reporting. **Remote Sensing of Environment**, v. 238, p. 111051, 1 mar. 2020. DOI: 10.1016/J.RSE.2019.01.013.

BAATZ, M.; SCHAPE, A. Multiresolution segmentation - An optimization approach for high quality multi-scale image segmentation. *In* ANGEWANDTE GEOGRAPHISCHE INFORMATIONS-VERARBEITUNG XII, 2000, Karlsruhe. **Anais eletrônicos…** Wichmann Verlag, 2000. Acesso em: 20 out. 2020

BALAGUER-BESER, A. et al. Using semivariogram indices to analyse heterogeneity in spatial patterns in remotely sensed images. **Computers & Geosciences**, v. 50, p. 115–127, 1 jan. 2013. DOI: 10.1016/J.CAGEO.2012.08.001.

BALAGUER, A. et al. Definition of a comprehensive set of texture semivariogram features and their evaluation for object-oriented image classification. **Computers & Geosciences**, v. 36, n. 2, p. 231–240, fev. 2010. DOI: 10.1016/j.cageo.2009.05.003.

BARTELS, S. F. et al. Trends in post-disturbance recovery rates of Canada's forests following wildfire and harvest. **Forest Ecology and Management**, v. 361, p. 194–207, fev. 2016. DOI: 10.1016/j.foreco.2015.11.015.

BELGIU, M.; DRĂGUŢ, L. Random forest in remote sensing: A review of applications and future directions. **ISPRS Journal of Photogrammetry and Remote Sensing**, v. 114, p. 24–31, abr. 2016. DOI: 10.1016/j.isprsjprs.2016.01.011.

BEUCHLE, R. et al. Land cover changes in the Brazilian Cerrado and Caatinga biomes from 1990 to 2010 based on a systematic remote sensing sampling approach. **Applied Geography**, v. 58, p. 116–127, mar. 2015. DOI: 10.1016/j.apgeog.2015.01.017.

BISCHL, B. et al. **mlr: Machine Learning in R**. R package version 2.19.0. 2021 Disponível em: https://mlr.mlr-org.com/.

BREIMAN, L. Random forests. **Machine Learning**, v. 45, n. 1, p. 5–32, out. 2001. DOI: 10.1023/A:1010933404324.

BUENO, I. T. et al. Object-Based Change Detection in the Cerrado Biome Using Landsat Time Series. **Remote Sensing**, v. 11, n. 5, p. 570, 8 mar. 2019. DOI: 10.3390/rs11050570.

BUENO, I. T. et al. Spatial Agreement among Vegetation Disturbance Maps in Tropical Domains Using Landsat Time Series. **Remote Sensing**, v. 12, n. 18, p. 2948, 11 set. 2020. DOI: 10.3390/rs12182948.

CURRAN, P. J. The semivariogram in remote sensing: An introduction. **Remote Sensing of Environment**, v. 24, n. 3, p. 493–507, 1 abr. 1988. DOI: 10.1016/0034-4257(88)90021-1.

DE JONG, S. M. et al. Mapping mangrove dynamics and colonization patterns at the Suriname coast using historic satellite data and the LandTrendr algorithm. **International Journal of Applied Earth Observation and Geoinformation**, v. 97, p. 102293, 1 maio 2021. DOI: 10.1016/j.jag.2020.102293.

DE MARZO, T. et al. Characterizing forest disturbances across the Argentine Dry Chaco based on Landsat time series. **International Journal of Applied Earth Observation and Geoinformation**, v. 98, p. 102310, 1 jun. 2021. DOI: 10.1016/j.jag.2021.102310.

DEFINIES AG. **Definiens eCognition Developer 8 User Guide**. Munich: Definies AG, 2009.

DESCLÉE, B.; BOGAERT, P.; DEFOURNY, P. Forest change detection by statistical object-based method. **Remote Sensing of Environment**, v. 102, n. 1–2, p. 1–11, maio 2006. DOI: 10.1016/j.rse.2006.01.013.

DRONOVA, I. Object-Based Image Analysis in Wetland Research: A Review. **Remote Sensing**, v. 7, n. 5, p. 6380–6413, 21 maio 2015. DOI: 10.3390/rs70506380.

DURO, D. C.; FRANKLIN, S. E.; DUBÉ, M. G. A comparison of pixel-based and object-based image analysis with selected machine learning algorithms for the classification of agricultural landscapes using SPOT-5 HRG imagery. **Remote Sensing of Environment**, v. 118, p. 259–272, 15 mar. 2012. DOI: 10.1016/j.rse.2011.11.020.

GIL-YEPES, J. L. et al. Description and validation of a new set of object-based temporal geostatistical features for land-use/land-cover change detection. **ISPRS Journal of Photogrammetry and Remote Sensing**, v. 121, p. 77–91, nov. 2016. DOI: 10.1016/j.isprsjprs.2016.08.010.

GORELICK, N. et al. Google Earth Engine: Planetary-scale geospatial analysis for everyone. **Remote Sensing of Environment**, v. 202, p. 18–27, dez. 2017. DOI: 10.1016/j.rse.2017.06.031.

HAMUNYELA, E.; VERBESSELT, J.; HEROLD, M. Using spatial context to improve early detection of deforestation from Landsat time series. **Remote Sensing of Environment**, v. 172, p. 126–138, jan. 2016. DOI: 10.1016/j.rse.2015.11.006.

HERMOSILLA, T. et al. Disturbance-Informed Annual Land Cover Classification Maps of Canada's Forested Ecosystems for a 29-Year Landsat Time Series. **Canadian Journal of Remote Sensing**, v. 44, n. 1, p. 67–87, 2 jan. 2018. DOI: 10.1080/07038992.2018.1437719.

HISLOP, S. et al. A fusion approach to forest disturbance mapping using time series ensemble techniques. **Remote Sensing of Environment**, v. 221, p. 188–197, fev. 2019. DOI: 10.1016/j.rse.2018.11.025.

HOEKSTRA, J. M. et al. Confronting a biome crisis: global disparities of habitat loss and protection. **Ecology Letters**, v. 8, n. 1, p. 23–29, 3 dez. 2004. DOI: 10.1111/j.1461-0248.2004.00686.x.

KENNEDY, R. et al. Implementation of the LandTrendr Algorithm on Google Earth Engine. **Remote Sensing**, v. 10, n. 5, p. 691, 1 maio 2018. DOI: 10.3390/rs10050691.

KENNEDY, R. E.; YANG, Z.; COHEN, W. B. Detecting trends in forest disturbance and recovery using yearly Landsat time series: 1. LandTrendr — Temporal segmentation algorithms. **Remote Sensing of Environment**, v. 114, n. 12, p. 2897–2910, 15 dez. 2010. DOI: 10.1016/j.rse.2010.07.008.

KUHN, M. Building Predictive Models in R Using the caret Package. **Journal of Statistical Software**, v. 28, n. 1, p. 1–26, 10 nov. 2008. DOI: 10.18637/jss.v028.i05.

LI, C. et al. A novel automatic phenology learning (APL) method of training sample selection using multiple datasets for time-series land cover mapping. **Remote Sensing of Environment**, v. 266, p. 112670, 1 dez. 2021. DOI: 10.1016/J.RSE.2021.112670.

LU, M. et al. Land cover change detection by integrating object-based data blending model of Landsat and MODIS. **Remote Sensing of Environment**, v. 184, p. 374–386, out. 2016. DOI: 10.1016/j.rse.2016.07.028.

MA, L. et al. A review of supervised object-based land-cover image classification. **ISPRS Journal of Photogrammetry and Remote Sensing**, v. 130, p. 277–293, ago. 2017. DOI: 10.1016/j.isprsjprs.2017.06.001.

MYERS, N. et al. Biodiversity hotspots for conservation priorities. **Nature**, v. 403, n. 6772, p. 853–858, 24 fev. 2000. DOI: 10.1038/35002501.

OLIVEIRA-FILHO, A. T. et al. Workshop: Definição e delimitação de domínios e subdomínios das paisagens naturais do Estado de Minas Gerais. In: **Mapeamento e inventário da flora nativa e dos reflorestamentos de Minas Gerais**. Lavras: Editora UFLA, 2006. p. 21–35.

OLOFSSON, P. et al. Good practices for estimating area and assessing accuracy of land change. **Remote Sensing of Environment**, v. 148, n. October, p. 42–57, maio 2014. DOI: 10.1016/j.rse.2014.02.015.

PEEL, M. C.; FINLAYSON, B. L.; MCMAHON, T. A. Updated world map of the Köppen-Geiger climate classification. **Hydrology and Earth System Sciences**, v. 11, n. 5, p. 1633–1644, 11 out. 2007. DOI: 10.5194/hess-11-1633-2007.

PITTOCK, J. et al. Managing freshwater, river, wetland and estuarine protected areas. In: WORBOYS, G. L. et al. (Eds.). . **Protected Area Governance and Management**. Camberra: ANU Press, 2015. p. 966.

POWERS, R. P. et al. Remote sensing and object-based techniques for mapping fine-scale industrial disturbances. **International Journal of Applied Earth Observation and Geoinformation**, v. 34, n. 1, p. 51–57, 1 fev. 2015. DOI: 10.1016/J.JAG.2014.06.015.

R CORE TEAM. **R: A language and environment for statistical computing.** Viena, 2016. R Foundation for Statistical Computing, Vienna, Austria. 2019. Disponível em: https://www.R-project.org/. Acesso em: 20 de out. 2020.

RIBEIRO, S. C. et al. Above- and belowground biomass in a Brazilian Cerrado. **Forest Ecology and Management**, v. 262, n. 3, p. 491–499, 1 ago. 2011. DOI: 10.1016/j.foreco.2011.04.017.

RUIZ, L. A. et al. A feature extraction software tool for agricultural object-based image analysis. **Computers and Electronics in Agriculture**, v. 76, n. 2, p. 284–296, maio 2011. DOI: 10.1016/j.compag.2011.02.007.

SCHWIEDER, M. et al. Mapping Brazilian savanna vegetation gradients with Landsat time series. **International Journal of Applied Earth Observation and Geoinformation**, v. 52, p. 361–370, out. 2016. DOI: 10.1016/j.jag.2016.06.019.

SILVEIRA, E. M. O. et al. Assessment of geostatistical features for object-based image classification of contrasted landscape vegetation cover. **Journal of Applied Remote Sensing**, v. 11, n. 3, p. 036004, 21 jul. 2017. DOI: 10.1117/1.JRS.11.036004.

SILVEIRA, E. M. O. et al. Object-based land-cover change detection applied to Brazilian seasonal savannahs using geostatistical features. **International Journal of Remote Sensing**, v. 39, n. 8, p. 2597–2619, 18 abr. 2018a. DOI: 10.1080/01431161.2018.1430397.

SILVEIRA, E. M. O. et al. Reducing the effects of vegetation phenology on change detection in tropical seasonal biomes. **GIScience and Remote Sensing**, v. 56, n. 5, p. 699–717, 4 jul. 2019. DOI: 10.1080/15481603.2018.1550245.

SILVEIRA, E. M. O. et al. Using spatial features to reduce the impact of seasonality for detecting tropical forest changes from landsat time series. **Remote Sensing**, v. 10, n. 6, p. 808, 23 maio 2018b. DOI: 10.3390/rs10060808.

SOUZA, A. A. et al. Dynamics of savanna clearing and land degradation in the newest agricultural frontier in Brazil. **GIScience and Remote Sensing**, v. 57, n. 7, p. 965–984, 2 out. 2020a. DOI: 10.1080/15481603.2020.1835080.

TRANCOSO, R.; SANO, E. E.; MENESES, P. R. The spectral changes of deforestation in the Brazilian tropical savanna. **Environmental Monitoring and Assessment**, v. 187, n. 1, p. 4145,

4 jan. 2015. DOI: 10.1007/s10661-014-4145-3.

TRUMBORE, S.; BRANDO, P.; HARTMANN, H. Forest health and global change. **Science**, v. 349, n. 6250, p. 814–818, 21 ago. 2015. DOI: 10.1126/science.aac6759.

VENKATAPPA, M. et al. Determination of vegetation thresholds for assessing land use and land use changes in Cambodia using the Google Earth Engine cloud-computing platform. **Remote Sensing**, v. 11, n. 13, 2019. DOI: 10.3390/rs11131514.

VERBESSELT, J. et al. Phenological change detection while accounting for abrupt and gradual trends in satellite image time series. **Remote Sensing of Environment**, v. 114, n. 12, p. 2970–2980, 15 dez. 2010. DOI: 10.1016/j.rse.2010.08.003.

VERMOTE, E. F. et al. Preliminary analysis of the performance of the Landsat 8/OLI land surface reflectance product. **Remote Sensing of Environment**, v. 185, p. 46–56, nov. 2016. DOI: 10.1016/j.rse.2016.04.008.

WU, X. et al. Evaluation of semivariogram features for object-based image classification. **Geo-spatial Information Science**, v. 18, n. 4, p. 159–170, 2 out. 2015. DOI: 10.1080/10095020.2015.1116206.

WULDER, M. A. et al. Satellite-based time series land cover and change information to map forest area consistent with national and international reporting requirements. **Forestry: An International Journal of Forest Research**, v. 93, n. 3, p. 331–343, 14 maio 2020. DOI: 10.1093/forestry/cpaa006.

YUE, A. et al. Texture extraction for object-oriented classification of high spatial resolution remotely sensed images using a semivariogram. **International Journal of Remote Sensing**, v. 34, n. 11, p. 3736–3759, 10 jun. 2013. DOI: 10.1080/01431161.2012.759298.

ZHOU, W.; TROY, A.; GROVE, M. Object-based Land Cover Classification and Change Analysis in the Baltimore Metropolitan Area Using Multitemporal High Resolution Remote Sensing Data. **Sensors**, v. 8, n. 3, p. 1613–1636, 10 mar. 2008. DOI: 10.3390/s8031613.

ZHU, Z. et al. Optimizing selection of training and auxiliary data for operational land cover classification for the LCMAP initiative. **ISPRS Journal of Photogrammetry and Remote Sensing**, v. 122, p. 206–221, 1 dez. 2016. DOI: 10.1016/J.ISPRSJPRS.2016.11.004.

ZHU, Z. Change detection using landsat time series: A review of frequencies, preprocessing, algorithms, and applications. **ISPRS Journal of Photogrammetry and Remote Sensing**, v. 130, p. 370–384, ago. 2017. DOI: 10.1016/j.isprsjprs.2017.06.013.

7 SUPPLEMENTARY MATERIAL

Table 1S – Data of acquisition of Landsat OLI images.

Orbit/row	Date of acquisition (mm/dd/yyyy)				
219/070	06/13/2013	07/02/2014	06/19/2015	07/07/2016	08/11/2017
219/071	06/13/2013	08/03/2014	06/19/2015	07/07/2016	08/11/2017
220/071	07/06/2013	08/10/2014	05/25/2015	07/14/2016	08/02/2017

Source: Author (2022).

Figure 1S – Correlation matrix of the 19 variables. See Table 2 for legend details.

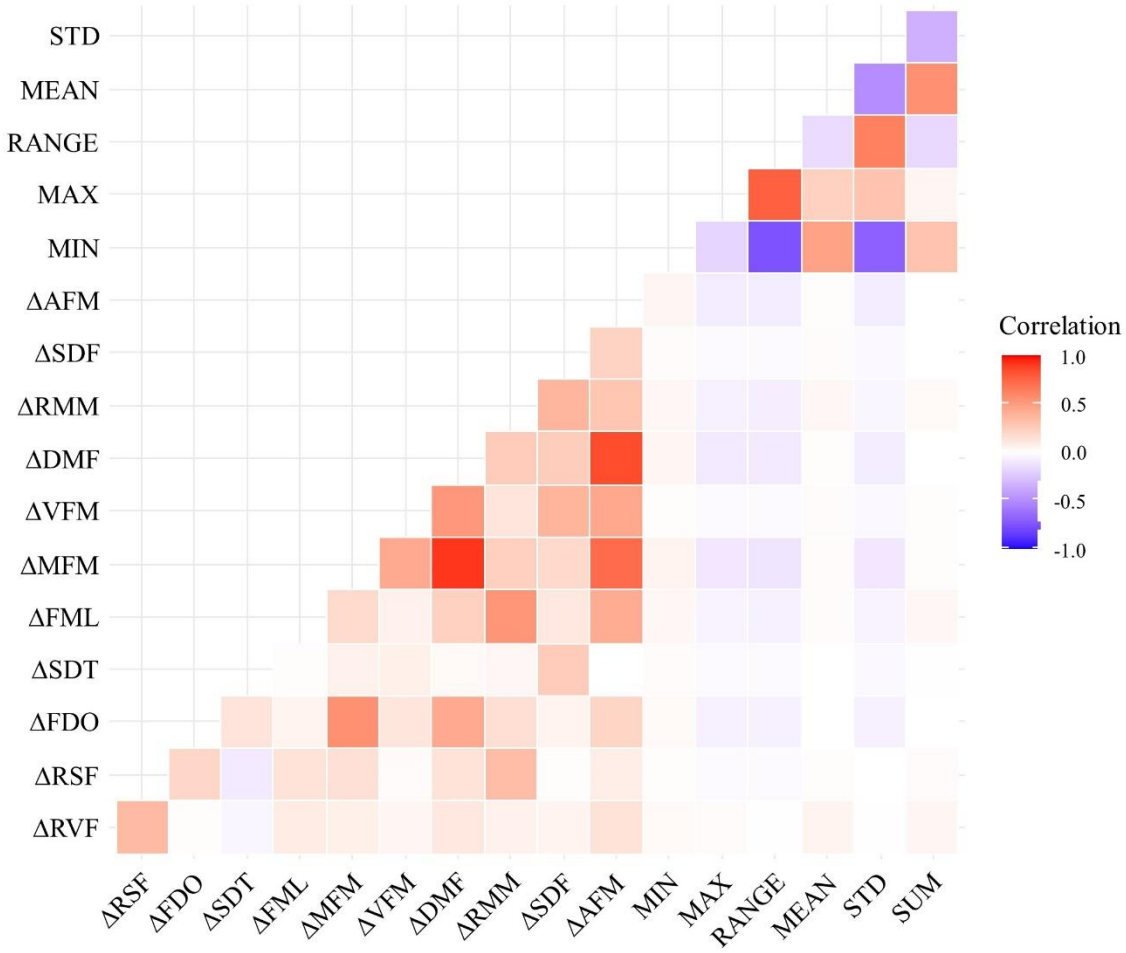

Source: Author (2022).